NASA Technical Memorandum 106344

Thermoelastic Response of Metal Matrix Composites With Large-Diameter Fibers Subjected to Thermal Gradients

Jacob Aboudi and Marek-Jerzy Pindera
University of Virginia
Charlottesville, Virginia

and

Steven M. Arnold
Lewis Research Center
Cleveland, Ohio

October 1993

NASA

THERMOELASTIC RESPONSE OF METAL MATRIX COMPOSITES WITH LARGE-DIAMETER FIBERS SUBJECTED TO THERMAL GRADIENTS

by

Jacob Aboudi[1] and Marek-Jerzy Pindera
University of Virginia
Charlottesville, Virginia

Steven M. Arnold
National Aeronautics and Space Administration
Lewis Research Center
Cleveland, Ohio

ABSTRACT

A new micromechanical theory is presented for the response of heterogeneous metal matrix composites subjected to thermal gradients. In contrast to existing micromechanical theories that utilize classical homogenization schemes in the course of calculating microscopic and macroscopic field quantities, in the present approach the actual microstructural details are explicitly coupled with the macrostructure of the composite. Examples are offered that illustrate limitations of the classical homogenization approach in predicting the response of thin-walled metal matrix composites with large-diameter fibers when subjected to thermal gradients. These examples include composites with a finite number of fibers in the thickness direction that may be uniformly or nonuniformly spaced, thus admitting so-called functionally gradient composites. The results illustrate that the classical approach of decoupling micromechanical and macro-mechanical analyses in the presence of a finite number of large-diameter fibers, finite dimensions of the composite, and temperature gradient may produce excessively conservative estimates for macroscopic field quantities, while both underestimating and overestimating the local fluctuations of the microscopic quantities in different regions of the composite. Also demonstrated is the usefulness of the present approach in generating favorable stress distributions in the presence of thermal gradients by appropriately tailoring the internal microstructural details of the composite.

NOMENCLATURE

$u_i(S), T_i(S)$	--	displacement and traction components on the surface S of a composite
$\varepsilon^0_{ij}, \sigma^0_{ij}$	--	average values of strains and stresses in a composite subjected to homogeneous boundary conditions
$\bar{\varepsilon}_{ij}, \bar{\sigma}_{ij}$	--	average values of strains and stresses in a representative volume element

[1]Visiting Professor, Faculty of Engineering, Tel-Aviv University, Ramat-Aviv 69978, Israel

$\varepsilon_{ij}(x_k)$, $\sigma_{ij}(x_k)$	--	strains and stresses at the point x_k in a composite
C_{ijkl}	--	elements of the effective stiffness tensor of a composite
p, q, r	--	indices used to identify the cell (p,q,r)
α, β, γ	--	indices used to identify the subcell $(\alpha\beta\gamma)$
$d_\alpha^{(p)}, h_\beta, l_\gamma$	--	dimensions of the subcell $(\alpha\beta\gamma)$ in the $p-th$ unit cell
$v_{(\alpha\beta\gamma)}^{(p)}$	--	volume of the subcell $(\alpha\beta\gamma)$
$\bar{x}_1^{(\alpha)}, \bar{x}_2^{(\beta)}, \bar{x}_3^{(\gamma)}$	--	local subcell coordinates
$k_i^{(\alpha\beta\gamma)}$	--	coefficients of heat conductivity of the material in the subcell $(\alpha\beta\gamma)$
$T^{(\alpha\beta\gamma)}$	--	temperature field in the subcell $(\alpha\beta\gamma)$
$T_0^{(\alpha\beta\gamma)}$	--	temperature at the center of the subcell $(\alpha\beta\gamma)$
$T_i^{(\alpha\beta\gamma)}$	--	coefficients in the temperature expansion within the subcell $(\alpha\beta\gamma)$
$q_i^{(\alpha\beta\gamma)}$	--	components of the heat flux vector in the subcell $(\alpha\beta\gamma)$
$Q_{i(l,m,n)}^{(\alpha\beta\gamma)}$	--	average values of the subcell heat flux component $q_i^{(\alpha\beta\gamma)}$ when $l = m = n = 0$; higher-order heat fluxes for other values of l,m,n
$L_{i(l,m,n)}^{(\alpha\beta\gamma)}$	--	surface integrals of subcell interfacial heat fluxes
$u_i^{(\alpha\beta\gamma)}$	--	displacement components in the subcell $(\alpha\beta\gamma)$
$w_1^{(\alpha\beta\gamma)}$	--	x_1 displacement component at the center of the subcell $(\alpha\beta\gamma)$
$\phi_1^{(\alpha\beta\gamma)}$	--	coefficients associated with the linear terms in the second-order expansion of the subcell displacement $u_1^{(\alpha\beta\gamma)}$
$\chi_2^{(\alpha\beta\gamma)}$	--	coefficients associated with the linear terms in the first-order expansion of the subcell displacement $u_2^{(\alpha\beta\gamma)}$
$\psi_3^{(\alpha\beta\gamma)}$	--	coefficients associated with the linear terms in the first-order expansion of the subcell displacement $u_3^{(\alpha\beta\gamma)}$
$U_1^{(\alpha\beta\gamma)}$	--	coefficients associated with the quadratic term $x_1^{(\alpha)2}$ in the second-order expansion of the subcell displacement $u_1^{(\alpha\beta\gamma)}$

$V_1^{(\alpha\beta\gamma)}$ -- coefficients associated with the quadratic term $x_2^{(\beta)2}$ in the second-order expansion of the subcell displacement $u_1^{(\alpha\beta\gamma)}$

$W_1^{(\alpha\beta\gamma)}$ -- coefficients associated with the quadratic term $x_3^{(\gamma)2}$ in the second-order expansion of the subcell displacement $u_1^{(\alpha\beta\gamma)}$

$\varepsilon_{ij}^{(\alpha\beta\gamma)}$ -- local strain components in the subcell $(\alpha\beta\gamma)$

$\sigma_{ij}^{(\alpha\beta\gamma)}$ -- local stress components in the subcell $(\alpha\beta\gamma)$

$c_{ijkl}^{(\alpha\beta\gamma)}$ -- elements of the stiffness tensor of the material in the subcell $(\alpha\beta\gamma)$

$\Gamma_{ij}^{(\alpha\beta\gamma)}$ -- elements of the thermal tensor of the material in the subcell $(\alpha\beta\gamma)$ (products of the stiffness tensor and the thermal expansion coefficients)

$S_{ij(l,m,n)}^{(\alpha\beta\gamma)}$ -- average values of the subcell stress components $\sigma_{ij}^{(\alpha\beta\gamma)}$ when $l = m = n = 0$; higher-order stress components for other values of l,m,n

$I_{1j(n,0,0)}^{(\alpha\beta\gamma)}$ -- surface integrals of the subcell interfacial stresses $\sigma_{1j}^{(\alpha\beta\gamma)}$ at $\bar{x}_1^{(\alpha)} = \pm d_\alpha^{(p)}/2$

$J_{2j(0,n,0)}^{(\alpha\beta\gamma)}$ -- surface integrals of the subcell interfacial stresses $\sigma_{2j}^{(\alpha\beta\gamma)}$ at $\bar{x}_2^{(\beta)} = \pm h_\beta/2$

$K_{3j(0,0,n)}^{(\alpha\beta\gamma)}$ -- surface integrals of the subcell interfacial stresses $\sigma_{3j}^{(\alpha\beta\gamma)}$ at $\bar{x}_3^{(\gamma)} = \pm l_\gamma/2$,

1.0 INTRODUCTION

The past thirty years have seen tremendous growth in the development and use of composite materials. The applications range from sporting and recreational accessories to advanced aerospace structural and engine components. Historically, composite materials have been classified into different categories based on the geometry and distribution of the reinforcement phase and the type of the matrix phase. For example, polymeric matrix (PMC), metal matrix (MMC), intermetallic matrix (IMC), and ceramic matrix (CMC) composites are four classes of composites based on the type of matrix used to contain the reinforcement phase. The reinforcement phase can be finite-length or continuous, oriented or random, thereby providing further classification into short-fiber, oriented or random composites, and unidirectional (continuous and oriented) composites.

Typically, the reinforcement phase in the various classes of composite materials is distributed in a statistically or macroscopically uniform fashion such that the resulting two-phase material is macroscopically homogeneous with properties that do not vary spatially. Numerous micromechanical approaches have been developed during the past thirty years, as discussed by

Aboudi (1991), to calculate the average (often called *effective* or *macroscopic*) properties of such composites given the geometry, distribution and properties of the individual phases. The micromechanical analysis makes it possible to replace the heterogeneous microstructure of the composite with an equivalent homogeneous continuum characterized by a set of effective elastic properties that subsequently can be used in more complicated structural analyses. The effective elastic properties are defined as the constitutive parameters that relate volume averages of the stress and strain components under so-called homogeneous boundary conditions, specified either in terms of surface displacements or prescribed surface tractions.

The **central assumption** in applying the various well-established micromechanical techniques is the **existence** of a definable representative volume element (RVE) at each point within the heterogeneous continuum and the ability to apply homogeneous boundary conditions to such an element. This amounts to decoupling the local and global analyses by evaluating the effective material properties at a given point based only on the local states of stress and deformation at that point which are assumed to be known **a priori**. Such decoupling is based on the assumption of the applicability of a principle sometimes referred to in the literature as **the principle of local action** (Malvern, 1969). The decoupling of local and global analyses clearly limits the range of applicability of the classical homogenization approach to composites with very fine microstructures (i.e., inclusion dimensions) with respect to the overall dimensions of the composite, and imposes constraints on the severity of deformation gradients that can be admitted. Composites with fine microstructures include unidirectional composites reinforced with small-diameter fibers such as graphite and carbon, for instance. Alternatively, in composites containing relatively large-diameter fibers with respect to the thickness of a single ply, such as B/Al or SiC/Ti, the applicability and reliability of the traditional microscopic approach based on the concept of an RVE and the classical homogenization treatment is suspect, and remains to be established due to potential coupling between the microstructure and the global response. This is illustrated in Figure 1 for situations involving thermal gradients, and will be discussed in more detail in the following section.

Recently, a new concept involving tailoring of the internal microstructure of the composite to achieve certain required response characteristics to given input parameters has taken root. This idea has been pursued vigorously by Japanese researchers (cf. Yamanouchi et al., 1990) who have coined the term **functionally gradient materials** to describe this newly emerging class of composites. The idea involves spatially grading the properties of the material by using variable spacings between individual inclusions, as well as by using inclusions with different properties, sizes and shapes. Such an approach offers a number of advantages over the more traditional methods of changing the compliance of composite structural elements by varying the

lamination sequence or dropping plies to reduce the cross-sectional geometry, for instance. Grading or tailoring the internal microstructure of a composite material or a structural component allows the designer to truly integrate both the material and structural considerations into the final design and final product. This brings the entire structural design process to the material level in the purest sense, thereby increasing the number of possible material configurations for specific design applications.

Composite materials with tailored microstructures are ideal candidates for applications involving severe thermal gradients, ranging from thermal structures in advanced aircraft and aerospace engines to circuit boards. For instance, a direct consequence of the temperature gradient across the thickness of a structural component (such as a combustor liner or airfoil) is the tendency to bend in the out-of-plane direction. This tendency will be present irrespective of whether a homogeneous or heterogeneous material is considered. However, by judiciously tailoring the microstructure of a heterogeneous material, the thermal bending moment can be reduced, if not eliminated, consequently decreasing the severity of warping.

The potential benefits that may be derived from composites with tailored microstructures have lead to increased activities in the areas of processing, and materials science, of these materials. These activities, however, are handicapped by the lack of appropriate computational strategies for the response of functionally graded materials that **explicitly couple the heterogeneous microstructure of the material with the global analysis**. As implied by the foregoing brief discussion on the limits of applicability of the classical homogenization approach, and further elaborated upon in the following section, traditional micromechanical schemes currently used in analyzing functionally graded materials, that is those which implicitly assume the existence of an RVE and the validity of the principle of local state, suffer from theoretical shortcomings and cannot be used with confidence. As a result, a new analytical approach is presented (that explicitly couples the heterogeneous microstructure of the material with the global analysis) in order to respond to the current need to analyze behavior of composites with tailored microstructures (e.g. functionally graded, large-diameter reinforcement) in the presence of thermal gradients. In particular, the problem considered herein is a composite plate with a finite thickness H extending to infinity in the x_2–x_3 plane and subjected to a temperature gradient, see Figure 2. The composite is reinforced by periodic arrays of fibers in the direction of the x_2 axis or the x_3 axis (Figure 2a), or both (Figure 2b). In the direction of the x_1 axis, hereafter called the functionally gradient (**FG**) direction, the fiber spacing between adjacent arrays may vary. The reinforcing fibers can be either continuous or finite-length. Further, each array of fibers can admit different thermoelastic properties. Consequently, the model admits a variety of tailored microstructural configurations whose response to the applied thermal gradient can be

investigated (including unidirectional and bi-directional arrays with uniform or variable fiber spacings in the **FG** direction, as well as multi-phase arrays). These configurations can include functionally graded materials consisting of metallic and ceramic phases that produce continuously changing properties for applications involving severe thermal gradients. In such applications, metallic-rich regions are placed in the vicinity of the surface exposed to lower temperatures whereas those regions exposed to elevated temperatures are ceramic-rich.

In addition, the present formulation makes it possible to test the applicability of the various homogenization schemes when predicting the response of composites with large-diameter fibers subjected to thermal gradients, i.e., when each ply consists of a single row of fibers in the thickness direction. Hence, the fundamental question of how many fibers (or plies) are required in the thickness direction for classical homogenization schemes to be valid in the presence of thermal gradients can therefore be finally answered using the present approach.

This question is the first to be addressed in the **APPLICATIONS** section by presenting inplane force and moment resultants in a composite with finite thickness reinforced with unidirectional SiC fibers, produced by the imposed temperature gradient, as a function of the number of uniformly spaced fibers in the **FG** direction for a fixed fiber volume fraction. These results are normalized by the continuum approach predictions obtained by first generating the effective thermoelastic properties of the individual rows of fibers using a suitable homogenization scheme and subsequently employing these effective properties in the thermal boundary-value problem of an equivalent homogeneous composite. Similarly, a bi-directionally reinforced composite with uniformly spaced fibers in both inplane directions is considered and the various quantities of interest compared with those obtained using the corresponding homogenized configuration. Finally, examples illustrating the effect of linearly, quadratically and cubically varying fiber spacing in the **FG** direction are compared to the uniformly spaced configuration, and the advantages of using functionally graded composites with regard to reducing inplane force and moment resultants are discussed.

2.0 APPLICABILITY OF THE CLASSICAL HOMOGENIZATION SCHEMES

The various micromechanical approaches used to calculate effective properties of composites include use of simple Reuss and Voigt hypotheses, self-consistent schemes and their generalizations, differential schemes, the Mori-Tanaka method, concentric cylinder models, bounding techniques and approximate or numerical analyses of periodic arrays of inclusions or fibers in the surrounding matrix phase. A discussion of these various approaches has recently been given by Aboudi (1991). As stated in the preceding section, the central assumption in applying these well-established techniques is the existence of an RVE and the ability to apply

homogeneous boundary conditions to such an element. These homogeneous boundary conditions can be specified either in terms of surface displacements

$$u_i(S) = \varepsilon^0_{ij} x_j \tag{1}$$

or in terms of prescribed surface tractions

$$T_i(S) = \sigma^0_{ij} n_j \tag{2}$$

where n_i is the unit outward normal vector on the boundary surface S of the composite, x_i are the Cartesian coordinates of the surface, ε^0_{ij} and σ^0_{ij} are constants, and repeated index implies summation. For an inhomogeneous medium the constants ε^0_{ij} and σ^0_{ij} are the volume averaged strains and stresses under the prescribed boundary conditions given by equations (1) and (2), respectively. This is a consequence of the following relations

$$\bar{\varepsilon}_{ij} = \frac{1}{V}\int_V \varepsilon_{ij}(x_k)dV = \frac{1}{V}\int_S \frac{1}{2}(u_i n_j + u_j n_i)dS \tag{3}$$

$$\bar{\sigma}_{ij} = \frac{1}{V}\int_V \sigma_{ij}(x_k)dV = \frac{1}{V}\int_S \frac{1}{2}(T_i x_j + T_j x_i)dS \tag{4}$$

where V is the volume enclosed by the surface S. The above relations hold provided that: the displacements u_i are continuous; the tractions T_i are continuous at all interfaces of the heterogeneous medium; and body forces vanish. Under the above conditions, the effective elastic moduli C_{ijkl} are defined as

$$\bar{\sigma}_{ij} = C_{ijkl}\bar{\varepsilon}_{kl} \tag{5}$$

In practice, the average strains and stresses that result from the application of homogeneous boundary conditions are calculated for an RVE whose macroscopic behavior is indistinguishable from the behavior of the composite-at-large. By applying the homogeneous boundary conditions to the bounding surface of the RVE, which are the same as the boundary conditions applied to the entire composite, its average behavior can be calculated. This average behavior, in turn, defines the composite's macroscopic properties. To qualify as an RVE, the volume of the

element used to calculate average composite behavior must meet two criteria. First, it must be sufficiently small with respect to the dimensions of the composite-at-large in order to be considered a material point in the equivalent homogeneous continuum (i.e. $h \ll H$, see Figure 1). Second, it must be sufficiently large with respect to the inclusion phase (i.e. $d \ll h$, see Figure 1) so that to the first order the elastic strain energy induced by both sets of homogeneous boundary conditions is the same, making the effective elastic properties in equation (5) independent of the manner in which boundary conditions are applied (Hill, 1963). In the case of periodic fiber arrays, the repeating unit cell is interpreted as the RVE provided that the homogeneous boundary conditions are replaced by either symmetry conditions on the deformation of the unit cell or periodic boundary conditions, depending on the type of loading.

Clearly, the range of applicability of the aforementioned approaches is limited to composites reinforced by fibers with very small diameters such as graphite or carbon fibers. In such composites, a typical RVE contains a sufficiently large number of fibers while occupying a very small volume of the entire composite, allowing one to disregard boundary-layer effects near the bounding surfaces of the RVE upon application of either type of homogeneous boundary conditions. As a result, even in the presence of highly inhomogeneous deformation gradients within the composite-at-large, the field quantities within the RVE will not vary significantly, thereby permitting the definition of a material property at a point in the equivalent homogeneous continuum. In contrast, in composites with relatively large-diameter fibers with respect to the thickness of a single ply, the variation of the quantities of interest within the RVE (assuming that it can be defined) invalidates the basic assumptions on which the concept of effective properties is based. These local variations of the field quantities within the RVE may give rise to unexpected phenomena rooted in the local-global coupling which is neglected in the traditional micromechanical homogenization schemes. For instance, different thermal conductivities of the individual phases together with their directional arrangement may produce thermal gradients in the individual phases which are quite different from the thermal gradients in the homogeneous composite with equivalent effective properties subjected to identical boundary conditions (Figure 1). This, in turn, may alter the local conductivity characteristics and produce unexpected effects such as localized "hot spots" for instance. The size of the RVE in relation to the thickness of the composite and the temperature gradient obviously will play an important role in the above scenario.

The preceding discussion raises questions about the applicability of the traditional microscopic approach based on the concept of an RVE in the presence of large thermal gradients and coarse or spatially variable microstructure. In light of this discussion, the current practice of decoupling the local response from the global response by calculating pointwise effective

thermoelastic properties of functionally graded materials without regard to whether the actual microstructure admits the presence of an RVE, and subsequently using these properties in the global analysis of the heterogeneous material, remains to be justified. These issues were discussed qualitatively as early as 1974 by Pagano (1974) with regard to mechanical loading of macroscopically homogeneous composites. No further work in this area appears to have been published in the open literature since then. In order to resolve these issues, a model is required that explicitly couples the microstructural and macrostructural analyses. The model presented in the following section is a step in this direction for applications involving composites with uniformly or nonuniformly spaced, large-diameter fibers subjected to through-the-thickness thermal gradients.

3.0 ANALYTICAL MODEL

The heterogeneous composite shown in Figure 2 can be constructed using the basic building block or repeating unit cell given in Figure 3. This unit cell consists of eight subcells designated by the triplet ($\alpha\beta\gamma$). Each index α, β, γ takes on the values 1 or 2 which indicate the relative position of the given subcell along the x_1, x_2 and x_3 axis, respectively. The dimensions of the unit cell along the x_2 and x_3 axes, h_1, h_2, and l_1, l_2, are fixed for the given configuration since these are the periodic directions, whereas the dimensions along the x_1 axis or the **FG** direction, $d_1^{(p)}$, $d_2^{(p)}$, can vary from unit cell to unit cell. The dimensions of the subcells within a given cell along the **FG** direction are designated with a running index p which identifies the cell number. We note that p remains constant in the x_2-x_3 plane. For the other two directions, x_2 and x_3, the corresponding indices q and r are introduced. Thus a given cell is designated by the triplet (p,q,r) for $p = 1, 2, ..., M$, where M is the number of fibers in the thickness or **FG** direction, and an infinite range of q and r due to the periodicity of the composite in the x_2 and x_3 directions. The material occupying each subcell within the unit cell can be represented by a different set of thermoelastic parameters, allowing considerations of multi-phase media as well as bi-directionally reinforced configurations. It is important to note that the repeating unit cell in the present framework is not taken to be the RVE whose effective properties can be obtained through homogenization as explained below. Rather, the RVE comprises an entire column of such cells spanning the thickness of the plate. Thus the principle of local action **cannot be applied** to an individual cell, requiring the response of each cell to be explicitly coupled to the response of the entire column of cells in the **FG** direction. This is what is meant by the statement that the present approach explicitly couples the microstructural details with the global analysis.

The thermal boundary-value problem outlined in the foregoing is solved in two steps. In the first step, the temperature distribution in the heterogeneous composite is determined by solving

the heat equation under steady-state conditions in each sub-region or cell of the composite. Since the composite is periodic in the x_2-x_3 plane, it is sufficient to determine the distribution of temperatures in a single row of cells spanning the **FG** dimensions only, provided that appropriate continuity and compatibility conditions are satisfied. These conditions ensure that the given cell is indeed indistinguishable from the adjacent cells in the x_2-x_3 plane. Given the temperature distribution in the entire volume occupying the composite, internal displacements, strains and stresses are subsequently generated by solving the equilibrium equations in each sub-region of the composite subject to appropriate continuity and boundary conditions. As in the case of the thermal problem, only a single row of cells is considered due to periodic nature of the composite in the x_2-x_3 plane.

The analytical technique for the above problem is a derivative of the approach developed by the first author in the treatment of the effective response of doubly and triply periodic composites, referred to as the **method of cells** (Aboudi, 1991) and most recently the **generalized method of cells** (Paley and Aboudi, 1992; Aboudi and Pindera, 1992). In the original formulation of the method of cells, a continously-reinforced, unidirectional fibrous composite is modeled as a doubly-periodic array of fibers embedded in a matrix phase. The periodic character of the assemblage allows one to identify a repeating unit cell that can be used as a building block to construct the entire composite. The properties of this repeating unit cell are thus representative of the properties of the entire assemblage. The unit cell consists of a single fiber subcell surrounded by three matrix subcells. Hence the name **method of cells**. The rectangular geometry of the repeating unit cell allows one to obtain an approximate, closed-form solution for the stresses and strains in the individual subcells given some macroscopically homogeneous state of strain or stress applied to the composite. The solution is obtained by approximating the displacement field in each of the subcells in terms of the displacement of the center of the subcell and a linear expansion in the local coordinates $\bar{x}^{(\alpha)}, \bar{x}^{(\beta)}, \bar{x}^{(\gamma)}$ centered at the subcell's mid-point. The coefficients or microvariables associated with the linear terms in the expansion, and the unknown displacements at the subcell centers are obtained by satisfying continuity of tractions and diplacements in an average sense between individual subcells of a given cell, and between adjacent cells. In addition, a **connectivity condition** is imposed on subcell center displacements of a given cell with respect to the corresponding subcell center displacements in adjacent cells, that provides the necessary expressions for homogenized strains in terms of the displacement gradients of the subcell mid-points. The approximate solution to the given boundary-value problem, in turn, is used to determine macroscopic (average) or effective properties of the composite. In the **generalized method of cells**, the repeating unit cell is subdivided into an arbitrary number of subcells which makes it possible to include multiple phases and additional geometric detail in

modeling the repeating unit cell. The procedure for analyzing local stress and strain fields in this case, however, is the same as that used in the original method of cells (i.e., by approximating local subcell displacements using linear expansions in terms of local coordinates in the individual subcells).

Conversely, in the present analysis a **higher-order theory** is required in order to capture the local effects created by the thermal gradient, the microstructure of the composite, and the finite dimension in the **FG** direction. Accordingly, in the thermal problem the temperature field in each subcell of a repeating unit cell is approximated using a **quadratic expansion** in local coordinates along the three coordinate directions associated with the given subcell. In the solution for the local strains and stresses, the displacement field in the **FG** direction in each subcell is also approximated using a **quadratic expansion** in local coordinates within the subcell. The displacement field in the x_2 and x_3 directions, however, is still approximated using a **linear expansion** in local coordinates to reflect the periodic character of the composite's microstructure in the x_2-x_3 plane.

The unknown coefficients associated with the linear and quadratic local coordinates in both the thermal problem and the solution for internal strains and stresses are obtained by satisfying continuity of displacements and tractions and boundary conditions in an average sense along similar lines as those employed in the original and generalized method of cells. A fundamental difference, however, between the present solution and the previous treatments lies in the fact that the considered composite contains elements of both material and structural effects which **cannot** be treated (i.e., decoupled) using the classical homogenization schemes. Accordingly, the connectivity conditions (which provide expressions for the homogenized strains in terms of the subcell mid-point displacement gradients) are not imposed in the **FG** direction in solving the given boundary-value problem since it is not possible to define homogenized strains in this direction using classical micromechanical concepts. This is due to the absence of homogeneous boundary conditions that hold for **both** the repeating unit cell and the composite-at-large, as well as the finite dimension of the composite in the **FG** direction. These features set the present model apart from the classical micromechanical approaches currently employed by researchers working in the area of functionally gradient materials.

An outline of this new analytical approach for both the thermal and mechanical problem that summarizes the governing equations for the determination of the temperature and displacement fields in the individual subcells will now be given. A detailed derivation of these equations is presented in the Appendix so as not to obscure the basic concepts by the involved algebraic manipulations necessary to generate the governing equations.

3.1 Thermal Analysis: Problem Formulation

Suppose that the composite material occupies the region $0 \le x_1 \le H$, $|x_2| < \infty$, $|x_3| < \infty$. Let the composite be subjected to the temperature T_T on the top surface ($x_1 = 0$) and to T_B on the bottom surface ($x_1 = H$). Also, let M denote the number of cells in the interval $0 \le x_1 \le H$, i.e., $M = H / \sum_{p=1}^{M} (d_1^{(p)} + d_2^{(p)})$. For $p = 2, \ldots, M-1$ the cells are internal, whereas for $p = 1$ and $p = M$ they are boundary cells.

3.1.1 Heat Conduction Equation

For a steady-state situation, the heat flux field in the material occupying the subcell ($\alpha\beta\gamma$) of the $p-th$ cell, in the region defined by $|\bar{x}_1^{(\alpha)}| \le \frac{1}{2} d_\alpha^{(p)}$, $|\bar{x}_2^{(\beta)}| \le \frac{1}{2} h_\beta$, $|\bar{x}_3^{(\gamma)}| \le \frac{1}{2} l_\gamma$, must satisfy the equation:

$$\partial_1 q_1^{(\alpha\beta\gamma)} + \partial_2 q_2^{(\alpha\beta\gamma)} + \partial_3 q_3^{(\alpha\beta\gamma)} = 0 \tag{6}$$

where $\partial_1 = \partial / \partial \bar{x}_1^{(\alpha)}$, $\partial_2 = \partial / \partial \bar{x}_2^{(\beta)}$, $\partial_3 = \partial / \partial \bar{x}_3^{(\gamma)}$. The components of the heat flux vector $q_i^{(\alpha\beta\gamma)}$ in this subcell are derived from the temperature field according to:

$$q_i^{(\alpha\beta\gamma)} = -k_i^{(\alpha\beta\gamma)} \partial_i T^{(\alpha\beta\gamma)} \quad , \quad (i = 1, 2, 3; \textit{ no sum}) \tag{7}$$

where $k_i^{(\alpha\beta\gamma)}$ are the coefficients of heat conductivity of the material in the subcell ($\alpha\beta\gamma$), and no summation is implied by repeated Greek letters in the above and henceforth.

Given the relation between the heat flux and temperature, a temperature distribution that satisfies the heat conduction equation is sought subject to the continuity and boundary conditions given below.

3.1.2 Heat Flux Continuity Conditions

The continuity of the heat flux vector $\mathbf{q}^{(\alpha\beta\gamma)}$ at the interfaces separating adjacent subcells within the repeating unit cell (p,q,r) is fulfilled by imposing the relations

$$q_1^{(1\beta\gamma)} \Big|^{(p,q,r)}_{\bar{x}_1^{(1)} = d_1^{(p)}/2} = q_1^{(2\beta\gamma)} \Big|^{(p,q,r)}_{\bar{x}_1^{(2)} = -d_2^{(p)}/2} \tag{8a}$$

$$q_2^{(\alpha 1\gamma)} \Big|^{(p,q,r)}_{\bar{x}_2^{(1)} = h_1/2} = q_2^{(\alpha 2\gamma)} \Big|^{(p,q,r)}_{\bar{x}_2^{(2)} = -h_2/2} \tag{8b}$$

$$q_3^{(\alpha\beta 1)} \Big|^{(p,q,r)}_{\bar{x}_3^{(1)} = l_1/2} = q_3^{(\alpha\beta 2)} \Big|^{(p,q,r)}_{\bar{x}_3^{(2)} = -l_2/2} \tag{8c}$$

In addition to the above continuity conditions within the $p-th$ cell, the heat flux continuity at the interfaces between neighboring cells must be ensured. The conditions that ensure this are given by

$$q_1^{(1\beta\gamma)} \Big|^{(p+1,q,r)}_{\bar{x}_1^{(1)} = -d_1^{(p+1)}/2} = q_1^{(2\beta\gamma)} \Big|^{(p,q,r)}_{\bar{x}_1^{(2)} = d_2^{(p)}/2} \tag{9a}$$

$$q_2^{(\alpha 1\gamma)} \Big|^{(p,q+1,r)}_{\bar{x}_2^{(1)} = -h_1/2} = q_2^{(\alpha 2\gamma)} \Big|^{(p,q,r)}_{\bar{x}_2^{(2)} = h_2/2} \tag{9b}$$

$$q_3^{(\alpha\beta 1)} \Big|^{(p,q,r+1)}_{\bar{x}_3^{(1)} = -l_1/2} = q_3^{(\alpha\beta 2)} \Big|^{(p,q,r)}_{\bar{x}_3^{(2)} = l_2/2} \tag{9c}$$

3.1.3 Thermal Continuity Conditions

The thermal continuity conditions at the interfaces separating adjacent subcells within the representative cell (p,q,r) are given by relations similar to the corresponding heat flux continuity conditions, i.e., equations (8a) - (8c),

$$T^{(1\beta\gamma)} \Big|^{(p,q,r)}_{\bar{x}_1^{(1)} = d_1^{(p)}/2} = T^{(2\beta\gamma)} \Big|^{(p,q,r)}_{\bar{x}_1^{(2)} = -d_2^{(p)}/2} \tag{10a}$$

$$T^{(\alpha 1\gamma)} \Big|^{(p,q,r)}_{\bar{x}_2^{(1)} = h_1/2} = T^{(\alpha 2\gamma)} \Big|^{(p,q,r)}_{\bar{x}_2^{(2)} = -h_2/2} \tag{10b}$$

$$T^{(\alpha\beta 1)} \Big|^{(p,q,r)}_{\bar{x}_3^{(1)} = l_1/2} = T^{(\alpha\beta 2)} \Big|^{(p,q,r)}_{\bar{x}_3^{(2)} = -l_2/2} \tag{10c}$$

while the thermal continuity at the interfaces between neighboring cells is ensured, as in the case of the heat flux field, by requiring that

$$T^{(1\beta\gamma)}\Big|^{(p+1,q,r)}_{\bar{x}_1^{(1)}=-d_1^{(p+1)}/2} = T^{(2\beta\gamma)}\Big|^{(p,q,r)}_{\bar{x}_1^{(2)}=d_2^{(p)}/2} \tag{11a}$$

$$T^{(\alpha 1\gamma)}\Big|^{(p,q+1,r)}_{\bar{x}_2^{(1)}=-h_1/2} = T^{(\alpha 2\gamma)}\Big|^{(p,q,r)}_{\bar{x}_2^{(2)}=h_2/2} \tag{11b}$$

$$T^{(\alpha\beta 1)}\Big|^{(p,q,r+1)}_{\bar{x}_3^{(1)}=-l_1/2} = T^{(\alpha\beta 2)}\Big|^{(p,q,r)}_{\bar{x}_3^{(2)}=l_2/2} \tag{11c}$$

3.1.4 Boundary Conditions

The final set of conditions that the solution for the temperature field must satisfy are the boundary conditions at the top and bottom surfaces. The temperature in the cell $p = 1$ at the top surface must equal the applied temperature T_T, whereas in the cell $p = M$ at the bottom surface the temperature must be T_B. That is,

$$T^{(1\beta\gamma)}\Big|^{(1,q,r)} = T_T\,,\quad \bar{x}_1^{(1)} = -\frac{1}{2}d_1^{(1)} \tag{12}$$

$$T^{(2\beta\gamma)}\Big|^{(M,q,r)} = T_B\,,\quad \bar{x}_1^{(2)} = \frac{1}{2}d_2^{(M)} \tag{13}$$

3.2 Thermal Analysis: Solution

The temperature distribution in the subcell $(\alpha\beta\gamma)$ of the $p-th$ cell, measured with respect to a reference temperature T_R, is denoted by $T^{(\alpha\beta\gamma)}$. We approximate this temperature field by a second order expansion in the local coordinates $\bar{x}_1^{(\alpha)}$, $\bar{x}_2^{(\beta)}$, and $\bar{x}_3^{(\gamma)}$ as follows:

$$T^{(\alpha\beta\gamma)} = T_0^{(\alpha\beta\gamma)} + \bar{x}_1^{(\alpha)}T_1^{(\alpha\beta\gamma)} + \frac{1}{2}(3\bar{x}_1^{(\alpha)2} - \frac{d_\alpha^{(p)2}}{4})T_2^{(\alpha\beta\gamma)} + \frac{1}{2}(3\bar{x}_2^{(\beta)2} - \frac{h_\beta^2}{4})T_3^{(\alpha\beta\gamma)} +$$

$$\frac{1}{2}(3\bar{x}_3^{(\gamma)2} - \frac{l_\gamma^2}{4})T_4^{(\alpha\beta\gamma)} \tag{14}$$

where $T_0^{(\alpha\beta\gamma)}$, which is the temperature at the center of the subcell, and $T_i^{(\alpha\beta\gamma)}$ ($i = 1, \ldots, 4$) are unknown coefficients which are determined from conditions that will be outlined subsequently.

Henceforth, for notational simplicity and in view of the fact that the composite material is periodic in the x_2-x_3 plane, the designation (p,q,r) for the $p-th$ cell will be replaced by (p) whenever appropriate in this section and in the corresponding section dealing with solution to the mechanical problem.

Given the five unknown quantities associated with each subcell (i.e., $T_0^{(\alpha\beta\gamma)}$, ... , $T_4^{(\alpha\beta\gamma)}$) and eight subcells within each unit cell, $40M$ unknown quantities must be determined for a composite with M rows of fibers in the **FG** direction. These unknown quantities are determined by first satisfying the heat conduction equation, as well as the first and second moment of this equation in each subcell. This is carried out in a volumetric sense for each subcell in view of the temperature field approximation given by equation (14). For this reason both first and second moments must be considered. Subsequently, continuity of heat flux and temperature is imposed in an average sense at the interfaces separating adjacent subcells, as well as neighboring cells. Fulfillment of these field equations and continuity conditions, in conjunction with the imposed thermal boundary conditions at the top and bottom surfaces of the composite, provide the necessary $40M$ equations for the $40M$ unknown coefficients in the temperature field expansion. We begin the outline of the sequence of steps to generate the required $40M$ equations by first considering an arbitrary $p-th$ cell in the interior of the composite material (i.e. $p = 2, \ldots, M-1$). This will produce $40(M-2)$ equations. The additional equations are obtained by considering the boundary cells (i.e. $p = 1$ and M). For these cells, most of the preceding relations will also hold, with the exception of some of the interfacial continuity conditions between adjacent cells. These conditions are replaced by the specified boundary conditions.

3.2.1 Heat Conduction Equations

In the course of satisfying the steady-state heat equation in a volumetric sense, it is convenient to define the following flux quantities:

$$Q_{i(l,m,n)}^{(\alpha\beta\gamma)} = \frac{1}{v_{(\alpha\beta\gamma)}^{(p)}} \int_{-d_\alpha^{(p)}/2}^{d_\alpha^{(p)}/2} \int_{-h_\beta/2}^{h_\beta/2} \int_{-l_\gamma/2}^{l_\gamma/2} (\bar{x}_1^{(\alpha)})^l (\bar{x}_2^{(\beta)})^m (\bar{x}_3^{(\gamma)})^n q_i^{(\alpha\beta\gamma)} d\bar{x}_1^{(\alpha)} d\bar{x}_2^{(\beta)} d\bar{x}_3^{(\gamma)} \tag{15}$$

where l, m, $n = 0$, 1, *or* 2 with $l + m + n \leq 2$, and $v_{(\alpha\beta\gamma)}^{(p)} = d_\alpha^{(p)} h_\beta \, l_\gamma$ is the volume of the subcell $(\alpha\beta\gamma)$ in the $p-th$ cell. For $l = m = n = 0$, $Q_{i(0,0,0)}^{(\alpha\beta\gamma)}$ is the average value of the heat flux component $q_i^{(\alpha\beta\gamma)}$ in the subcell, whereas for other values of (l,m,n) equation (15) defines higher-order heat fluxes. These flux quantities can be evaluated explicitly in terms of the coefficients $T_i^{(\alpha\beta\gamma)}$ by performing the required volume integration using equations (7) and (14) in equation

(15). This yields the following non-vanishing zeroth-order and first-order heat fluxes in terms of the unknown coefficients appearing in the temperature field expansion:

$$Q^{(\alpha\beta\gamma)}_{1(0,0,0)} = -k_1^{(\alpha\beta\gamma)} T_1^{(\alpha\beta\gamma)} \tag{16}$$

$$Q^{(\alpha\beta\gamma)}_{1(1,0,0)} = -\frac{1}{4} k_1^{(\alpha\beta\gamma)} d_\alpha^{(p)2} T_2^{(\alpha\beta\gamma)} \tag{17}$$

$$Q^{(\alpha\beta\gamma)}_{2(0,1,0)} = -\frac{1}{4} k_2^{(\alpha\beta\gamma)} h_\beta^2 T_3^{(\alpha\beta\gamma)} \tag{18}$$

$$Q^{(\alpha\beta\gamma)}_{3(0,0,1)} = -\frac{1}{4} k_3^{(\alpha\beta\gamma)} l_\gamma^2 T_4^{(\alpha\beta\gamma)} \tag{19}$$

Satisfaction of the zeroth, first and second moment of the steady-state heat equation results in the following eight (8) relationships among the first-order heat fluxes $Q^{(\alpha,\beta,\gamma)}_{i(l,m,n)}$ in the different subcells $(\alpha\beta\gamma)$ of the $p-th$ cell, after some involved algebraic manipulations (see the Appendix):

$$[\, Q^{(\alpha\beta\gamma)}_{1(1,0,0)} / d_\alpha^{(p)2} + Q^{(\alpha\beta\gamma)}_{2(0,1,0)} / h_\beta^2 + Q^{(\alpha\beta\gamma)}_{3(0,0,1)} / l_\gamma^2 \,]^{(p)} = 0 \tag{20}$$

where the triplet $(\alpha\beta\gamma)$ assumes all permutations of the integers 1 and 2.

3.2.2 Heat Flux Continuity Equations

The continuity of heat fluxes at the subcell interfaces, as well as between individual cells, associated with the x_1 (**FG**) direction, equations (8a) and (9a) imposed in an average sense, is ensured by the following relations:

$$[\, 12 Q^{(1\beta\gamma)}_{2(0,1,0)} / h_\beta^2 + 12 Q^{(1\beta\gamma)}_{3(0,0,1)} / l_\gamma^2 \,]^{(p)} + 6 \frac{d_2^{(p)}}{d_1^{(p)}} [\, Q^{(2\beta\gamma)}_{2(0,1,0)} / h_\beta^2 + Q^{(2\beta\gamma)}_{3(0,0,1)} / l_\gamma^2 \,]^{(p)} +$$

$$6 \frac{d_2^{(p-1)}}{d_1^{(p)}} [\, Q^{(2\beta\gamma)}_{2(0,1,0)} / h_\beta^2 + Q^{(2\beta\gamma)}_{3(0,0,1)} / l_\gamma^2 \,]^{(p-1)} + \frac{1}{d_1^{(p)}} [\, Q^{(2\beta\gamma)}_{1(0,0,0)} \Big|^{(p)} - Q^{(2\beta\gamma)}_{1(0,0,0)} \Big|^{(p-1)} \,] = 0 \tag{21}$$

and

$$Q^{(1\beta\gamma)}_{1(0,0,0)}\Big|^{(p)} = \frac{1}{2}Q^{(2\beta\gamma)}_{1(0,0,0)}\Big|^{(p)} + \frac{1}{2}Q^{(2\beta\gamma)}_{1(0,0,0)}\Big|^{(p-1)} + 3d_2^{(p)}[Q^{(2\beta\gamma)}_{2(0,1,0)}/h_\beta^2 + Q^{(2\beta\gamma)}_{3(0,0,1)}/l_\gamma^2]^{(p)} -$$

$$3d_2^{(p-1)}[\,Q^{(2\beta\gamma)}_{2(0,1,0)} + Q^{(2\beta\gamma)}_{3(0,0,1)}\,]^{(p-1)} \tag{22}$$

while the equations that ensure heat flux continuity at the subcell interfaces associated with the x_2 and x_3 directions, equations (8b) and (8c) are given by

$$[\,Q^{(\alpha 1\gamma)}_{2(0,1,0)}/h_1 + Q^{(\alpha 2\gamma)}_{2(0,1,0)}/h_2\,]^{(p)} = 0 \tag{23}$$

$$[\,Q^{(\alpha\beta 1)}_{3(0,0,1)}/l_1 + Q^{(\alpha\beta 2)}_{3(0,0,1)}/l_2\,]^{(p)} = 0 \tag{24}$$

We note that equations (9b) and (9c) are identically satisfied by the chosen temperature field representation due to the periodicity of the composite in the x_2-x_3 plane.

Equations (21) - (24) provide us with sixteen (16) additional relations among the zeroth-order and first-order heat fluxes. These relations, together with equation (20), can be expressed in terms of the unknown coefficients $T_i^{(\alpha\beta\gamma)}$ (i = 1, ..., 4) by making use of equations (16) - (19), providing a total of twenty-four (24) of the required forty (40) equations necessary for the determination of these coefficients in the $p-th$ cell.

3.3.3 Thermal Continuity Equations

An additional set of sixteen (16) equations necessary to determine the unknown coefficients in the temperature field expansion is subsequently generated by the thermal continuity conditions imposed on an average basis at each subcell and cell interface. Imposing the thermal continuity at each subcell interface, equations (10a) through (10c), we obtain the following conditions for the $p-th$ cell:

$$[\,T_0^{(1\beta\gamma)} + d_1^{(p)}T_1^{(1\beta\gamma)} + \frac{1}{4}d_1^{(p)2}T_2^{(1\beta\gamma)}\,]^{(p)} = [\,T_0^{(2\beta\gamma)} - d_2^{(p)}T_1^{(2\beta\gamma)} + \frac{1}{4}d_2^{(p)2}T_2^{(2\beta\gamma)}\,]^{(p)} \tag{25}$$

$$[\,T_0^{(\alpha 1\gamma)} + \frac{1}{4}h_1^2T_3^{(\alpha 1\gamma)}\,]^{(p)} = [\,T_0^{(\alpha 2\gamma)} + \frac{1}{4}h_2^2T_3^{(\alpha 2\gamma)}\,]^{(p)} \tag{26}$$

$$[\,T_0^{(\alpha\beta 1)} + \frac{1}{4}l_1^2T_4^{(\alpha\beta 1)}\,]^{(p)} = [\,T_0^{(\alpha\beta 2)} + \frac{1}{4}l_2^2T_4^{(\alpha\beta 2)}\,]^{(p)} \tag{27}$$

The continuity of temperature between neighboring cells in the **FG** direction, equation (11a), on the other hand, yields

$$[\,T_0^{(1\beta\gamma)} - \frac{1}{2}d_1^{(p+1)}T_1^{(1\beta\gamma)} + \frac{1}{4}d_1^{(p+1)2}T_2^{(1\beta\gamma)}\,]^{(p+1)} = [\,T_0^{(2\beta\gamma)} + \frac{1}{2}d_2^{(p)}T_1^{(2\beta\gamma)} + \frac{1}{4}d_2^{(p)2}T_2^{(2\beta\gamma)}\,]^{(p)} \quad (28)$$

We note that the continuity of temperature between neighboring cells in the x_2 and x_3-directions, equations (11b) and (11c), is automatically satisfied by the chosen temperature field representation which reflects the periodic character of the composite in these directions.

3.3.4 Governing Equations for the Unknown Coefficients in the Temperature Expansion

The equilibrium equations, equation (20), together with the heat flux and thermal continuity equations, equations (21) - (24) and equations (25) - (28), respectively, form altogether 40 linear algebraic equations which govern the 40 field variables $T_i^{(\alpha\beta\gamma)}$ ($i = 0, \ldots, 4$) in the eight subcells ($\alpha\beta\gamma$) of an interior cell p; $p = 2, \ldots, M-1$. For the boundary cells $p = 1$ and $p = M$, a different treatment must be applied. For $p = 1$, the governing equations, equations (20), and (23) - (28), are operative. Relations (21) - (22), on the other hand, which follow from the continuity of heat flux between a given cell and the preceding one are not applicable. They are replaced by the condition that the heat flux at the interface between subcell ($1\beta\gamma$) and ($2\beta\gamma$) of the cell $p = 1$ is continuous, as well as the applied temperature relation at the surface $x_1 = 0$. For the cell $p = M$, the previous equations are applicable except equations (28) which are obviously not operative. These equations are replaced by the specific temperature applied at the surface $x_1 = H$.

The governing equations at the interior and boundary cells form a system of $40M$ linear algebraic equations in the unknown coefficients $T_i^{(\alpha\beta\gamma)\,|P}$ (i = 0, ... , 4; $\alpha,\beta,\gamma = 1,2$; p = 1, ... , M). Their solution determines the temperature distribution within the **FG** composite subjected to the boundary conditions (12) and (13). The final form of this system of equations is symbolically represented below

$$\boldsymbol{\kappa}\, T = t \quad (29)$$

where the structural thermal conductivity matrix $\boldsymbol{\kappa}$ contains information on the geometry and thermal conductivities of the individual subcells ($\alpha\beta\gamma$) in the M cells spanning the thickness of the **FG** plate, the thermal coefficient vector T contains the unknown coefficients that describe the thermal field in each subcell, i.e., $T = (T_1^{(111)}, \ldots, T_M^{(222)})$ where $T_p^{(\alpha\beta\gamma)} = (T_0, T_1, T_2, T_3, T_4)_p^{(\alpha\beta\gamma)}$, and the thermal force vector $t = (T_T, 0, \ldots, 0, T_B)$ contains

information on the boundary conditions.

3.3 Mechanical Analysis: Problem Formulation

Given the temperature distribution generated by the applied surface temperatures T_T and T_B obtained in the preceding section, we now proceed to determine the resulting displacement and stress fields. This is carried out for uniform normal (i.e., no shearing) mechanical loading applied to the surfaces of the composite.

3.3.1 Equations of Equilibrium

The stress field in the subcell ($\alpha\beta\gamma$) of the $p-th$ cell generated by the given temperature field must satisfy the equilibrium equations

$$\partial_1 \sigma_{1j}^{(\alpha\beta\gamma)} + \partial_2 \sigma_{2j}^{(\alpha\beta\gamma)} + \partial_3 \sigma_{3j}^{(\alpha\beta\gamma)} = 0 \ , \ j = 1, 2, 3 \tag{30}$$

where the operator ∂_i has been defined previously. The components of the stress tensor, assuming that the material occupying the subcell ($\alpha\beta\gamma$) of the $p-th$ cell is orthotropic, are related to the strain components through the familiar generalized Hooke's law:

$$\sigma_{ij}^{(\alpha\beta\gamma)} = c_{ijkl}^{(\alpha\beta\gamma)} \varepsilon_{kl}^{(\alpha\beta\gamma)} - \Gamma_{ij}^{(\alpha\beta\gamma)} T^{(\alpha\beta\gamma)} \tag{31}$$

where $c_{ijkl}^{(\alpha\beta\gamma)}$ are the elements of the stiffness tensor and the elements $\Gamma_{ij}^{(\alpha\beta\gamma)}$ of the so-called thermal tensor are the products of the stiffness tensor and the thermal expansion coefficients. The components of the strain tensor in the individual subcells are, in turn, obtained from the strain-displacement relations

$$\varepsilon_{ij}^{(\alpha\beta\gamma)} = \frac{1}{2}(\partial_i u_j^{(\alpha\beta\gamma)} + \partial_j u_i^{(\alpha\beta\gamma)}) \ , \ i, j = 1, 2, 3 \tag{32}$$

Given the relation between the stresses and displacement gradients obtained from equations (31) and (32), a displacement field is sought that satisfies the three equilibrium equations together with the continuity and boundary conditions that follow.

3.3.2 Traction Continuity Conditions

The continuity of tractions at the interfaces separating adjacent subcells within the repeating unit cell (p,q,r) is fulfilled by requiring that

$$\sigma_{1i}^{(1\beta\gamma)} \Big|_{\bar{x}_1^{(1)} = d_1^{(p)}/2}^{(p,q,r)} = \sigma_{1i}^{(2\beta\gamma)} \Big|_{\bar{x}_1^{(2)} = -d_2^{(p)}/2}^{(p,q,r)} \tag{33a}$$

$$\sigma_{2i}^{(\alpha 1\gamma)} \Big|_{\bar{x}_2^{(1)} = h_1/2}^{(p,q,r)} = \sigma_{2i}^{(\alpha 2\gamma)} \Big|_{\bar{x}_2^{(2)} = -h_2/2}^{(p,q,r)} \tag{33b}$$

$$\sigma_{3i}^{(\alpha\beta 1)} \Big|_{\bar{x}_3^{(1)} = l_1/2}^{(p,q,r)} = \sigma_{3i}^{(\alpha\beta 2)} \Big|_{\bar{x}_3^{(2)} = -l_2/2}^{(p,q,r)} \tag{33c}$$

In addition to the above continuity conditions within the $p-th$ cell, the traction continuity at the interfaces between neighboring cells must be ensured. These conditions are fulfilled by requiring that

$$\sigma_{1i}^{(1\beta\gamma)} \Big|_{\bar{x}_1^{(1)} = -d_1^{(p+1)}/2}^{(p+1,q,r)} = \sigma_{1i}^{(2\beta\gamma)} \Big|_{\bar{x}_1^{(2)} = d_2^{(p)}/2}^{(p,q,r)} \tag{34a}$$

$$\sigma_{2i}^{(\alpha 1\gamma)} \Big|_{\bar{x}_2^{(1)} = -h_1/2}^{(p,q+1,r)} = \sigma_{2i}^{(\alpha 2\gamma)} \Big|_{\bar{x}_2^{(2)} = h_2/2}^{(p,q,r)} \tag{34b}$$

$$\sigma_{3i}^{(\alpha\beta 1)} \Big|_{\bar{x}_3^{(1)} = -l_1/2}^{(p,q,r+1)} = \sigma_{3i}^{(\alpha\beta 2)} \Big|_{\bar{x}_3^{(2)} = l_2/2}^{(p,q,r)} \tag{34c}$$

3.3.3 Displacement Continuity Conditions

At the interfaces of the subcells within the repeating unit cell (p,q,r) the displacements $\boldsymbol{u} = (u_1, u_2, u_3)$ must be continuous,

$$\boldsymbol{u}^{(1\beta\gamma)} \Big|_{\bar{x}_2^{(1)} = d_1^{(p)}/2}^{(p,q,r)} = \boldsymbol{u}^{(2\beta\gamma)} \Big|_{\bar{x}_1^{(2)} = -d_2^{(p)}/2}^{(p,q,r)} \tag{35a}$$

$$\boldsymbol{u}^{(\alpha 1\gamma)} \Big|_{\bar{x}_2^{(1)} = h_1/2}^{(p,q,r)} = \boldsymbol{u}^{(\alpha 2\gamma)} \Big|_{\bar{x}_2^{(2)} = -h_2/2}^{(p,q,rP} \tag{35b}$$

$$\boldsymbol{u}^{(\alpha\beta 1)} \Big|_{\bar{x}_3^{(1)} = l_1/2}^{(p,q,r)} = \boldsymbol{u}^{(\alpha\beta 2)} \Big|_{\bar{x}_3^{(2)} = -l_2/2}^{(p,q,r)} \tag{35c}$$

while the continuity of displacements between neighboring cells is ensured by requiring that

$$\boldsymbol{u}^{(1\beta\gamma)} \Big|^{(p+1,q,r)}_{\bar{x}_1^{(1)} = -d_1^{(p+1)}/2} = \boldsymbol{u}^{(2\beta\gamma)} \Big|^{(p,q,r)}_{\bar{x}_1^{(2)} = d_2^{(p)}/2} \tag{36a}$$

$$\boldsymbol{u}^{(\alpha 1\gamma)} \Big|^{(p,q+1,r)}_{\bar{x}_2^{(1)} = -h_1/2} = \boldsymbol{u}^{(\alpha 2\gamma)} \Big|^{(p,q,r)}_{\bar{x}_2^{(2)} = h_2/2} \tag{36b}$$

$$\boldsymbol{u}^{(\alpha\beta 1)} \Big|^{(p,q,r+1)}_{\bar{x}_3^{(1)} = -l_1/2} = \boldsymbol{u}^{(\alpha\beta 1)} \Big|^{(p,q,r)}_{\bar{x}_3^{(2)} = l_2/2} \tag{36c}$$

3.3.4 Boundary Conditions

The final set of conditions that the solution for the displacement field must satisfy are the boundary conditions at the top and bottom surfaces. The normal stress in the cell $p = 1$ at the top surface must equal the normal stress f(t),

$$\sigma_{11}^{(1\beta\gamma)} \Big|^{(1,q,r)} = f(t)\,, \qquad \bar{x}_1^{(1)} = -\frac{1}{2} d_1^{(1)} \tag{37}$$

with f(t) describing the temporal variation of this loading, whereas in the cell $p = M$ at the bottom surface the condition that the surface $x_1 = H$ is rigidly clamped (say) is imposed

$$u_1^{(2\beta\gamma)} \Big|^{(M,q,r)} = 0\,, \qquad \bar{x}_1^{(2)} = \frac{1}{2} d_2^{(M)} \tag{38}$$

For other types of boundary conditions, equation (38) should be modified accordingly.

3.4 Mechanical Analysis: Solution

Due to symmetry considerations, the displacement field in the subcell $(\alpha\beta\gamma)$ of the $p-th$ cell is approximated by a second-order expansion in the local coordinates $\bar{x}_1^{(\alpha)}$, $\bar{x}_2^{(\beta)}$, and $\bar{x}_3^{(\gamma)}$ as follows:

$$u_1^{(\alpha\beta\gamma)} = w_1^{(\alpha\beta\gamma)} + \bar{x}_1^{(\alpha)} \phi_1^{(\alpha\beta\gamma)} + \frac{1}{2}(3\bar{x}_1^{(\alpha)2} - \frac{1}{4} d_\alpha^{(p)2}) U_1^{(\alpha\beta\gamma)} + \frac{1}{2}(3\bar{x}_2^{(\beta)2} - \frac{1}{4} h_\beta^2) V_1^{(\alpha\beta\gamma)}$$

$$+ \frac{1}{2}(3\bar{x}_3^{(\gamma)2} - \frac{1}{4} l_\gamma^2) W_1^{(\alpha\beta\gamma)}$$

$$u_2^{(\alpha\beta\gamma)} = \bar{x}_2^{(\beta)} \chi_2^{(\alpha\beta\gamma)} \tag{39}$$

$$u_3^{(\alpha\beta\gamma)} = \bar{x}_3^{(\gamma)} \psi_3^{(\alpha\beta\gamma)}$$

where $w_1^{(\alpha\beta\gamma)}$, which are the displacements at the center of the subcell, and $U_1^{(\alpha\beta\gamma)}$, $V_1^{(\alpha\beta\gamma)}$, $W_1^{(\alpha\beta\gamma)}$, $\phi_1^{(\alpha\beta\gamma)}$, $\chi_2^{(\alpha\beta\gamma)}$, and $\psi_3^{(\alpha\beta\gamma)}$ must be determined from conditions similar to those employed in the thermal problem. In this case, there are $56M$ unknown quantities. The determination of these quantities parallels that of the thermal problem. Here, the heat conduction equation is replaced by the three equilibrium equations, and the continuity of tractions and displacements at the various interfaces replaces the continuity of heat fluxes and temperature. Finally, the boundary conditions involve the appropriate mechanical quantities. As in the thermal problem, we start with the internal cells and subsequently modify the governing equations to accommodate the boundary cells $p = 1$ and M.

3.4.1 Equations of Equilibrium

In the course of satisfying the equilibrium equations in a volumetric sense, it is convenient to define the following stress quantities:

$$S_{ij\,(l,m,n)}^{(\alpha\beta\gamma)} = \frac{1}{v_{(\alpha\beta\gamma)}^{(p)}} \int_{-d_\alpha^{(p)}/2}^{d_\alpha^{(p)}/2} \int_{-h_\beta/2}^{h_\beta/2} \int_{-l_\gamma/2}^{l_\gamma/2} (\bar{x}_1^{(\alpha)})^l (\bar{x}_2^{(\beta)})^m (\bar{x}_3^{(\gamma)})^n \sigma_{ij}^{(\alpha\beta\gamma)} \, d\bar{x}_1^{(\alpha)} d\bar{x}_2^{(\beta)} d\bar{x}_3^{(\gamma)} \tag{40}$$

For $l = m = n = 0$, equation (40) provides average stresses in the subcell, whereas for other values of (l,m,n) higher-order stresses are obtained which are needed to describe the governing field equations of the higher-order continuum. These stress quantities can be evaluated explicitly in terms of the unknown coefficients $U_1^{(\alpha\beta\gamma)}$, ..., $\phi_1^{(\alpha\beta\gamma)}$, ..., $\psi_3^{(\alpha\beta\gamma)}$ by performing the required volume integration using equations (31), (32) and (39) in equation (40). This yields the following non-vanishing zeroth-order and first-order stress components in terms of the unknown coefficients in the displacement field expansion:

$$S_{11(0,0,0)}^{(\alpha\beta\gamma)} = c_{11}^{(\alpha\beta\gamma)} \phi_1^{(\alpha\beta\gamma)} + c_{12}^{(\alpha\beta\gamma)} \chi_2^{(\alpha\beta\gamma)} + c_{13}^{(\alpha\beta\gamma)} \psi_3^{(\alpha\beta\gamma)} - \Gamma_1^{(\alpha\beta\gamma)} T_0^{(\alpha\beta\gamma)} \tag{41}$$

$$S_{22(0,0,0)}^{(\alpha\beta\gamma)} = c_{12}^{(\alpha\beta\gamma)} \phi_1^{(\alpha\beta\gamma)} + c_{22}^{(\alpha\beta\gamma)} \chi_2^{(\alpha\beta\gamma)} + c_{23}^{(\alpha\beta\gamma)} \psi_3^{(\alpha\beta\gamma)} - \Gamma_2^{(\alpha\beta\gamma)} T_0^{(\alpha\beta\gamma)} \tag{42}$$

$$S_{33(0,0,0)}^{(\alpha\beta\gamma)} = c_{13}^{(\alpha\beta\gamma)} \phi_1^{(\alpha\beta\gamma)} + c_{23}^{(\alpha\beta\gamma)} \chi_2^{(\alpha\beta\gamma)} + c_{33}^{(\alpha\beta\gamma)} \psi_3^{(\alpha\beta\gamma)} - \Gamma_3^{(\alpha\beta\gamma)} T_0^{(\alpha\beta\gamma)} \tag{43}$$

$$S^{(\alpha\beta\gamma)}_{11(1,0,0)} = \frac{1}{4} c^{(\alpha\beta\gamma)}_{11} d^{(p)2}_{\alpha} U^{(\alpha\beta\gamma)}_{1} - \frac{1}{12} d^{(p)2}_{\alpha} \Gamma^{(\alpha\beta\gamma)}_{1} T^{(\alpha\beta\gamma)}_{1} \tag{44}$$

$$S^{(\alpha\beta\gamma)}_{12(0,1,0)} = \frac{1}{4} c^{(\alpha\beta\gamma)}_{44} h^{2}_{\beta} V^{(\alpha\beta\gamma)}_{1} \tag{45}$$

$$S^{(\alpha\beta\gamma)}_{13(0,0,1)} = \frac{1}{4} c^{(\alpha\beta\gamma)}_{55} l^{2}_{\gamma} W^{(\alpha\beta\gamma)}_{1} \tag{46}$$

Satisfaction of the equilibrium equations results in the following eight (8) relations among the volume-averaged first-order stresses $S^{(\alpha\beta\gamma)}_{ij(l,m,n)}$ in the different subcells $(\alpha\beta\gamma)$ of the $p-th$ cell, after lengthy algebraic manipulations (see the Apendix):

$$[\, S^{(\alpha\beta\gamma)}_{11(1,0,0)} / d^{(p)2}_{\alpha} + S^{(\alpha\beta\gamma)}_{12(0,1,0)} / h^{2}_{\beta} + S^{(\alpha\beta\gamma)}_{13(0,0,1)} / l^{2}_{\gamma} \,]^{(p)} = 0 \tag{47}$$

where, as in the case of equation (20), the triplet $(\alpha\beta\gamma)$ assumes all permutations of the integers 1 and 2.

3.4.2 Traction Continuity Equations

The continuity of tractions at the subcell interfaces, as well as between individual cells, associated with the x_1 (**FG**) direction, equations (33a) and (34a) imposed in an average sense, is ensured by the following relations:

$$[\, 12 S^{(1\beta\gamma)}_{12(0,1,0)} / h^{2}_{\beta} + 12 S^{(1\beta\gamma)}_{13(0,0,1)} / l^{2}_{\gamma} \,]^{(p)} + 6 \frac{d^{(p)}_{2}}{d^{(p)}_{1}} [\, S^{(2\beta\gamma)}_{12(0,1,0)} / h^{2}_{\beta} + S^{(2\beta\gamma)}_{13(0,0,1)} / l^{2}_{\gamma} \,]^{(p)} +$$

$$6 \frac{d^{(p-1)}_{2}}{d^{(p)}_{1}} [\, S^{(2\beta\gamma)}_{12(0,1,0)} / h^{2}_{\beta} + S^{(2\beta\gamma)}_{13(0,0,1)} / l^{2}_{\gamma} \,]^{(p-1)} + \frac{1}{d^{(p)}_{1}} [\, S^{(2\beta\gamma)}_{11(0,0,0)} \Big|^{(p)} - S^{(2\beta\gamma)}_{11(0,0,0)} \Big|^{(p-1)} \,] = 0 \tag{48}$$

$$S^{(1\beta\gamma)}_{11(0,0,0)} \Big|^{(p)} = \frac{1}{2} S^{(2\beta\gamma)}_{11(0,0,0)} \Big|^{(p)} + \frac{1}{2} S^{(2\beta\gamma)}_{11(0,0,0)} \Big|^{(p-1)} + 3 d^{(p)}_{2} [\, S^{(2\beta\gamma)}_{12(0,1,0)} / h^{2}_{\beta} + S^{(2\beta\gamma)}_{13(0,0,1)} / l^{2}_{\gamma} \,]^{(p)} -$$

$$3 d^{(p-1)}_{2} [\, S^{(2\beta\gamma)}_{12(0,1,0)} / h^{2}_{\beta} + S^{(2\beta\gamma)}_{13(0,0,1)} / l^{2}_{\gamma} \,]^{(p-1)} \tag{49}$$

while the equations that ensure traction continuity between individual subcells associated with the x_2 and x_3 directions, equations (33b) and (33c), are given by

$$[\, S^{(\alpha 1\gamma)}_{12(0,1,0)}/h_1 + S^{(\alpha 2\gamma)}_{12(0,1,0)}/h_2 \,]^{(p)} = 0 \tag{50}$$

$$[\, S^{(\alpha\beta 1)}_{13(0,0,1)}/l_1 + S^{(\alpha\beta 2)}_{13(0,0,1)}/l_2 \,]^{(p)} = 0 \tag{51}$$

$$S^{(\alpha 1\gamma)}_{22(0,0,0)} \Big|^{(p)} = S^{(\alpha 2\gamma)}_{22(0,0,0)} \Big|^{(p)} \tag{52}$$

$$S^{(\alpha\beta 1)}_{33(0,0,1)} \Big|^{(p)} = S^{(\alpha\beta 2)}_{33(0,0,1)} \Big|^{(p)} \tag{53}$$

We note that equations (34b) and (34c) are identically satisfied by the chosen displacement field representation due to the periodic character of the composite material in the x_2-x_3 plane.

Equations (48) - (53) provide us with twenty-four (24) additional relations among the zeroth-order and first-order stresses. These relations, together with equation (47), can be expressed in terms of the unknown coefficients $U_1^{(\alpha\beta\gamma)}$, ..., $\phi_1^{(\alpha\beta\gamma)}$, ..., $\psi_3^{(\alpha\beta\gamma)}$ by making use of equations (41) - (46), providing a total of thirty-two (32) of the required fifty-six (56) equations necessary for the determination of these coefficients in the $p-th$ cell.

3.4.3 Displacement Continuity Equations

The additional twenty-four (24) relations necessary to determine the unknown coefficients in the displacement field expansion are subsequently obtained by imposing displacement continuity conditions on an average basis at each subcell and cell interface. The continuity of displacements at each subcell interface of the $p-th$ cell, equations (35a) through (35c), is satisfied by the following conditions:

$$[\, w_1^{(1\beta\gamma)} + \frac{1}{2} d_1^{(p)} \phi_1^{(1\beta\gamma)} + \frac{1}{4} d_1^2 U_1^{(1\beta\gamma)} \,]^{(p)} = [\, w_1^{(2\beta\gamma)} - \frac{1}{2} d_2^{(p)} \phi_1^{(2\beta\gamma)} + \frac{1}{4} d_2^2 U_1^{(2\beta\gamma)} \,]^{(p)} \tag{54}$$

$$[\, w_1^{(\alpha 1\gamma)} + \frac{1}{2} h_1^2 V_1^{(\alpha 2\gamma)} \,]^{(p)} = [\, w_1^{(\alpha 2\gamma)} + \frac{1}{4} h_2^2 V_1^{(\alpha 2\gamma)} \,]^{(p)} \tag{55}$$

$$h_1 \chi_2^{(\alpha 1\gamma)} \Big|^{(p)} = -h_2 \chi_2^{(\alpha 2\gamma)} \Big|^{(p)} \tag{56}$$

$$[\, w_1^{(\alpha\beta 1)} + \frac{1}{4} l_1^2 W_1^{(\alpha\beta 1)} \,]^{(p)} = [\, w_1^{(\alpha\beta 2)} + \frac{1}{4} l_2^2 W_1^{(\alpha\beta 2)} \,]^{(p)} \tag{57}$$

$$l_1 \psi_3^{(\alpha\beta 1)} \Big|^{(p)} = -l_2 \psi_3^{(\alpha\beta 2)} \Big|^{(p)} \tag{58}$$

while the continuity of displacements between neighboring cells in the **FG** direction, equation (36a), requires that

$$[w_1^{(1\beta\gamma)} - \frac{1}{2}d_1^{(p+1)}\phi_1^{(1\beta\gamma)} + \frac{1}{4}d_1^{(p+1)2}U_1^{(1\beta\gamma)}]^{(p+1)} = [w_1^{(2\beta\gamma)} + \frac{1}{2}d_2^{(p)}\phi_1^{(2\beta\gamma)} + \frac{1}{4}d_2^{(p)2}U_1^{(2\beta\gamma)}]^{(p)} \quad (59)$$

The displacement continuity between neighboring cells in the x_2 and x_3-directions, equations (36b) and (36c), is automatically satisfied by the chosen displacement field representation which reflects the periodic character of the composite in these directions.

3.4.4 Governing Equations for the Unknown Coefficients in the Displacement Expansion

The equilibrium equations, equation (47), together with the traction and displacement continuity equations, equations (48) - (53) and equations (54) - (59), respectively, form altogether 56 equations in the 56 unknowns $w_1^{(\alpha\beta\gamma)}$, $\phi_1^{(\alpha\beta\gamma)}$, $U_1^{(\alpha\beta\gamma)}$, $V_1^{(\alpha\beta\gamma)}$, $W_1^{(\alpha\beta\gamma)}$, $\chi_2^{(\alpha\beta\gamma)}$, $\psi_3^{(\alpha\beta\gamma)}$, which govern the equilibrium of a subcell $(\alpha\beta\gamma)$ within the $p-th$ cell in the interior. As in the thermal problem, a different treatment must be adopted for the boundary cells $p = 1$ and $p = M$. For $p = 1$, equations (47), (50) - (53), and the displacement continuity relations, equations (54) through (59), are operative, whereas equations (48) and (49), which follow from the continuity of tractions between a given cell and the preceeding one, are not applicable. These eight equations must be replaced by the conditions of continuity of tractions at the interior interfaces of the cell $p = 1$ and by the applied normal stress at $x_1 = 0$, equation (37). For the cell $p = M$, the previously derived governing equations are operative except for the four relations given by equations (59) which are obviously not applicable. These are replaced by the condition that the surface $x_1 = H$ is rigidly clamped, equation (38). Consequently, the governing equations at both interior and boundary cells form a system of $56M$ linear algebraic equations in the field variables of the cells along $0 \le x_1 \le H$. The final form of this system of equations is symbolically represented below

$$\boldsymbol{K}\,\boldsymbol{U} = \boldsymbol{f} \quad (60)$$

where the structural stiffness matrix $\boldsymbol{K}$ contains information on the geometry and thermomechanical properties of the individual subcells $(\alpha\beta\gamma)$ in the M cells spanning the thickness of the **FG** plate, the displacement coefficient vector $\boldsymbol{U}$ contains the unknown coefficients that describe the displacement field in each subcell, i.e., $\boldsymbol{U} = (\,\boldsymbol{U}_1^{(111)}, \ldots, \boldsymbol{U}_M^{(222)}\,)$ where $\boldsymbol{U}_p^{(\alpha\beta\gamma)} = (\,w_1, \phi_1, U_1, V_1, W_1, \chi_2, \psi_3\,)_p^{(\alpha\beta\gamma)}$, and the mechanical force vector $\boldsymbol{f} = (\,f(t), 0, \ldots, 0\,)$

contains information on the boundary conditions.

4.0 APPLICATIONS

The approach outlined in the foregoing is employed to investigate the response of thin-walled composites subjected to a thermal gradient in the through-the-thickness direction, i.e., in the **FG** direction. The investigated composites are reinforced with continuous SiC fibers embedded in a titanium aluminide matrix, with the fiber volume fraction, v_f, equal to 0.4. The temperature T_T at the top surface of the composite ($x_1 = 0$) is 0°C while the temperature T_B at the bottom surface ($x_1 = H$) is 500°C. The composite is constrained from deforming due to the applied thermal loading by imposing zero displacement at the bottom surface. At the top surface, the normal traction component is required to vanish (i.e., $\sigma_{11} = 0$).

The properties of the fiber and matrix phases are provided in Table 1. We note that these properties are assumed to be independent of temperature. Although this may be a reasonably good approximation for the SiC fiber, the titanium matrix properties will change with temperature in the range of the imposed thermal gradient across the plate's thickness. This temperature dependence will also be accompanied by viscoplastic effects that are not considered herein. These effects will be considered in a follow-up communication. In view of the lack of accurate knowledge of the thermal conductivity for the SiC fiber, four values of the fiber's thermal conductivity were employed in generating the results. These values resulted in fiber-to-matrix conductivity ratios, κ_m / κ_f, of 50, 25, 5 and 2.2, providing additional insight into the effect of the conductivity mismatch on the resulting temperature and stress fields.

As a first step, unidirectional composites with fibers uniformly spaced in the thickness direction and oriented in the x_3 direction are considered. Results for temperature distributions, stresses and inplane force and moment resultants generated with the present approach that explicitly couples local micromechanical and global structural effects are compared with predictions based on the continuum and a "primitive" micromechanics approaches in which local and global effects are decoupled. The continuum results are obtained by first generating the effective properties of the individual rows of fibers along the x_2 coordinate, or "plies", using the generalized method of cells without regard to whether a representative volume exists or not. That is, these effective properties are generated on the premise that no coupling exists between local and global responses. This is the standard approach currently employed by researchers working in the area of micromechanics. These effective properties, given in Table 2, are subsequently used in the thermal boundary-value problem of an equivalent homogeneous composite subjected to the specified thermal loading. With the knowledge of the continuum or macroscopic thermal fields, the stresses in the individual phases of a repeating unit cell are then calculated by applying an

average temperature over a given cell, treating it as an RVE within the framework of the generalized method of cells. In addition, bi-directionally reinforced composites with uniform fiber spacing in the **FG** direction are also considered, with fibers oriented along the x_3 axis in some layers and along the x_2 axis in others. Again, comparison with the results of the continuum approach is given, using cross-ply laminates subjected to the imposed thermal gradient. The solution to the thermal boundary-value problem of unidirectional and bi-directional laminates based on the continuum approach is briefly outlined in Section 4.1. We note that the continuum approach yields results that, for the considered geometry and applied boundary conditions, are identical to those that would be obtained using the classical lamination theory (cf. Christensen (1979)). Thus, we employ the familiar terminology used in the classical lamination theory in developing the pertinent solution based on the continuum approach in Section 4.1.

Finally, application to functionally graded composites (or those with a tailored mesostructure) is illustrated by considering unidirectional composites with nonuniformly spaced fibers in the **FG** direction. Only continuous fiber configurations are considered with fibers oriented along the x_3 coordinate. Data generated for linear, quadratic and cubic variation in the fiber spacing is compared with results obtained for configurations with uniformly spaced fibers occupying the same total volume of the composite.

4.1 Continuum Approach (Classical Lamination Approach)

Consider a laminate composed of M plies subjected to a thermal gradient by the imposition of the temperature T_T on the top surface and T_B on the bottom surface, Figure 4. The total thickness of the laminate is H with t_i representing the thickness of individual plies. Let $h_0 = -H/2$ designate the coordinate of the top surface of the first ply measured from the mid-plane of the laminate denoted by $z = 0$. The top surface of the $i-th$ ply is thus given by $h_i = h_{i-1} + t_i$ for $i = 1, 2, ..., M$. The solution of the Laplace's equation for the given geometry subjected to the specified boundary conditions yields a linear temperature distribution in each ply. Letting $T_1 = T_T$, the temperature at the interfaces of the laminate can be shown to be given by:

$$T_{i+1} = T_i + \Delta T_i\,, \quad i = 1, 2, \cdots, M \tag{61}$$

where

$$\Delta T_i = \frac{t_i}{\kappa_i} \frac{T_T - T_B}{\sum_{j=1}^{M} \frac{t_j}{\kappa_j}} \tag{62}$$

We note that in our case, κ_i are the effective transverse conductivities κ_T^* of the $i-th$ ply calculated using the method of cells (see Table 2) and $t_i = 199\ \mu m$.

Given the temperature distribution throughout the laminate, the inplane stress distributions in the $i-th$ lamina in the absence of mid-plane strains and curvatures (which is the situation here for the specified boundary constraints) are simply calculated in the following manner:

$$\boldsymbol{\sigma}_{(x-y)}^{(i)} = \overline{\boldsymbol{Q}}^{(i)} \boldsymbol{\alpha}_{(x-y)}^{(i)} T(z) \tag{63}$$

where $\overline{\boldsymbol{Q}}^{(i)}$ and $\boldsymbol{\alpha}_{(x-y)}^{(i)}$ are the transformed reduced stiffness matrix and the thermal expansion coefficient vector, respectively, of the $i-th$ ply referred to the laminate coordinate system $x-y$.

The resulting inplane force and moment resultants can be obtained by multiplying by -1 the so-called thermal inplane force and moment resultants defined as follows:

$$\boldsymbol{N}^T = \int_{-H/2}^{+H/2} \overline{\boldsymbol{Q}} \boldsymbol{\alpha}_{(x-y)} T(z)\, dz \tag{64}$$

$$\boldsymbol{M}^T = \int_{-H/2}^{+H/2} \overline{\boldsymbol{Q}} \boldsymbol{\alpha}_{(x-y)} T(z)\, z\, dz \tag{65}$$

where the previously defined $\overline{\boldsymbol{Q}}$ and $\boldsymbol{\alpha}_{(x-y)}$ are piecewise uniform throughout the laminate, and the superscript (i) that associates these quantities with the $i-th$ ply has been omitted for obvious reasons. Substitution of the linear temperature variation into equations (64) and (65) and performing the necessary integration yields the following explicit expressions for $\boldsymbol{N}^T$ and $\boldsymbol{M}^T$ in terms of the previously defined quantities:

$$\boldsymbol{N}^T = \sum_{i=1}^{M} \overline{\boldsymbol{Q}}^{(i)} \boldsymbol{\alpha}_{(x-y)}^{(i)} \left[T_i (h_i - h_{i-1}) + \frac{1}{2} \frac{\Delta T_i}{t_i} (h_i^2 - h_{i-1}^2) - \frac{\Delta T_i}{t_i} [h_{i-1}(h_i - h_{i-1})] \right] \tag{66}$$

$$\boldsymbol{M}^T = \sum_{i=1}^{M} \overline{\boldsymbol{Q}}^{(i)} \boldsymbol{\alpha}_{(x-y)}^{(i)} \left[\frac{1}{2} T_i (h_i^2 - h_{i-1}^2) + \frac{1}{3} \frac{\Delta T_i}{t_i} (h_i^3 - h_{i-1}^3) - \frac{1}{2} \frac{\Delta T_i}{t_i} h_{i-1} (h_i^2 - h_{i-1}^2) \right] \tag{67}$$

4.2 Response of Composites with Uniform Mesostructure

Here, the response of unidirectional and bi-directional composites with uniformly spaced fibers is investigated. The results are useful in answering the fundamental question of the

validity of the classical homogenization scheme in the presence of thermal gradients and finite boundary effects. Just as importantly, the results give useful estimates on the number of fibers that are required in the thickness direction to produce data that can be reliably generated with the standard homogenization approach wherein the micromechanics and macromechanics analyses are decoupled (which clearly is less expensive than the present scheme).

4.2.1 Unidirectional Composites

Consider the response of a continuously-reinforced unidirectional composite having a fixed thickness of 199 μm with fibers oriented in the x_3 direction. This thickness is based on a single ply of a SiC/Ti composite with 40% fiber volume and a fiber diameter of 142 μm. The thermal conductivity of the SiC fiber is taken to be fifty (50) times that of the matrix, which provides the greatest mismatch between the fiber and matrix thermal conductivities herein considered. The effect of varying the thermal conductivity mismatch on the thermal and stress fields, and the resulting force and moment resultants, will be investigated in Section 4.2.2. The objective in this section is to determine the number of fibers in the thickness direction that are required for the results to approach those obtained using the standard homogenization procedure.

To this end, we consider configurations with M number of fibers, where M = 1, 2, 3, 5, 8, 12, 16, and 20. The volume of fibers occupying the total volume of the composite, i.e., the fiber volume fraction, is fixed at 0.40 for all the considered cases. Since the thickness of the composite is held constant, the size of the fibers must decrease when the number of fibers, M, is increased. However, since the problem is linear, the above is **equivalent** to increasing the number of fibers in the thickness direction by adding more layers in this direction, and thus increasing the thickness of the plate. For this reason the various distributions in the thickness direction are given as a function of the normalized coordinate x_1/M.

The results generated for such a large number of configurations provide a comprehensive library that can be used in future work to verify the applicability of various schemes in analyzing the thermal response of composites with tailored or coarse microstructures. The results also provide a continuous spectrum whose limiting behavior can be used as a basis for verification of the developed scheme. A more quantitative verification of the developed model based on the finite-element analysis of a finite thickness composite plate with a finite number of through-the-thickness fibers will be provide elsewhere. Further, these results demonstrate the power of the developed analytical model, in that a researcher can efficiently generate results by merely changing a few lines in the input data file of a computer code each time a new configuration is investigated.

First, temperature distributions are presented for six of the eight investigated configurations, namely $M = 1, 3, 5, 8, 16$, and 20. Figure 5 illustrates the temperature distributions in the representative cross-section (RCS) along the x_1 direction that includes both matrix and fiber phases (see Figure 2), whereas in Figure 6 the temperature distributions for a RCS containing matrix phase material are shown. Included in the figures are the linear distributions (denoted by dashed lines) obtained from the homogenized thermal boundary-value problem based on the lamination theory (i.e., continuum) equations. In the RCS containing both phases, the temperature profiles exhibit "staircase" patterns, charactarized by jumps or discontinuities between the fiber and matrix phases indicated by connected vertical lines. The temperature gradient in the fiber phase is much smaller than the gradient in the matrix phase since the thermal conductivity of the SiC fiber is much higher (fifty times) than that of the Ti-Al matrix (see Table 1). The staircase patterns intersect the linear distributions at $M + 1$ locations, as the step size decreases with increasing number of fibers (M) in the thickness direction. Alternatively, the temperature profiles in the RCS containing only matrix do not exhibit such a staircase pattern. These profiles exhibit smoother deviations from the linear distributions. It is clear that the temperature profiles generated using the standard homogenization approach, although conservative, exhibit substantial deviations from those of the present theory for $M \leq 8$ for the RCS containing both phases, with smaller differences observed in the RCS containing matrix only.

Figures 7 and 8 illustrate the corresponding normal stress profiles, σ_{22} and σ_{33}, in the RCS containing both fiber and matrix phases, whereas Figures 9 and 10 present the stress profiles in the matrix only RCS. As in the preceding cases, the linear normal stress distributions in the two directions generated with the standard homogenization approach (denoted by dashed lines) are included for comparison. Also presented are the results obtained using the primitive micromechanics approach discussed earlier. We first compare the predictions of the present theory with those of the standard homogenization approach and then with those of the primitive micromechanics approach.

The stress profiles generated with the present model are radically different from the profiles obtained with the standard homogenization approach for small values of M for both RCS's. In the case of the RCS containing both phases (see Figures 7 and 8), the stress profiles exhibit characteristic patterns, with substantially smaller gradients in the fiber phase than in the matrix phase, as suggested by the corresponding temperature profiles in Figure 5. When M is small, the stress profiles predicted by the present model are lower, i.e., conservative, than those obtained using the standard homogenization approach. As M increases, the normal stress distributions begin to oscillate around the linear or "mean" distribution predicted by the standard homogenization analysis. A clear pattern of oscillations emerges when M is about 5. As M increases beyond

5, the oscillations take on a characteristic pattern, forming a "fan" whose envelope grows with increasing distance from the top surface along the x_1 axis, with the actual gradients in the fiber and matrix phases being preserved. The stress magnitudes in the fiber phase are now greater that the mean distribution, and thus non-conservative, whereas in the matrix phase they are lower and consequently conservative. These oscillations are a direct result of the mismatch in the Young's moduli of the fiber and matrix phases. It is interesting to note that the envelope of the normal stress σ_{22} grows at a significantly smaller rate with x_1 than the envelope of the normal stress σ_{33}. This is clearly rooted in the microstructure of the composite which has preferred orientation along the x_3 axis. In other words, the normal stress carried by the individual fibers in the x_3 direction, that is required to maintain the composite flat in the presence of the thermal gradient, is significantly greater than the stress carried by the fibers in the x_2 direction. This is due to the fibers being continuous along the x_3 coordinate and discontinuous along the x_2 coordinate. In contrast, the differences in the normal stress distributions in the x_2 and x_3 directions predicted by the continuum calculations are significantly smaller than the differences predicted by the present model. Clearly, the continuum approach is insensitive to the actual microstructure of the material in the presence of large fiber diameter, finite boundaries, and thermal gradient.

In the case of the matrix only RCS (see Figures 9 and 10), a clear pattern for both normal stress distributions also emerges when M is about 5. In this case however, the situation is reversed, with the normal stress σ_{22} exhibiting greater oscillations than σ_{33}. Further, while the average behavior of the normal stress σ_{22} tends to the distribution predicted by the continuum approach, the average behavior of σ_{33} is below that of the linear distribution obtained from the continuum theory. The oscillations observed in the σ_{22} stress profiles are nonconservative in the matrix subcell adjacent to a fiber subcell in the $x_2 - x_3$ plane, and conservative in the matrix subcell adjacent to another matrix subcell in the same plane, as required by the continuity of tractions between adjacent cells. In contrast, the oscillations observed in the σ_{33} stress profiles are conservative everywhere.

The results generated using the primitive micromechanics approach included in Figures 7 through 10 for M = 1, 3, 5 and 8 exhibit "square" stair-case patterns, characterized by piece-wise uniform (no gradients) stresses in the fiber and matrix phases. The piece-wise uniform stress field is a direct consequence of applying an average temperature obtained from the continuum analysis over the unit cell, and subsequently treating it as an RVE in generating the microscopic stresses. For the considered cases, this approach is seen to always overestimate the stresses in the fiber phase, with the deviations from the present **FG** theory decreasing with increasing M. When M = 16 (not shown), the differences are quite small. In contrast, the matrix stresses are underestimated in some regions, and consequently non-conservative, while in others they are

overestimated. This is due to the stress gradients observed in the matrix phase that are predicted by the present theory, which cannot be reproduced locally with the primitive micromechanics approach. These differences depend on the considered stress component and the characteristic cross-section. As in the preceding case, the differences between the two micromechanical approaches in the matrix phase diminish with increasing M. For small values of M, these differences are significant and may be important in matrix-dominated failure modes. It is reassuring that the actual character, or pattern, of the stress field is captured by the primitive micromechanics approach for M as low as 3.

Finally, Figures 11 and 12 illustrate the normalized inplane force and moment resultants in the x_2 and x_3 directions, respectively, as a function of the number of fibers, M, in the thickness direction, that result from the normal stress distributions presented in Figures 7 - 10. Normalization is carried out with respect to the corresponding continuum model predictions. The inplane force resultants N_2 and N_3 shown in Figure 11 exhibit virtually identical behavior as a function of M, and asymptotically approach the predictions of the continuum model from below for increasing values of M. The continuum results thus provide a **conservative estimate** of the actual inplane resultant forces that are required to maintain the various composite configurations in place, for the applied loading and boundary conditions. A major conclusion obtained from these figures is that the continuum approach significantly overpredicts the magnitudes of the inplane force resultants for M less than about 10. Consequently, any design based on these quantities should be safe, albeit inefficient. In contrast to the identical asymptotic behavior exhibited by the inplane force resultants, the inplane moment resultants M_2 and M_3 presented in Figures 12 approach the continuum predictions at different rates for increasing M, with M_2 approaching the continuum results faster than M_3. In both cases, the asymptotic behavior is faster than for the inplane force resultants. A major conclusion once again is that the continuum model overpredicts the magnitudes of the moment resultants for M less than about 8. However, as in the preceding case, the predictions are conservative.

4.2.2 Effect of the Thermal Conductivity Mismatch

In this section, we investigate the effect of varying the thermal conductivity of the SiC fiber on the thermal and stress fields, as well as the force and moment resultants. Figure 13 illustrates the temperature and normal stress distributions in a unidirectional composite with three through-the-thickness SiC fibers having different thermal conductivities that yield κ_f / κ_m ratios of 25, 5 and 2.2. The profiles are given in the RCS containing both phases. As observed in the temperature distributions presented in Figure 13a, the effect of decreasing the fiber thermal conductivity is to increase the temperature gradient in the fiber which, in turn, results in a smaller

temperature gradient in the matrix. The higher temperature gradients in the fiber due to the lower thermal conductivities, generate higher normal stress gradients in the fiber and correspondingly lower stress gradients in the matrix. In summary, lowering the mismatch in the thermal conductivities of the fiber and matrix phases tends to smooth out the staircase pattern observed in the temperature distributions, and decreases the differences in the gradients of the normal stress distributions. One important difference should be noted in the two types of distributions. While the temperature distribution will tend to a linear distribution with decreasing mismatch in the fiber and matrix thermal conductivities, the corresponding normal stress distributions, because they are also governed by the mismatch in the mechanical properties, will retain not only distinct gradients in the fiber and matrix regions, but also the characteristic jumps or discontinuities across the interfaces.

Temperature and normal stress profiles were also generated for a unidirectional composite with twenty through-the-thickness fibers for the three fiber conductivities. In this case, the fine microstructure produced temperature distributions whose macroscopic behavior was essentially identical, with the differences due to the differences in the thermal conductivities only changing the local gradients rather than the global character. The global behavior for these cases was the same as that observed in Figures 5f, 7f and 8f generated for κ_f / κ_m ratio of fifty.

The inplane force and moment resultants for the considered composite configurations with three and twenty fibers in the thickness direction are presented in Table 3 for the three ratios of thermal conductivities. The inplane force and moment resultants for κ_f / κ_m ratio of fifty employed in generating Figures 5 through 12 are included for comparison. The resultants have been normalized with respect to the corresponding inplane force and moment resultants generated with the continuum approach. In this case, the effective or macroscopic thermal conductivity of the composite decreases from 16.2 to 10.7 (W / m-°C) as the thermal conductivity ratio κ_f / κ_m decreases from 50 to 2.2. However, since only unidirectionally-reinforced composite materials are considered, the inplane force and moment resultants remain the same, as dictated by the solution of the Laplace's equation for the temperature distribution in a homogeneous strip subjected to the given steady-state temperatures on the top and bottom surfaces. The inplane force resultants N_2 and N_3 generated by the imposed temperature gradient were 0.87×10^5 N/m and 0.95×10^5 N/m, respectively, while the inplane moment resultants M_2 and M_3 were 2.88 N and 3.16 N. As observed in the table, and intuitively expected, the effect of decreasing the thermal conductivity mismatch is to decrease the discrepancy between the inplane force resultants predicted by the **FG** theory and the continuum approach for both configurations. When the κ_f / κ_m ratio decreases from 50 to 2.2, the difference between the **FG** and continuum predictions decreases from approximately 20% to 8% for the three-ply (M=3) configuration, whereas for the

twenty-ply (M=20) configuration the corresponding percentage differences are on the order of 3% and 1%. An opposite trend is observed for the inplane moment resultants where decreasing the thermal conductivity mismatch produces a greater discrepancy between the two approaches. The increase in the discrepancy with decreasing κ_m / κ_f ratio is relatively small for both configurations, namely 2% and less than 1% for the three-ply and twenty-ply configurations, respectively. For both sets of inplane resultants, very little difference is seen in the results for the κ_f / κ_m ratios of 50 and 25, indicating existence of a saturation limit beyond a certain κ_f / κ_m ratio.

4.2.3 Bi-directional Composites

Consider next the response of a continuously-reinforced bi-directional composite with fibers oriented in both the x_3 and x_2 directions. The composite is constructed by starting with a ply having fibers oriented in the x_3 direction, followed by a ply with fibers along the x_2 direction, which in the terminology of the lamination theory is called an alternating 90°/0° laminate. This sequence is repeated as many times as desired. The thickness of each ply in this case is 199 μm with the fiber volume fraction of 0.40 as before. Since now the ply thickness is kept constant but the number of alternating 90° and 0° plies is allowed to increase, the total composite thickness increases. However, since the problem is linear, this arrangement is equivalent to keeping the ply thickness constant but decreasing the fiber diameter while maintaining a constant fiber volume fraction. Therefore, although the various distributions in the thickness direction are now given as a function of the coordinate x_1, they can be directly compared with those of the unidirectional configurations. As before, the objective is to determine the number of fibers in the thickness direction that are required for the results to approach those obtained using the standard homogenization procedure. In view of the extensive results and the well-established trends for the unidirectional configurations presented in the foregoing, we limit the discussion to bi-directional configurations containing 8 and 20 rows of fibers.

As before, the temperature distributions for the two configurations are illustrated first in Figure 14. These distributions are in the RCS containing both fiber and matrix phases. Clearly, the distributions exhibit the same characteristic staircase pattern seen previously in the unidirectional configurations, with the step size decreasing with increasing M. As expected, the temperature distributions predicted by the continuum approach are the same as those for the unidirectional cases because the transverse conductivity in the x_1 direction is the same for both the 0° and 90° configurations. The temperature distributions obtained using the present approach are also the same as those obtained for the unidirectional configurations. This is a somewhat unexpected result in view of the different conductivities of the fiber and matrix phases, and the

different microstructural details in the x_1 direction observed in the unidirectional and bi-directional configurations. It is not clear at this time why the present model predicts identical temperature distributions for the two different microstructural configurations.

The normal stress distributions σ_{22} and σ_{33}, in the RCS containing both phases, are presented in Figures 15 and 16, respectively. Due to the presence of alternating 0° and 90° layers, the envelopes of these distributions grow with increasing distance along the x_1 direction at approximately the same rate. This is in contrast with the normal distributions observed in the unidirectional configurations where the σ_{33} stress component grew faster than the σ_{22} stress component. We note that although the normal stresses in the fiber phase increased monotonically along the x_1 axis in the unidirectional configurations, this is not the case for the bi-directional configurations. In fact, here the normal stresses increase at two different rates depending on whether the fiber associated with the 90° or 0° layer is considered. Consequently, the pattern that is observed for the RCS in the bi-directional configurations is bi-modal, thereby giving the appearance of nonuniformity for $M = 8$. Alternatively, when $M = 20$, the full pattern emerges from which the growth of the two normal stresses (σ_{22} and σ_{33}) at two different rates can be easily discerned. The distribution of the normal stresses predicted by the present model follows the results of the continuum model in an average sense. Comparison with the predictions obtained using the primitive micromechanics approach will be presented elsewhere.

Figures 17 and 18 show the inplane force and moment resultants obtained from the normal stress distributions presented in Figures 15 and 16. As in the case of unidirectional configurations, these quantities have been normalized with respect to the continuum predictions and plotted as a function of the number of layers, M, in the thickness direction. The trends observed for the behavior of the inplane force and moment resultants for the bi-directional configurations generally follow the same pattern as in the preceding cases. However, a characteristic difference in the behavior of the inplane moment resultants is observed. Whereas for the unidirectional configurations, the inplane moment resultants approached the lamination theory predictions in a uniformly asymptotic manner, the asymptotic behavior for the bi-directional configurations is not uniform. This is particularly true for small values of M where the initially rapid increase of M_2 and M_3 is followed by a pattern of alternating slow and rapid growth rates, resembling a staircase pattern.

4.3 Response of Composites with Tailored Mesostructure

In the final set of examples, we investigate the response of unidirectional composites with nonuniformly spaced fibers to thermal gradients. Three fiber spacing variations in the **FG** direction are considered, namely linear, quadratic and cubic. The total thickness of the composite is

kept fixed and the total fiber volume fraction of the composite is 0.40 as in the preceding unidirectional composites with uniformly spaced fibers. The $p-th$ cell dimension, D_p, in the **FG** direction which determines the fiber spacing for the three variations was obtained from the following formulas:

linear fiber spacing

$$D_p = A(p-1) + B \tag{68}$$

quadratic fiber spacing

$$D_p = A(p-1)^2 + B \tag{69}$$

cubic fiber spacing

$$D_p = A(p-1)^3 + B \tag{70}$$

where $p = 1, 2, ..., M$, B is a pre-assigned constant, and A governs the rate of increase of the cell **FG** dimension. Let M be the number of fibers in the **FG** composite as before. The total thickness of the composite, $H = \sum_{p=1}^{M} D_p$, is then calculated from the following formulas:

linear fiber spacing

$$H = A\frac{(M^2 - M)}{2} + MB \tag{71}$$

quadratic fiber spacing

$$H = A[\frac{M}{6}(M+1)(2M+1) - M^2] + MB \tag{72}$$

cubic fiber spacing

$$H = A[\frac{(1+M)^2 M^2}{4} - M^3] + MB \tag{73}$$

The following results have been generated for the case when $M = 10$, $B = 199\ \mu m$ and $H = 20B$. Given these values, one can determine A directly, and since the total fiber volume fraction in the **FG** composite is given by:

$$v_f = \frac{M d_1^{(p)2}}{H(h_1 + h_2)} \tag{74}$$

the parameters $d_1^{(p)} = h_1$ and $d_2^{(p)} = h_2 = D_1 - d_1^{(p)}$ are determined for all values of p.

The temperature distributions for the three nonuniform configurations, as well as the uniformly spaced reference configuration, are illustrated in Figure 19. Clearly, in all nonuniformly spaced cases the temperature profiles are below that generated with uniformly spaced fibers. The linear fiber spacing variation produced the smallest deviation from the temperature profile obtained with uniformly spaced fibers, followed by the quadratic and then cubic fiber spacing variations. The above results are consistent with the observation that decreasing the fiber spacing close to the top surface increases the effective or "average" thermal conductivity in that region, thus lowering the temperature profile.

The associated normal stress distributions σ_{22} and σ_{33} produced by the resulting temperature distributions are given in Figures 20 and 21. These stress distributions are explicitly compared with the distribution obtained for the configuration with uniformly spaced fibers. As expected, those configurations that have been tailored to give lower temperature distributions necessarily produce lower stress distributions when compared to the stress distribution in the presence of uniform fiber spacing. Consequently, the greatest reduction in the normal stress distributions occurs for the cubic fiber spacing variation, followed by the quadratic and linear variations.

The resulting inplane force and moment resultants for the three fiber spacing configurations are illustrated in Figure 22 in bar chart form. The actual magnitudes have been normalized by the corresponding quantities obtained for the uniformly spaced fiber configuration. The results, as expected given Figures 20 and 21, indicate that the greatest reductions in the presence of nonuniformly spaced fiber configurations occur for the cubic variation, followed by the quadratic and linear. Of the two sets of resultants, the inplane force resultants exhibit the greatest relative reductions.

The last example discussed herein addresses the effect of reversing the temperature gradient on the temperature and stress distributions in the presence of nonuniformly spaced fibers. Again, the three configurations, i.e., linear, quadratic and cubic fiber spacings, discussed

previously are considered, however now the top surface ($x_1 = 0$) is exposed to the elevated temperature of 500°C and the bottom surface ($x_1 = H$) is maintained at 0°C. In practical terms for instance, this situation may arise in aircraft applications involving frictional heating of the wing skin during flight which, in turn, requires active internal cooling, causing the given temperature gradient. In light of the preceding results, only the results for the cubic fiber spacing case are presented.

The temperature distribution for the cubic fiber spacing variation and reference uniform spacing is presented in Figure 23a. In contrast with the preceding case, the temperature distribution is now higher than the distribution generated with uniformly spaced fibers, as one would expect since the ceramic rich zone corresponds to the elevated temperature zone. In fact, the temperature distribution with the reversed thermal gradient is the mirror image of the distribution with the original thermal gradient. The results presented in Figure 23a suggest that the magnitudes of the normal stress distributions σ_{22} and σ_{33} will now be greater than the corresponding magnitudes obtained for uniformly spaced fibers. This is indeed the case as seen in Figures 23b and 23c. Clearly, these normal stress distributions will generate inplane stress and moment resultants that will be higher than the resultants obtained from the uniformly spaced fiber configuration. Therefore, in order to reduce these quantities with respect to the reference quantities in the presence of uniform fiber spacing, the reversal of the thermal gradient should be accompanied by the reversal of the fiber spacing gradient.

5.0 CONCLUSIONS

A new approach has been presented for analyzing the response of thin-walled, metal matrix composites subjected to a thermal gradient, with a finite number of large-diameter fibers uniformly or nonuniformly spaced in the thickness direction. In this approach, the microstructural and macrostructural details are **explicitly coupled** when solving the thermomechanical boundary-value problem. This is in stark contrast to the standard micromechanical schemes, based on the classical homogenization procedures, which treat the local (micromechanics) and global (macromechanics) problems separately. Coupling of the local and global analyses allows one to rationally analyze the response of metal matrix composites such as SiC/TiAl that contain relatively few through-the-thickness fibers, as well as so-called functionally gradient composites with continuously changing properties due to nonuniform fiber spacing or the presence of several phases. In such composites, it is difficult, if not impossible, to define the representative volume element (RVE) used in the traditional micromechanical analyses.

The numerical examples presented herein indicate that the standard homogenization procedure based on the premise of an RVE yields inaccurate results for thin-walled composites with

a small number of large-diameter fibers in the thickness direction. In particular, the inplane force and moment resultants obtained using the standard homogenization approach, that are necessary to maintain the composite flat in the presence of a through-the-thickness thermal gradient, are significantly overpredicted (i.e., conservative) for fewer than about 10 fibers when the mismatch in the thermal conductivities of the fiber and matrix phases is large. For a larger number of through-the-thickness fibers, the results of the present theory asymptotically approach the results of the standard homogenization scheme. The local stresses, on the other hand, only converge to the classical homogenized stresses **in an average sense** with increasing number of through-the-thickness fibers, and can exhibit large non-conservative local fluctuations depending on the microstructural details of the composite and the mismatch in the thermal and mechanical properties. An estimate of the local stresses can be obtained from the continuum approach by applying an average temperature over a given volume containing both the fiber and matrix phases, and solving the associated micromechanics problem, treating the given volume as an RVE. Such an approach, herein called "primitive" micromechanics approach, must be employed with caution since it may underestimate the local stresses in the presence of stress gradients at the micromechanical level. The accuracy of this approach increases with increasing number of through-the-thickness fibers, and may be acceptable when the number of fibers is greater than 10. For small number of through-the-thickness fibers, on the other hand, the present theory is more suitable. These observations suggest that the use of the effective modulus concept must be approached with caution when analyzing the thermal response of composites with relatively few, large-diameter fibers in the thickness direction in the presence of thermal gradients.

The results obtained for composites with tailored mesostructures, i.e. nonuniformly spaced fibers in the through-the-thickness direction, and large mismatch in both thermal and mechanical properties, indicate that it is possible to reduce the temperature distribution, and thus obtain more favorable stress distributions, by appropriately grading the microstructure of the composite. This, in turn, reduces the inplane force and moment resultants, necessary to maintain the composite flat in the presence of a thermal gradient, with respect to the corresponding quantities that arise in composites with uniformly spaced fibers. The manner in which the microstructure of the composite is graded must take into account the sign of the thermal gradient. Consequently, tailoring of microstructure appears to be useful in those applications where the sign of the thermal gradient is preserved.

The results presented point to the potential usefulness of the developed theoretical framework for analyzing the response of advanced composites with tailored microstructures to thermal gradients in the presence of elastic phases with temperature-independent properties. In the future, the approach will be extended to include inelastic effects as well as temperature-

dependent response of the constituent phases exhibited by advanced metal matrix composites at elevated temperatures. Finally, the full potential of the presented method as a design tool for functionally graded or tailored composites can only be realized, however, when it is combined with an appropriate optimization approach (cf. Saravanos and Chamis, 1992; Saravanos and Pereira, 1992). This too will be addressed in future work.

6.0 ACKNOWLEDGEMENTS

The first two authors gratefully acknowledge the support provided by the NASA-Lewis Research Center through the grant **NASA NAG 3-1377**. The authors are grateful to Drs. Dimitris Saravanos, Thomas Wilt and Don Petrasek for their comments during the preparation of this report. They would also like to express their appreciation to Professor Carl T. Herakovich for fruitful discussions during the inital stages of this investigation.

7.0 REFERENCES

Aboudi, J. (1991), *Mechanics of Composite Materials - A Unified Micromechanical Approach*, Elsevier, New York.

Aboudi, J. and Pindera, M-J. (1992), "Micromechanics of Metal Matrix Composites Using the Generalized Method of Cells Model: User's Guide," *NASA CR 190756*, NASA-Lewis Research Center, Cleveland, OH.

Christensen, R. M. (1979), *Mechanics of Composite Materials*, John Wiley & Sons, Inc., New York

Hill, R. (1963), "Elastic Properties of Reinforced Solids: Some Theoretical Principles," *J. Mech. Phys. Solids*, **11**, 357.

Malvern, L. E. (1969), *Introduction to the Mechanics of a Continuous Medium*, Prentice-Hall, Inc., Englewood Cliffs, New Jersey.

Pagano, N. J. (1974), "The Role of Effective Moduli in the Elastic Analysis of Composite Laminates," in *Composite Materials. Volume II: Mechanics of Composite Materials*, G. P. Sendeckyj, Ed., pp. 1 - 22, Academic Press, New York.

Paley, M. and Aboudi, J. (1992), "Micromechanical Analysis of Composites by the Generalized Cells Model," *Mechanics of Materials*, **14**, 127.

Saravanos, D. A. and Chamis, C. C. (1992), "Multiobjective Shape and Material Optimization of Composite Structures Including Damping", *AIAA Journal*, **30**, (3), 805.

Saravanos, D. A. and Pereira, J. M. (1992), "Effects of Interply Damping Layers on the Dynamic Characteristics of Composite Plates", *AIAA Journal*, **30**, (12), 2906.

Yamanouchi, M., Koizumi, M., Hirai, T., and Shiota, I. (1990), *Proceedings of the First International Symposium on Functionally Gradient Materials*, Sendai, Japan.

8.0 APPENDIX

8.1 Thermal Analysis

8.1.1 Heat Conduction Equations

Let us multiply equation (6) by $(\bar{x}_1^{(\alpha)})^l\ (\bar{x}_2^{(\beta)})^m(\bar{x}_3^{(\gamma)})^n$, where l, m, $n = 0$, 1, or 2 with $l+m+n \le 2$. Integrating the resulting equation by parts and using the temperature expansion given in equation (14), the following set of equations is obtained:

$$L^{(\alpha\beta\gamma)}_{1(0,0,0)} + L^{(\alpha\beta\gamma)}_{2(0,0,0)} + L^{(\alpha\beta\gamma)}_{3(0,0,0)} = 0 \tag{A1}$$

$$L^{(\alpha\beta\gamma)}_{1(1,0,0)} - Q^{(\alpha\beta\gamma)}_{1(0,0,0)} = 0 \tag{A2}$$

$$\frac{1}{4}d_\alpha^{(p)2}\ [\,L^{(\alpha\beta\gamma)}_{1(0,0,0)} + \frac{1}{3}L^{(\alpha\beta\gamma)}_{2(0,0,0)} + \frac{1}{3}L^{(\alpha\beta\gamma)}_{3(0,0,0)}\,] - 2Q^{(\alpha\beta\gamma)}_{1(1,0,0)} = 0 \tag{A3}$$

$$\frac{1}{12}h_\beta^2\ [\,L^{(\alpha\beta\gamma)}_{1(0,0,0)} + 3L^{(\alpha\beta\gamma)}_{2(0,0,0)} + L^{(\alpha\beta\gamma)}_{3(0,0,0)}\,] - 2Q^{(\alpha\beta\gamma)}_{2(0,1,0)} = 0 \tag{A4}$$

$$\frac{1}{12}l_\gamma^2\ [\,L^{(\alpha\beta\gamma)}_{1(0,0,0)} + L^{(\alpha\beta\gamma)}_{2(0,0,0)} + 3L^{(\alpha\beta\gamma)}_{3(0,0,0)}\,] - 2Q^{(\alpha\beta\gamma)}_{3(0,0,1)} = 0 \tag{A5}$$

where in the above equations $Q^{(\alpha\beta\gamma)}_{i\,(l,m,n)}$ has been defined previously (see equation (15)), and is reproduced below for convenience,

$$Q^{(\alpha\beta\gamma)}_{i\,(l,m,n)} = \frac{1}{v^{(p)}_{(\alpha\beta\gamma)}} \int_{-d_\alpha^{(p)}/2}^{d_\alpha^{(p)}/2} \int_{-h_\beta/2}^{h_\beta/2} \int_{-l_\gamma/2}^{l_\gamma/2} (\bar{x}_1^{(\alpha)})^l (\bar{x}_2^{(\beta)})^m (\bar{x}_3^{(\gamma)})^n q_i^{(\alpha\beta\gamma)} d\bar{x}_1^{(\alpha)} d\bar{x}_2^{(\beta)} d\bar{x}_3^{(\gamma)}$$

with $v^{(p)}_{(\alpha\beta\gamma)} = d_\alpha^{(p)} h_\beta\, l_\gamma$ representing the volume of the subcell $(\alpha\beta\gamma)$ in the $p-th$ cell, and

$$L^{(\alpha\beta\gamma)}_{1(n,0,0)} = \frac{1}{v^{(p)}_{(\alpha\beta\gamma)}} \left(\frac{d_\alpha^{(p)}}{2}\right)^n \int_{-h_\beta/2}^{h_\beta/2} \int_{-l_\gamma/2}^{l_\gamma/2} [q_1^{(\alpha\beta\gamma)}\left(\frac{d_\alpha^{(p)}}{2}\right) + (-1)^{n+1} q_1^{(\alpha\beta\gamma)}\left(-\frac{d_\alpha^{(p)}}{2}\right)] d\bar{x}_2^{(\beta)} d\bar{x}_3^{(\gamma)} \tag{A6}$$

$$L^{(\alpha\beta\gamma)}_{2(0,n,0)} = \frac{1}{v^{(p)}_{(\alpha\beta\gamma)}} \left(\frac{h_\beta}{2}\right)^n \int_{-d_\alpha^{(p)}/2}^{d_\alpha^{(p)}/2} \int_{-l_\gamma/2}^{l_\gamma/2} [q_2^{(\alpha\beta\gamma)}\left(\frac{h_\beta}{2}\right) + (-1)^{n+1} q_2^{(\alpha\beta\gamma)}\left(-\frac{h_\beta}{2}\right)] d\bar{x}_1^{(\alpha)} d\bar{x}_3^{(\gamma)} \tag{A7}$$

$$L^{(\alpha\beta\gamma)}_{3(0,0,n)} = \frac{1}{v^{(p)}_{(\alpha\beta\gamma)}}\left(\frac{l_\gamma}{2}\right)^n \int_{-d^{(p)}_\alpha/2}^{d^{(p)}_\alpha/2} \int_{-h_\beta/2}^{h_\beta/2} [q_3^{(\alpha\beta\gamma)}(\tfrac{l_\gamma}{2}) + (-1)^{n+1} q_3^{(\alpha\beta\gamma)}(-\tfrac{l_\gamma}{2})] d\bar{x}_1^{(\alpha)} d\bar{x}_2^{(\beta)} \qquad \text{(A8)}$$

where $n = 0$ or 1, and $q_1^{(\alpha\beta\gamma)}(\pm\frac{d^{(p)}_\alpha}{2})$, $q_2^{(\alpha\beta\gamma)}(\pm\frac{h_\beta}{2})$, $q_3^{(\alpha\beta\gamma)}(\pm\frac{l_\gamma}{2})$ denote the interfacial fluxes at $\bar{x}_1^{(\alpha)} = \pm\frac{1}{2}d^{(p)}_\alpha$, $\bar{x}_2^{(\beta)} = \pm\frac{1}{2}h_\beta$, $\bar{x}_3^{(\gamma)} = \pm\frac{1}{2}l_\gamma$, respectively.

Equations (A1) through (A5) provide relations between the zeroth-order and first order heat fluxes $Q^{(\alpha\beta\gamma)}_{i(l,m,n)}$ and the interfacial fluxes $L^{(\alpha\beta\gamma)}_{i(l,m,n)}$. Explicit expressions for the interfacial fluxes $L^{(\alpha\beta\gamma)}_{i(l,m,n)}$ given solely in terms of $Q^{(\alpha\beta\gamma)}_{i(l,m,n)}$ are obtained through the following sequence of manipulations, noting that equation (A2) already provides a direct relation between $Q^{(\alpha\beta\gamma)}_{1(0,0,0)}$ and $L^{(\alpha\beta\gamma)}_{1(0,0,0)}$. First, substituting equation (A1) into equations (A4) and (A5), respectively, gives the following direct expressions for $L^{(\alpha\beta\gamma)}_{2(0,0,0)}$ and $L^{(\alpha\beta\gamma)}_{3(0,0,0)}$.

$$\frac{1}{6}h_\beta^2 L^{(\alpha\beta\gamma)}_{2(0,0,0)} = 2Q^{(\alpha\beta\gamma)}_{2(0,1,0)} \qquad \text{(A9)}$$

$$\frac{1}{6}l_\gamma^2 L^{(\alpha\beta\gamma)}_{3(0,0,0)} = 2Q^{(\alpha\beta\gamma)}_{3(0,0,1)} \qquad \text{(A10)}$$

Then upon substitution of equations (A9) and (A10) into equation (A1) we obtain the following expression for $L^{(\alpha\beta\gamma)}_{1(0,0,0)}$.

$$L^{(\alpha\beta\gamma)}_{1(0,0,0)} = -12(Q^{(\alpha\beta\gamma)}_{2(0,1,0)}/h_\beta^2 + Q^{(\alpha\beta\gamma)}_{3(0,0,1)}/l_\gamma^2) \qquad \text{(A11)}$$

Equations (A9) through (A11) will be used to reduce the heat conduction and heat flux continuity equations to expressions involving only the heat flux quantities $Q^{(\alpha\beta\gamma)}_{i(l,m,n)}$. These can subsequently be expressed in terms of the fundamental unknown coefficients $T_i^{(\alpha\beta\gamma)}$, appearing in the temperature expansion given by equations (14), using equations (16) through (19).

8.1.2 Heat Flux Continuity Equations

The heat flux continuity conditions (8) - (9) are imposed on an average basis at each subcell and cell interface. Prior to imposing these continuity conditions, let us define intermediate quantities $f_i^{(1\beta\gamma)}$ and $g_i^{(1\beta\gamma)}$ as follows:

$$f_i^{(1\beta\gamma)} = q_i^{(1\beta\gamma)} \Big|_{\bar{x}_1^{(1)} = d_1^{(p)}/2} - q_i^{(1\beta\gamma)} \Big|_{\bar{x}_1^{(1)} = -d_1^{(p)}/2} \tag{A12}$$

$$g_i^{(1\beta\gamma)} = q_i^{(1\beta\gamma)} \Big|_{\bar{x}_1^{(1)} = d_1^{(p)}/2} + q_i^{(1\beta\gamma)} \Big|_{\bar{x}_1^{(1)} = -d_1^{(p)}/2} \tag{A13}$$

These quantities will simplify the algebra associated with application of the heat flux continuity requirement on an average basis in the **FG** direction. Then substituting equations (8a) and (9a) into the above definitions we have,

$$f_1^{(1\beta\gamma)} \Big|^{(p)} = q_1^{(2\beta\gamma)} \Big|^{(p)}_{\bar{x}_1^{(2)} = -d_2^{(p)}/2} - q_1^{(2\beta\gamma)} \Big|^{(p-1)}_{\bar{x}_1^{(2)} = d_2^{(p-1)}/2} \tag{A14}$$

$$g_1^{(1\beta\gamma)} \Big|^{(p)} = q_1^{(2\beta\gamma)} \Big|^{(p)}_{\bar{x}_1^{(2)} = -d_2^{(p)}/2} + q_1^{(2\beta\gamma)} \Big|^{(p-1)}_{\bar{x}_1^{(2)} = d_2^{(p-1)}/2} \tag{A15}$$

Adding and subtracting equal quantities to and from equations (A14) and (A15) it can easily be verified that

$$2f_1^{(1\beta\gamma)} \Big|^{(p)} = [-f_1^{(2\beta\gamma)} + g_1^{(2\beta\gamma)}]^{(p)} - [f_1^{(2\beta\gamma)} + g_1^{(2\beta\gamma)}]^{(p-1)} \tag{A16}$$

$$2g_1^{(1\beta\gamma)} \Big|^{(p)} = [-f_1^{(2\beta\gamma)} + g_1^{(2\beta\gamma)}]^{(p)} + [f_1^{(2\beta\gamma)} + g_1^{(2\beta\gamma)}]^{(p-1)} \tag{A17}$$

Then using equations (A16) and (A17) in equation (A6), we obtain the following heat flux continuity conditions for the **FG** direction:

$$d_1^{(p)} L_{1(0,0,0)}^{(1\beta\gamma)} \Big|^{(p)} = [L_{1(1,0,0)}^{(2\beta\gamma)} - \frac{1}{2} d_2^{(p)} L_{1(0,0,0)}^{(2\beta\gamma)}]^{(p)} - [L_{1(1,0,0)}^{(2\beta\gamma)} + \frac{1}{2} d_2^{(p-1)} L_{1(0,0,0)}^{(2\beta\gamma)}]^{(p-1)} \tag{A18}$$

$$L_{1(1,0,0)}^{(1\beta\gamma)} \Big|^{(p)} = \frac{1}{2}[L_{1(1,0,0)}^{(2\beta\gamma)} - \frac{1}{4} d_2^{(p)} L_{1(0,0,0)}^{(2\beta\gamma)}]^{(p)} + \frac{1}{2}[L_{1(1,0,0)}^{(2\beta\gamma)} + \frac{1}{4} d_2^{(p-1)} L_{1(0,0,0)}^{(2\beta\gamma)}]^{(p-1)} \tag{A19}$$

The heat flux continuity conditions in the remaining two directions are obtained using equations (8b) and (8c) in equations (A7) and (A8), repectively. From equations (8b) and (A7) we have

$$h_1 L^{(\alpha 1\gamma)}_{2(0,0,0)} \Big|^{(p)} = -h_2 L^{(\alpha 2\gamma)}_{2(0,0,0)} \Big|^{(p)} \tag{A20}$$

while from equations (8c) and (A8)

$$l_1 L^{(\alpha\beta 1)}_{3(0,0,0)} \Big|^{(p)} = -l_2 L^{(\alpha\beta 2)}_{3(0,0,0)} \Big|^{(p)} \tag{A21}$$

We note that equations (9b) and (9c) are identically satisfied for a material that is periodic in the x_2 and x_3 directions by the chosen temperature field representation.

Equations (A9) through (A11), together with equation (A2), will be employed in reducing the heat flux continuity conditions (A18) through (A21) to expressions involving only the volume-averaged zeroth-order and first-order heat flux quantities $Q^{(\alpha\beta\gamma)}_{i(l,m,n)}$.

8.1.3 Reduction of Heat Conduction and Heat Flux Continuity Equations

Substituting equation (A1) into (A3), and using equations (A9) and (A10), reduces the volume-averaged heat conduction equations to a set of 8 equations given by equation (20) on page 16.

$$[\, Q^{(\alpha\beta\gamma)}_{1(1,0,0)}/d_\alpha^{(p)2} + Q^{(\alpha\beta\gamma)}_{2(0,1,0)}/h_\beta^2 + Q^{(\alpha\beta\gamma)}_{3(0,0,1)}/l_\gamma^2 \,]^{(p)} = 0 \tag{20}$$

Using the expression for $L^{(\alpha\beta\gamma)}_{1(0,0,0)}$ given by equation (A11), and the expression for $L^{(\alpha\beta\gamma)}_{1(1,0,0)}$ given by equation (A2), in the continuity relations (A18) and (A19), we obtain equations (21) and (22) on page 16 and 17.

$$[\, 12Q^{(1\beta\gamma)}_{2(0,1,0)}/h_\beta^2 + 12Q^{(1\beta\gamma)}_{3(0,0,1)}/l_\gamma^2 \,]^{(p)} + 6\frac{d_2^{(p)}}{d_1^{(p)}}[\, Q^{(2\beta\gamma)}_{2(0,1,0)}/h_\beta^2 + Q^{(2\beta\gamma)}_{3(0,0,1)}/l_\gamma^2 \,]^{(p)} +$$

$$6\frac{d_2^{(p-1)}}{d_1^{(p)}}[\, Q^{(2\beta\gamma)}_{2(0,1,0)}/h_\beta^2 + Q^{(2\beta\gamma)}_{3(0,0,1)}/l_\gamma^2]^{(p-1)} + \frac{1}{d_1^{(p)}}\,[\, Q^{(2\beta\gamma)}_{1(0,0,0)} \Big|^{(p)} - Q^{(2\beta\gamma)}_{1(0,0,0)} \Big|^{(p-1)} \,] = 0 \tag{21}$$

and

$$Q^{(1\beta\gamma)}_{1(0,0,0)}\Big|^{(p)} = \frac{1}{2}Q^{(2\beta\gamma)}_{1(0,0,0)}\Big|^{(p)} + \frac{1}{2}Q^{(2\beta\gamma)}_{1(0,0,0)}\Big|^{(p-1)} + 3d_2^{(p)}[Q^{(2\beta\gamma)}_{2(0,1,0)}/h_\beta^2 + Q^{(2\beta\gamma)}_{3(0,0,1)}/l_\gamma^2]^{(p)} -$$

$$3d_2^{(p-1)}[\,Q^{(2\beta\gamma)}_{2(0,1,0)} + Q^{(2\beta\gamma)}_{3(0,0,1)}\,]^{(p-1)} \tag{22}$$

Finally, combining equations (A9) and (A20), as well as equations (A10) and (A21), gives equations (23) and (24) on page 17.

$$[\,Q^{(\alpha 1\gamma)}_{2(0,1,0)}/h_1 + Q^{(\alpha 2\gamma)}_{2(0,1,0)}/h_2\,]^{(p)} = 0 \tag{23}$$

$$[\,Q^{(\alpha\beta 1)}_{3(0,0,1)}/l_1 + Q^{(\alpha\beta 2)}_{3(0,0,1)}/l_2\,]^{(p)} = 0 \tag{24}$$

As indicated previously, equations (20) through (24) are easily expressed in terms of the fundamental unknown coefficients $T_i^{(\alpha\beta\gamma)}$ using equations (16) through (19).

8.1.4 Thermal Continuity Equations

As in the case of the heat flux field, the thermal continuity conditions (10) - (11) are imposed on an average basis at each subcell and cell interface. Thus substituting equation (14) into equations (10a) - (10c), respectively, we obtain at each subcell interface the following conditions:

$$[\,T_0^{(1\beta\gamma)} + d_1^{(p)}T_1^{(1\beta\gamma)} + \frac{1}{4}d_1^{(p)2}T_2^{(1\beta\gamma)}\,]^{(p)} = [\,T_0^{(2\beta\gamma)} - d_2^{(p)}T_1^{(2\beta\gamma)} + \frac{1}{4}d_2^{(p)2}T_2^{(2\beta\gamma)}\,]^{(p)} \tag{25}$$

$$[\,T_0^{(\alpha 1\gamma)} + \frac{1}{4}h_1^2T_3^{(\alpha 1\gamma)}\,]^{(p)} = [\,T_0^{(\alpha 2\gamma)} + \frac{1}{4}h_2^2T_3^{(\alpha 2\gamma)}\,]^{(p)} \tag{26}$$

$$[\,T_0^{(\alpha\beta 1)} + \frac{1}{4}l_1^2T_4^{(\alpha\beta 1)}\,]^{(p)} = [\,T_0^{(\alpha\beta 2)} + \frac{1}{4}l_2^2T_4^{(\alpha\beta 2)}\,]^{(p)} \tag{27}$$

Furthermore, substituting equation (14) into equation (11a) to ensure continuity of temperature between neighboring cells in the **FG** direction, we obtain the condition

$$[\,T_0^{(1\beta\gamma)} - \frac{1}{2}d_1^{(p+1)}T_1^{(1\beta\gamma)} + \frac{1}{4}d_1^{(p+1)2}T_2^{(1\beta\gamma)}\,]^{(p+1)} = [\,T_0^{(2\beta\gamma)} + \frac{1}{2}d_2^{(p)}T_1^{(2\beta\gamma)} + \frac{1}{4}d_2^{(p)2}T_2^{(2\beta\gamma)}\,]^{(p)} \tag{28}$$

The remaining two conditions (11b) and (11c) are identically satisfied for a functionally graded material in the x_1-direction that is periodic in the x_2 and x_3-directions.

8.2 Mechanical Analysis

8.2.1 Equations of Equilibrium

Let us multiply equation (30) by $(\bar{x}_1^{(\alpha)})^l\ (\bar{x}_2^{(\beta)})^m\ (\bar{x}_3^{(\gamma)})^n$, where again l, m, $n = 0$, 1, *or* 2 with $l+m+n \le 2$. Integrating the resulting equations by parts, and using the displacement expansions (39), we obtain the equations of equilibrium in the subcell region $(\alpha\beta\gamma)$ in the form:

$$I^{(\alpha\beta\gamma)}_{11(0,0,0)} + J^{(\alpha\beta\gamma)}_{21(0,0,0)} + K^{(\alpha\beta\gamma)}_{31(0,0,0)} = 0 \tag{A22}$$

$$I^{(\alpha\beta\gamma)}_{11(1,0,0)} - S^{(\alpha\beta\gamma)}_{11(0,0,0)} = 0 \tag{A23}$$

$$J^{(\alpha\beta\gamma)}_{22(0,1,0)} - S^{(\alpha\beta\gamma)}_{22(0,0,0)} = 0 \tag{A24}$$

$$K^{(\alpha\beta\gamma)}_{33(0,0,1)} - S^{(\alpha\beta\gamma)}_{33(0,0,0)} = 0 \tag{A25}$$

$$3I^{(\alpha\beta\gamma)}_{11(0,0,0)} + J^{(\alpha\beta\gamma)}_{21(0,0,0)} + K^{(\alpha\beta\gamma)}_{31(0,0,0)} - 24S^{(\alpha\beta\gamma)}_{11(1,0,0)}/d_\alpha^{(p)2} = 0 \tag{A26}$$

$$I^{(\alpha\beta\gamma)}_{11(0,0,0)} + 3J^{(\alpha\beta\gamma)}_{21(0,0,0)} + K^{(\alpha\beta\gamma)}_{31(0,0,0)} - 24S^{(\alpha\beta\gamma)}_{12(0,1,0)}/h_\beta^2 = 0 \tag{A27}$$

$$I^{(\alpha\beta\gamma)}_{11(0,0,0)} + J^{(\alpha\beta\gamma)}_{21(0,0,0)} + 3K^{(\alpha\beta\gamma)}_{31(0,0,0)} - 24S^{(\alpha\beta\gamma)}_{13(0,0,1)}/l_\gamma^2 = 0 \tag{A28}$$

where $S^{(\alpha\beta\gamma)}_{ij(l,m,n)}$ has been defined previously (see equation (40)), and is reproduced below for convenience,

$$S^{(\alpha\beta\gamma)}_{ij(l,m,n)} = \frac{1}{v^{(p)}_{(\alpha\beta\gamma)}} \int_{-d_\alpha^{(p)}/2}^{d_\alpha^{(p)}/2} \int_{-h_\beta/2}^{h_\beta/2} \int_{-l_\gamma/2}^{l_\gamma/2} (\bar{x}_1^{(\alpha)})^l\ (\bar{x}_2^{(\beta)})^m\ (\bar{x}_3^{(\gamma)})^n\ \sigma_{ij}^{(\alpha\beta\gamma)}\, d\bar{x}_1^{(\alpha)} d\bar{x}_2^{(\beta)} d\bar{x}_3^{(\gamma)}$$

for i, $j = 1$, 2, and 3, with $v^{(p)}_{(\alpha\beta\gamma)} = d_\alpha^{(p)} h_\beta l_\gamma$, and

$$I^{(\alpha\beta\gamma)}_{1j(n,0,0)} = \frac{1}{v^{(p)}_{(\alpha\beta\gamma)}} \left(\frac{1}{2} d_\alpha^{(p)}\right)^n \int_{-h_\beta/2}^{h_\beta/2} \int_{-l_\gamma/2}^{l_\gamma/2} \left[\sigma_{1j}^{(\alpha\beta\gamma)}\left(\frac{1}{2} d_\alpha^{(p)}\right) + (-1)^{n+1} \sigma_{1j}^{(\alpha\beta\gamma)}\left(-\frac{1}{2} d_\alpha^{(p)}\right)\right] d\bar{x}_2^{(\beta)} d\bar{x}_3^{(\gamma)} \tag{A29}$$

$$J^{(\alpha\beta\gamma)}_{2j(0,n,0)} = \frac{1}{v^{(p)}_{(\alpha\beta\gamma)}}(\frac{1}{2}h_\beta)^n \int_{-d^{(p)}_\alpha/2}^{d^{(p)}_\alpha/2} \int_{-l_\gamma/2}^{l_\gamma/2} [\sigma^{(\alpha\beta\gamma)}_{2j}(\frac{1}{2}h_\beta) + (-1)^{n+1}\sigma^{(\alpha\beta\gamma)}_{2j}(-\frac{1}{2}h_\beta)]d\bar{x}^{(\alpha)}_1 d\bar{x}^{(\gamma)}_3 \qquad \text{(A30)}$$

$$K^{(\alpha\beta\gamma)}_{3j(0,0,n)} = \frac{1}{v^{(p)}_{(\alpha\beta\gamma)}}(\frac{1}{2}l_\gamma)^n \int_{-d^{(p)}_\alpha/2}^{d^{(p)}_\alpha/2} \int_{-h_\beta/2}^{h_\beta/2} [\sigma^{(\alpha\beta\gamma)}_{3j}(\frac{1}{2}l_\gamma) + (-1)^{n+1}\sigma^{(\alpha\beta\gamma)}_{3j}(-\frac{1}{2}l_\gamma)]d\bar{x}^{(\alpha)}_1 d\bar{x}^{(\beta)}_2 \qquad \text{(A31)}$$

and where $\sigma^{(\alpha\beta\gamma)}_{1j}(\pm\frac{1}{2}d^{(p)}_\alpha)$, $\sigma^{(\alpha\beta\gamma)}_{2j}(\pm\frac{1}{2}h_\beta)$, $\sigma^{(\alpha\beta\gamma)}_{3j}(\pm\frac{1}{2}l_\gamma)$, stand for the interfacial stresses at $\bar{x}^{(\alpha)}_1 = \pm\frac{1}{2}d^{(p)}_\alpha, \bar{x}^{(\beta)}_2 = \pm\frac{1}{2}h_\beta, \bar{x}^{(\gamma)}_3 = \pm\frac{1}{2}l_\gamma$, respectively.

Equations (A22) through (A28) provide relations between the zeroth-order and first order, volume-averaged stresses $S^{(\alpha\beta\gamma)}_{ij(l,m,n)}$ and the interfacial tractions $I^{(\alpha\beta\gamma)}_{1j(n,0,0)}$, $J^{(\alpha\beta\gamma)}_{2j(0,n,0)}$ and $K^{(\alpha\beta\gamma)}_{3j(0,0,n)}$. Direct "one-to-one" relations are obtained through the following sequence of manipulations, noting that equations (A23) through (A25) already provide direct relations between $S^{(\alpha\beta\gamma)}_{11(0,0,0)}$ and $I^{(\alpha\beta\gamma)}_{11(1,0,0)}$, $S^{(\alpha\beta\gamma)}_{22(0,0,0)}$ and $J^{(\alpha\beta\gamma)}_{22(0,1,0)}$, $S^{(\alpha\beta\gamma)}_{33(0,0,0)}$ and $K^{(\alpha\beta\gamma)}_{33(0,0,1)}$. First, substituting equation (A22) into equations (A27) and (A28), respectively, gives direct expressions for $J^{(\alpha\beta\gamma)}_{21(0,0,0)}$ and $K^{(\alpha\beta\gamma)}_{31(0,0,0)}$.

$$\frac{1}{6}h^2_\beta J^{(\alpha\beta\gamma)}_{21(0,0,0)} = 2S^{(\alpha\beta\gamma)}_{12(0,1,0)} \qquad \text{(A32)}$$

$$\frac{1}{6}l^2_\gamma K^{(\alpha\beta\gamma)}_{31(0,0,0)} = 2S^{(\alpha\beta\gamma)}_{13(0,0,1)} \qquad \text{(A33)}$$

Then, upon substitution of equations (A32) and (A33) into equation (A22), we have the following expression for $I^{(\alpha\beta\gamma)}_{11(0,0,0)}$:

$$I^{(\alpha\beta\gamma)}_{11(0,0,0)} = -12(S^{(\alpha\beta\gamma)}_{12(0,1,0)}/h^2_\beta + S^{(\alpha\beta\gamma)}_{13(0,0,1)}/l^2_\gamma) \qquad \text{(A34)}$$

Equations (A32) through (A34) will be used to reduce the equilibrium equations and traction continuity equations to expressions involving only the zeroth-order and first-order, volume-averaged stress quantities $S^{(\alpha\beta\gamma)}_{ij(l,m,n)}$. These can subsequently be expressed in terms of the fundamental unknown coefficients $w^{(\alpha\beta\gamma)}_1$, $U^{(\alpha\beta\gamma)}_1$, $V^{(\alpha\beta\gamma)}_1$, $W^{(\alpha\beta\gamma)}_1$, $\phi^{(\alpha\beta\gamma)}_1$, $\chi^{(\alpha\beta\gamma)}_2$, and $\psi^{(\alpha\beta\gamma)}_3$ appearing in the displacement field expansion given by equations (39), using equations (41) through (46).

8.2.2 Traction Continuity Conditions

The traction continuity conditions, equations (33) - (34), are imposed on an average basis at the subcell and cell interfaces. These conditions imply existence of certain relationships between the surface integrals of the interfacial traction components defined by equations (A29) - (A31). To assist in establishing these relations, let us define two new quantities $F_{ij}^{(1\beta\gamma)}$ and $G_{ij}^{(1\beta\gamma)}$ as follows

$$F_{ij}^{(1\beta\gamma)} = \sigma_{ij}^{(1\beta\gamma)} \Big|_{\bar{x}_1^{(1)} = d_1^{(p)}/2} - \sigma_{ij}^{(1\beta\gamma)} \Big|_{\bar{x}_1^{(1)} = -d_1^{(p)}/2} \tag{A35}$$

$$G_{ij}^{(1\beta\gamma)} = \sigma_{ij}^{(1\beta\gamma)} \Big|_{\bar{x}_1^{(1)} = d_1^{(p)}/2} + \sigma_{ij}^{(1\beta\gamma)} \Big|_{\bar{x}_1^{(1)} = -d_1^{(p)}/2} \tag{A36}$$

Substituting equations (33a) and (34a) into the above definitions, we obtain, respectively:

$$F_{11}^{(1\beta\gamma)} \Big|^{(p)} = \sigma_{11}^{(2\beta\gamma)} \Big|_{\bar{x}_1^{(2)} = -d_2^{(p)}/2}^{(p)} - \sigma_{11}^{(2\beta\gamma)} \Big|_{\bar{x}_1^{(2)} = d_2^{(p-1)}/2}^{(p-1)} \tag{A37}$$

$$G_{11}^{(1\beta\gamma)} \Big|^{(p)} = \sigma_{11}^{(2\beta\gamma)} \Big|_{\bar{x}_1^{(2)} = -d_2^{(p)}/2}^{(p)} + \sigma_{11}^{(2\beta\gamma)} \Big|_{\bar{x}_1^{(2)} = d_2^{(p-1)}/2}^{(p-1)} \tag{A38}$$

By addition and subtraction of equal quantities to and from equations (A34) and (A35) it can easily be verified that

$$2F_{11}^{(1\beta\gamma)} \Big|^{(p)} = [-F_{11}^{(2\beta\gamma)} + G_{11}^{(2\beta\gamma)}]^{(p)} - [F_{11}^{(2\beta\gamma)} + G_{11}^{(2\beta\gamma)}]^{(p-1)} \tag{A39}$$

$$2G_{11}^{(1\beta\gamma)} \Big|^{(p)} = [G_{11}^{(2\beta\gamma)} - F_{11}^{(2\beta\gamma)}]^{(p)} + [G_{11}^{(2\beta\gamma)} + F_{11}^{(2\beta\gamma)}]^{(p-1)} \tag{A40}$$

Then employing equations (A36) and (A37) in equation (A29) with j = 1, we obtain the corresponding relations:

$$d_1^{(p)} I_{11(0,0,0)}^{(1\beta\gamma)} \Big|^{(p)} = [I_{11(1,0,0)}^{(2\beta\gamma)} - \frac{1}{2} d_2^{(p)} I_{11(0,0,0)}^{(2\beta\gamma)}]^{(p)} - [I_{11(1,0,0)}^{(2\beta\gamma)} + \frac{1}{2} d_2^{(p-1)} I_{11(0,0,0)}^{(2\beta\gamma)}]^{(p-1)} \tag{A41}$$

$$I_{11(1,0,0)}^{(1\beta\gamma)} \Big|^{(p)} = \frac{1}{2}[I_{11(1,0,0)}^{(2\beta\gamma)} - \frac{1}{4} d_2^{(p)} I_{11(0,0,0)}^{(2\beta\gamma)}]^{(p)} + \frac{1}{2}[I_{11(1,0,0)}^{(2\beta\gamma)} + \frac{1}{2} d_2^{(p-1)} I_{11(0,0,0)}^{(2\beta\gamma)}]^{(p-1)} \tag{A42}$$

Similarly, using equations (33b) and (A30) we have

$$h_1 J^{(\alpha 1\gamma)}_{21(0,0,0)} \Big|^{(p)} = -h_2 J^{(\alpha 2\gamma)}_{21(0,0,0)} \Big|^{(p)} \tag{A43}$$

$$J^{(\alpha 1\gamma)}_{22(0,1,0)} \Big|^{(p)} = J^{(\alpha 2\gamma)}_{22(0,1,0)} \Big|^{(p)} \tag{A44}$$

and from equations (33c) and (A31) we obtain

$$l_1 K^{(\alpha\beta 1)}_{31(0,0,0)} \Big|^{(p)} = -l_2 K^{(\alpha\beta 2)}_{31(0,0,0)} \Big|^{(p)} \tag{A45}$$

$$K^{(\alpha\beta 1)}_{33(0,0,1)} \Big|^{(p)} = K^{(\alpha\beta 2)}_{33(0,0,1)} \Big|^{(p)} \tag{A46}$$

We note that the other two traction continuity conditions, equations (34b) and (34c), are identically satisfied for the present case of an applied normal mechanical loading in the x_1-direction.

As a result of the above manipulations, 24 relations, given by equations (A41) through (A46), arise from the traction continuity conditions between subcells and between neighboring cells. These equations, in conjunction with equations (A22) through (A26), and equations (A32) through (A34), will be employed in reducing the equilibrium and traction continuity equations to expressions involving only volume-averaged zeroth-order and first-order stresses $S^{(\alpha\beta\gamma)}_{ij(l,m,n)}$.

8.2.3 Reduction of Equilibrium and Traction Continuity Equations

Substituting equation (A22) into equation (A26) and using equations (A32) and (A33), reduces the volume-averaged equilibrium equations to a set of 8 equations given by equation (47) on page 23, reproduced below for convenience.

$$[\, S^{(\alpha\beta\gamma)}_{11(1,0,0)} / d^{(p)2}_{\alpha} + S^{(\alpha\beta\gamma)}_{12(0,1,0)} / h^2_{\beta} + S^{(\alpha\beta\gamma)}_{13(0,0,1)} / l^2_{\gamma} \,]^{(p)} = 0 \tag{47}$$

Combining the expressions for $I^{(\alpha\beta\gamma)}_{11(1,0,0)}$ and $I^{(\alpha\beta\gamma)}_{11(0,0,0)}$, provided by equations (A23) and (A34), and the continuity relations (A41) - (A42), respectively, we obtain the following eight equations

$$[\ 12S^{(1\beta\gamma)}_{12(0,1,0)}/h_\beta^2 + 12S^{(1\beta\gamma)}_{13(0,0,1)}/l_\gamma^2\ ]^{(p)} + 6\frac{d_2^{(p)}}{d_1^{(p)}}[\ S^{(2\beta\gamma)}_{12(0,1,0)}/h_\beta^2 + S^{(2\beta\gamma)}_{13(0,0,1)}/l_\gamma^2\ ]^{(p)} +$$

$$6\frac{d_2^{(p-1)}}{d_1^{(p)}}[\ S^{(2\beta\gamma)}_{12(0,1,0)}/h_\beta^2 + S^{(2\beta\gamma)}_{13(0,0,1)}/l_\gamma^2\ ]^{(p-1)} + \frac{1}{d_1^{(p)}}[\ S^{(2\beta\gamma)}_{11(0,0,0)}\Big|^{(p)} - S^{(2\beta\gamma)}_{11(0,0,0)}\Big|^{(p-1)}\ ] = 0 \quad (48)$$

and

$$S^{(1\beta\gamma)}_{11(0,0,0)}\Big|^{(p)} = \frac{1}{2}S^{(2\beta\gamma)}_{11(0,0,0)}\Big|^{(p)} + \frac{1}{2}S^{(2\beta\gamma)}_{11(0,0,0)}\Big|^{(p-1)} + 3d_2^{(p)}[\ S^{(2\beta\gamma)}_{12(0,1,0)}/h_\beta^2 + S^{(2\beta\gamma)}_{13(0,0,1)}/l_\gamma^2\ ]^{(p)} -$$

$$3d_2^{(p-1)}[\ S^{(2\beta\gamma)}_{12(0,1,0)}/h_\beta^2 + S^{(2\beta\gamma)}_{13(0,0,1)}/l_\gamma^2\ ]^{(p-1)} \quad (49)$$

Continuing, if we substitute equation (A32) into equation (A43) directly, and equation (A33) into equation (A45), we obtain, respectively:

$$[\ S^{(\alpha 1\gamma)}_{12(0,1,0)}/h_1 + S^{(\alpha 2\gamma)}_{12(0,1,0)}/h_2\ ]^{(p)} = 0 \quad (50)$$

$$[\ S^{(\alpha\beta 1)}_{13(0,0,1)}/l_1 + S^{(\alpha\beta 2)}_{13(0,0,1)}/l_2\ ]^{(p)} = 0 \quad (51)$$

Finally combining equations (A24) and (A44), and equations (A25) and (A46), yields, respectively,

$$S^{(\alpha 1\gamma)}_{22(0,0,0)}\Big|^{(p)} = S^{(\alpha 2\gamma)}_{22(0,0,0)}\Big|^{(p)} \quad (52)$$

$$S^{(\alpha\beta 1)}_{33(0,0,1)}\Big|^{(p)} = S^{(\alpha\beta 2)}_{33(0,0,1)}\Big|^{(p)} \quad (53)$$

As indicated previously, equations (47) through (53) are easily expressed in terms of the fundamental unknown coefficients $w_1^{(\alpha\beta\gamma)}$, $U_1^{(\alpha\beta\gamma)}$, $V_1^{(\alpha\beta\gamma)}$, $W_1^{(\alpha\beta\gamma)}$, $\phi_1^{(\alpha\beta\gamma)}$, $\chi_2^{(\alpha\beta\gamma)}$, and $\psi_3^{(\alpha\beta\gamma)}$ using equations (41) through (46).

8.2.4 Displacement Continuity Conditions

The displacement continuity conditions, i.e. equations (35) - (36), are now imposed on an average basis at the interfaces. This is accomplished by first substituting equation (39) into

equation (35a),

$$[\, w_1^{(1\beta\gamma)} + \frac{1}{2} d_1^{(p)} \phi_1^{(1\beta\gamma)} + \frac{1}{4} d_1^2 U_1^{(1\beta\gamma)} \,]^{(p)} = [\, w_1^{(2\beta\gamma)} - \frac{1}{2} d_2^{(p)} \phi_1^{(2\beta\gamma)} + \frac{1}{4} d_2^2 U_1^{(2\beta\gamma)} \,]^{(p)} \tag{54}$$

then into equation (35b)

$$[\, w_1^{(\alpha 1\gamma)} + \frac{1}{2} h_1^2 V_1^{(\alpha 2\gamma)} \,]^{(p)} = [\, w_1^{(\alpha 2\gamma)} + \frac{1}{4} h_2^2 V_1^{(\alpha 2\gamma)} \,]^{(p)} \tag{55}$$

$$h_1 \chi_2^{(\alpha 1\gamma)} \Big|^{(p)} = -h_2 \chi_2^{(\alpha 2\gamma)} \Big|^{(p)} \tag{56}$$

followed by equation (35c)

$$[\, w_1^{(\alpha\beta 1)} + \frac{1}{4} l_1^2 W_1^{(\alpha\beta 1)} \,]^{(p)} = [\, w_1^{(\alpha\beta 2)} + \frac{1}{4} l_2^2 W_1^{(\alpha\beta 2)} \,]^{(p)} \tag{57}$$

$$l_1 \psi_3^{(\alpha\beta 1)} \Big|^{(p)} = -l_2 \psi_3^{(\alpha\beta 2)} \Big|^{(p)} \tag{58}$$

and finally into equation (36a)

$$[\, w_1^{(1\beta\gamma)} - \frac{1}{2} d_1^{(p+1)} \phi_1^{(1\beta\gamma)} + \frac{1}{4} d_1^{(p+1)2} U_1^{(1\beta\gamma)} \,]^{(p+1)} = [\, w_1^{(2\beta\gamma)} + \frac{1}{2} d_2^{(p)} \phi_1^{(2\beta\gamma)} + \frac{1}{4} d_2^{(p)2} U_1^{(2\beta\gamma)} \,]^{(p)} \tag{59}$$

The other two displacement continuity relations (36b) and (36c) are identically satisfied for the present case of normal loading applied in the x_1-direction. Consequently, equations (54) - (59) provide 24 relations which must be imposed to guarantee the continuity of the displacements between the subcells and between neighboring cells.

Table 1. Material properties of SCS6 SiC fiber and titanium matrix.

Material	E (GPa)	ν	α (10^{-6} m / m / °C)	κ (W / m-°C)
SiC fiber	414.0	0.3	4.9	400.0, 200.0, 40.0, 17.6
Ti-Al matrix	100.0	0.3	9.6	8.0

E and ν denote the Young's modulus and Poisson's ratio, respectively, α is the coefficient of thermal expansion, and κ is the thermal conductivity.

Table 2. Material properties of the SCS6 SiC/Ti composite ($v_f = 0.40$).

E_A^* (GPa)	ν_A^*	E_T^* (GPa)	G_A^* (GPa)
226.0	0.30	167.0	60.9

α_A^* (10^{-6} m / m / °C)	α_T^* (10^{-6} m / m / °C)	κ_A^* (W / m-°C)	κ_T^* (W / m-°C)
6.15	7.90	164.80	16.20

Subindices A and T denote axial and transverse quantities, respectively.

Table 3. Normalized inplane force and moment resultants for different κ_f / κ_m ratios.

κ_f / κ_m	N_2 / N_2^{LAM}	N_3 / N_3^{LAM}	M_2 / M_2^{LAM}	M_3 / M_3^{LAM}
M = 3				
50.0	0.7954	0.7895	0.9444	0.9209
25.0	0.8046	0.8000	0.9409	0.9177
5.0	0.8621	0.8631	0.9271	0.9019
2.2	0.9195	0.9158	0.9201	0.8924
M = 20				
50.0	0.9655	0.9684	0.9930	0.9873
25.0	0.9655	0.9684	0.9930	0.9873
5.0	0.9770	0.9789	0.9896	0.9842
2.2	0.9885	0.9895	0.9896	0.9842

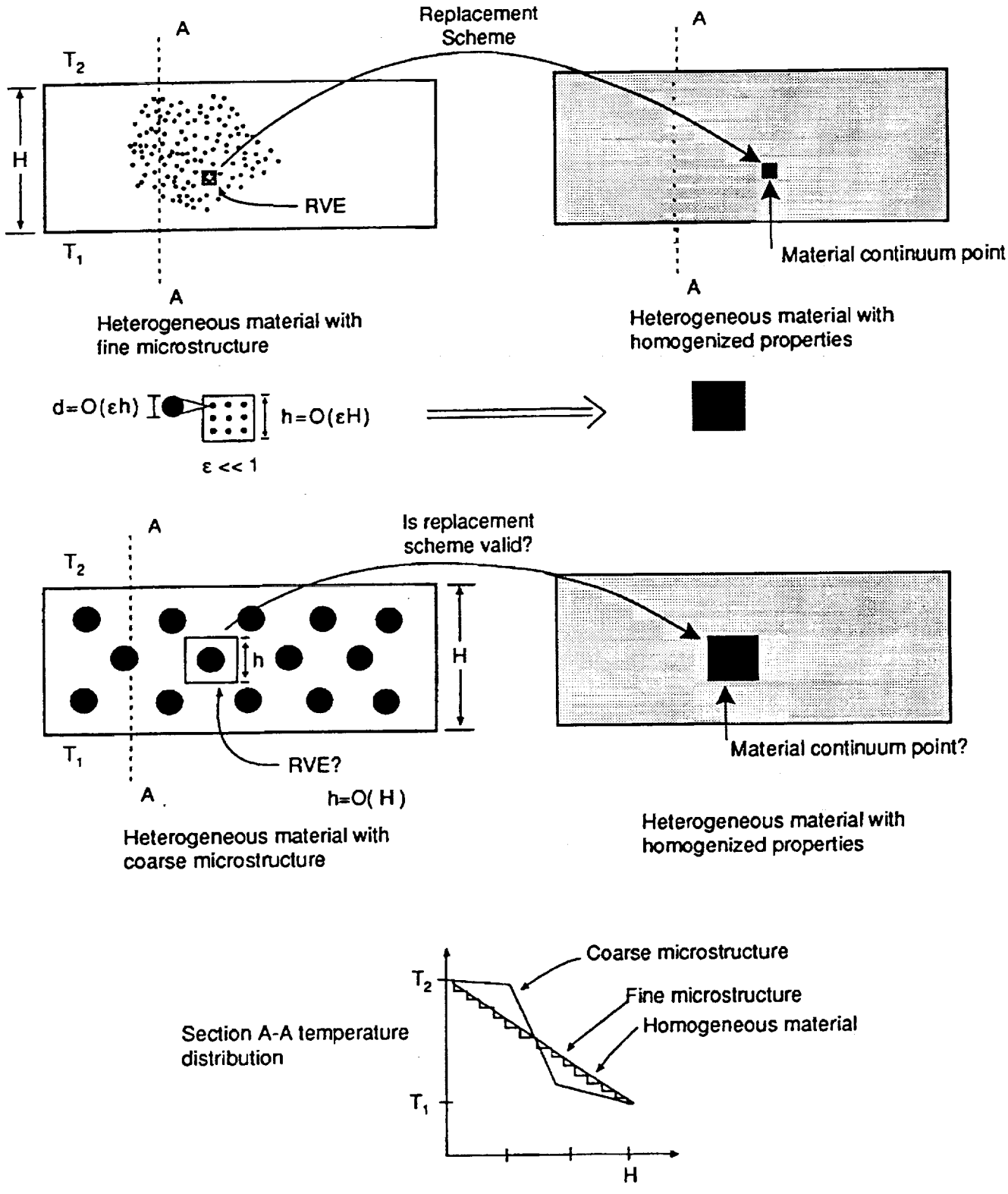

Figure 1 - Applicability of the representative volume elment for heterogeneous materials in the presence of thermal gradients.

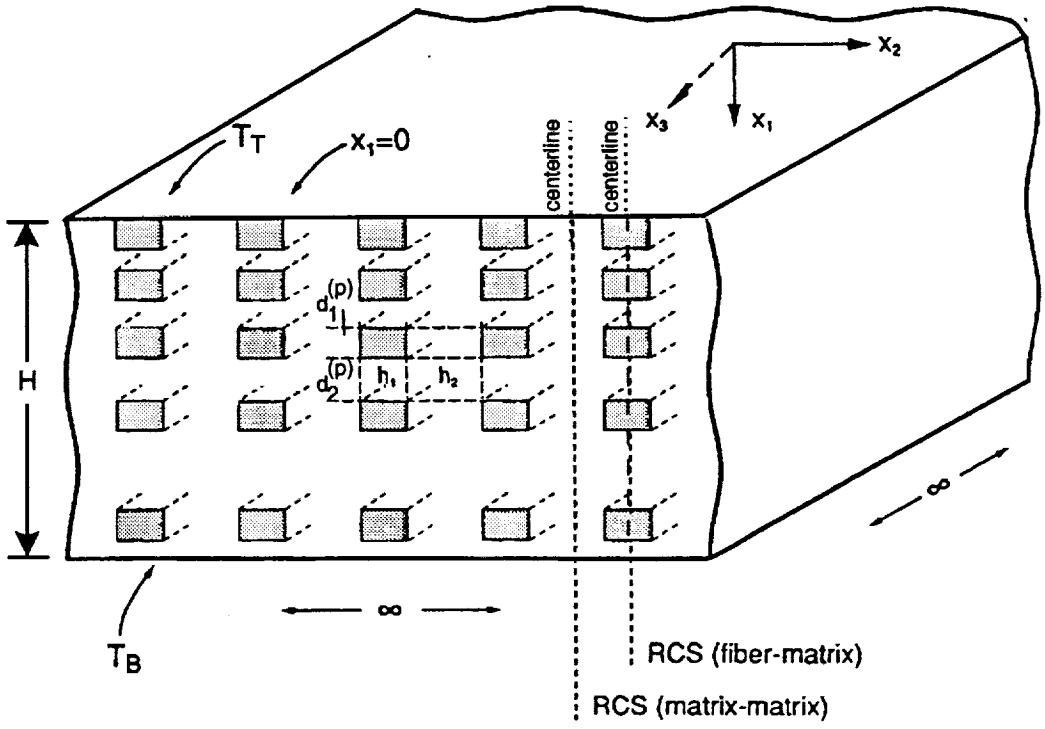

a) unidirectionally-reinforced material

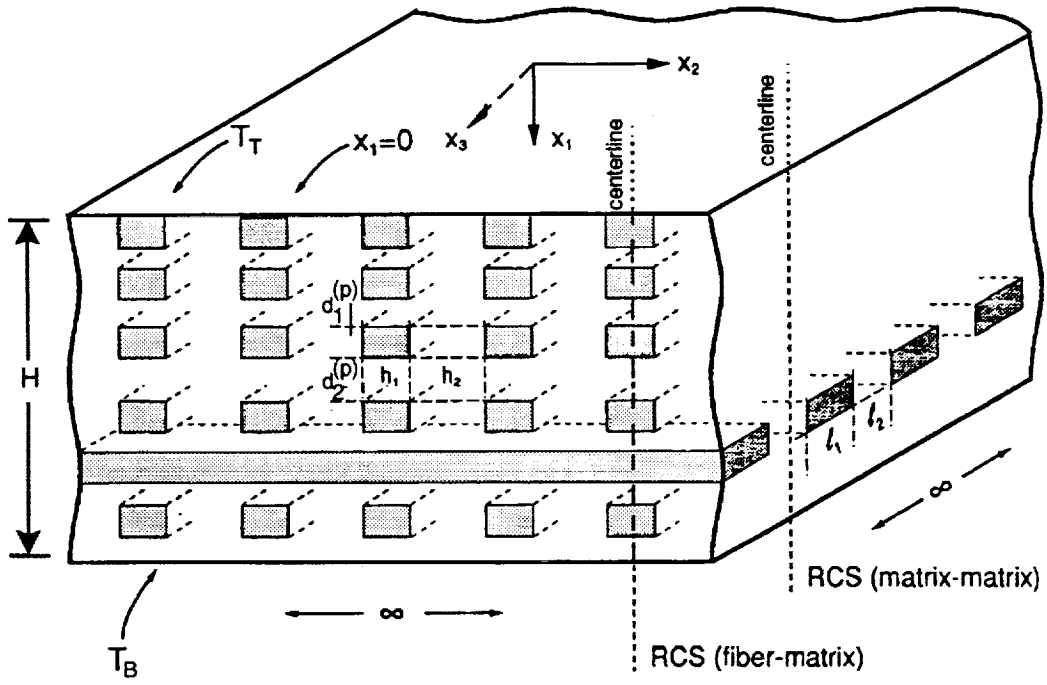

b) bidirectionally-reinforced material

Figure 2 - Composite with nonperiodic fiber distribution in x_1 direction.

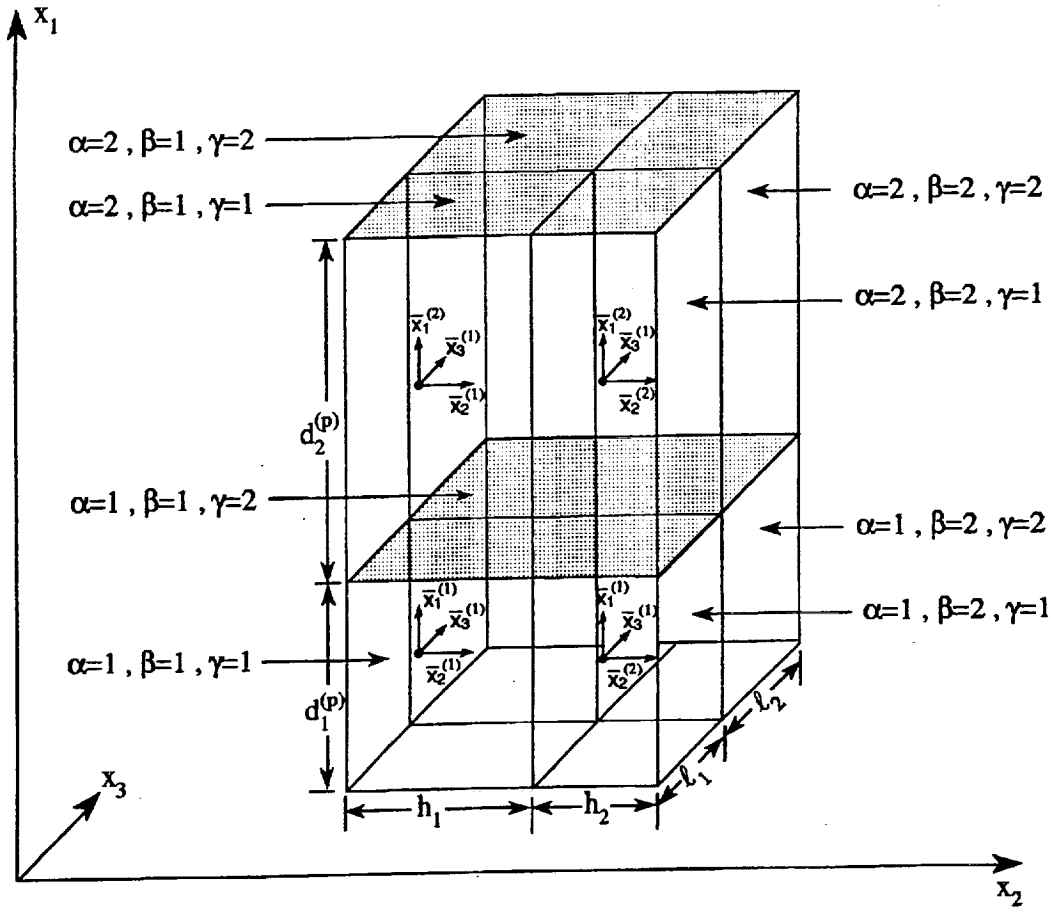

Figure 3 - The repeating unit cell of a composite with nonperiodic fiber distribution in the x_1 direction.

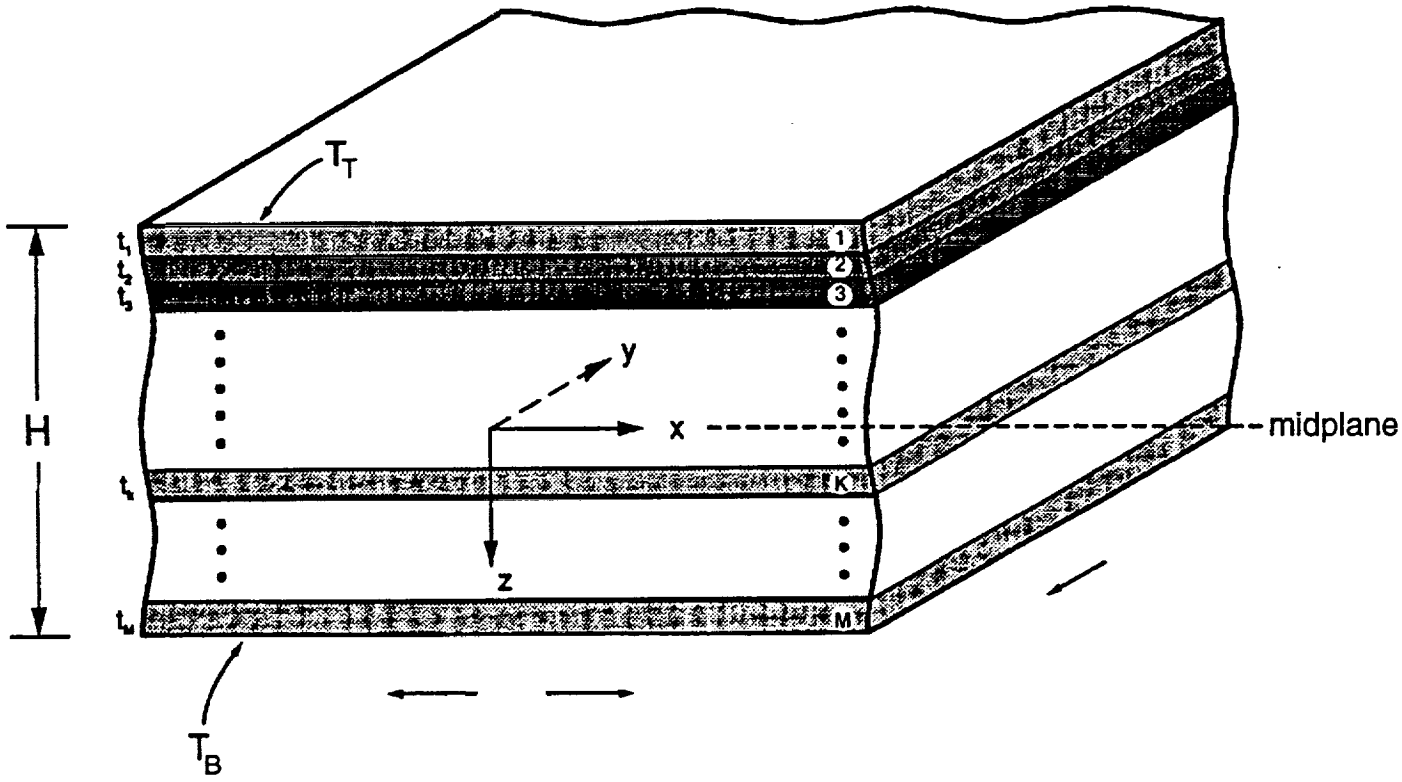

Figure 4 - Laminate geometry.

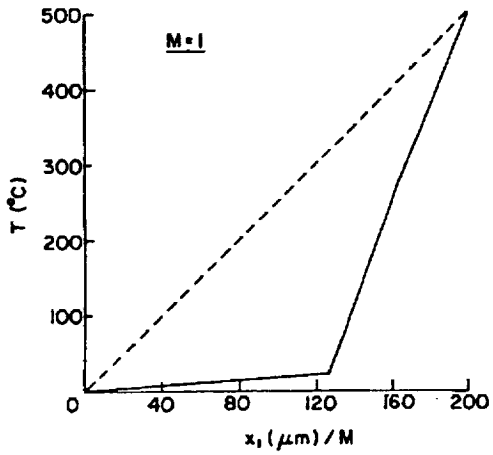

a) M = 1

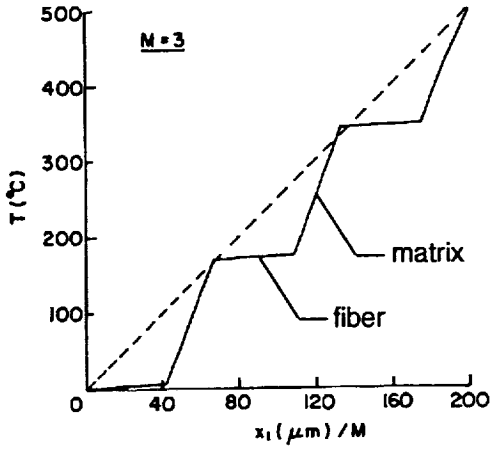

b) M = 3

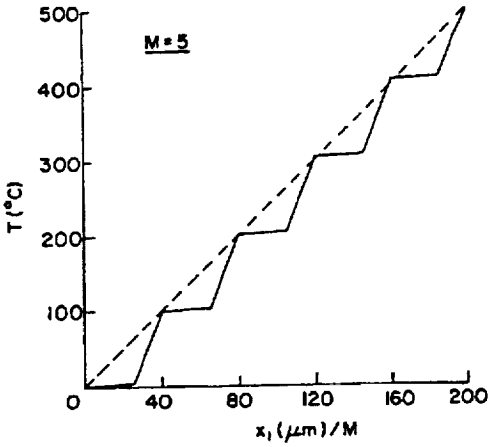

c) M = 5

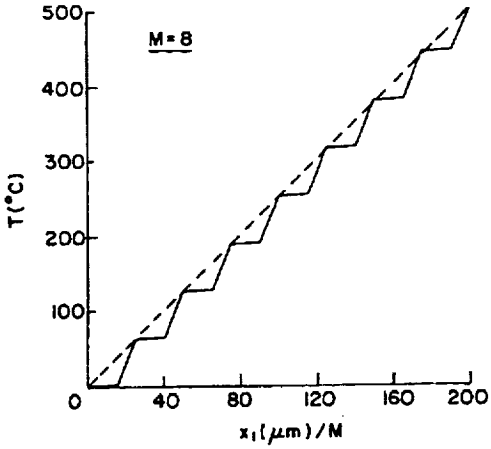

d) M = 8

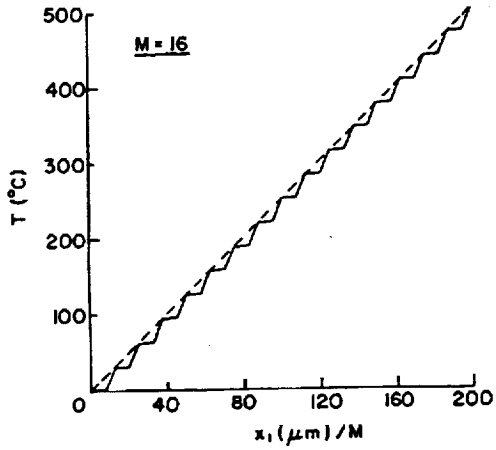

d) M = 16

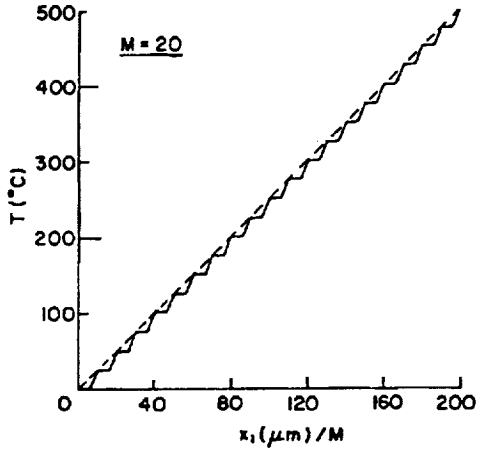

e) M = 20

Figure 5 - Through-the-thickness temperature distribution in a unidirectional composite with uniformly spaced fibers in the cross-section containing both phases (——) FG theory, (- - -) continuum theory.

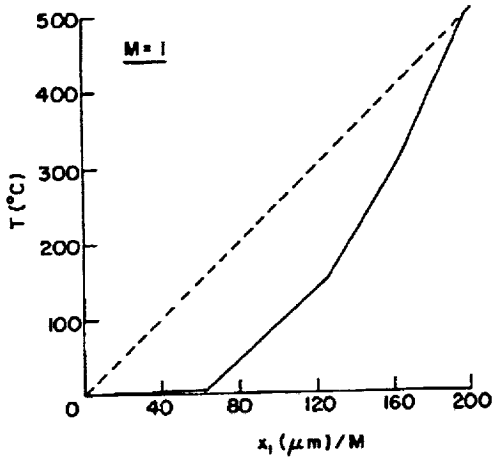

a) M = 1

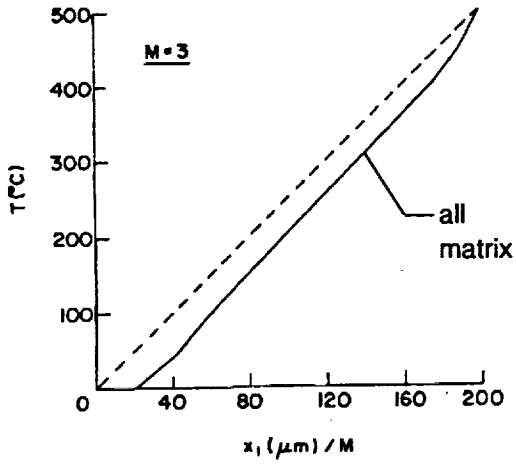

b) M = 3

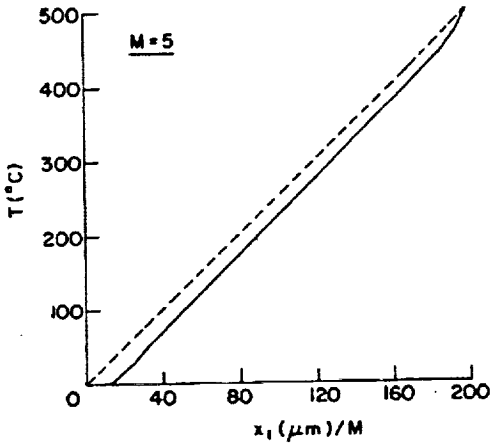

c) M = 5

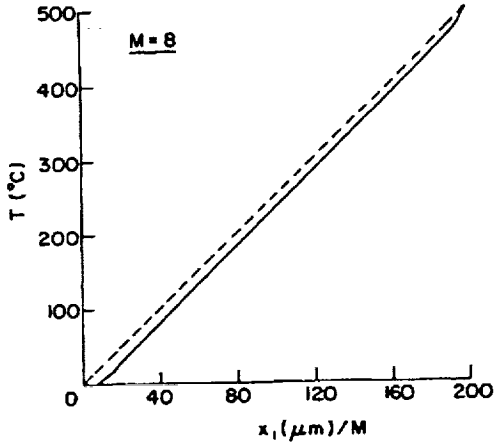

d) M = 8

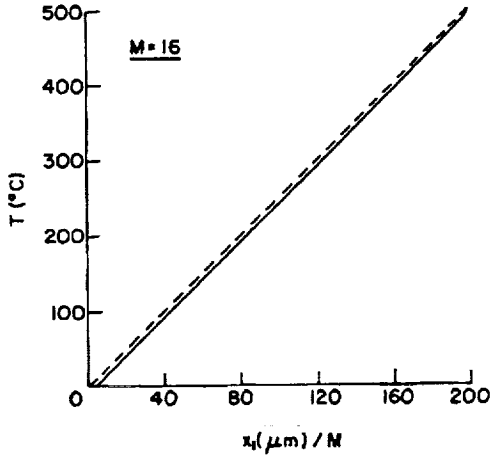

e) M = 16

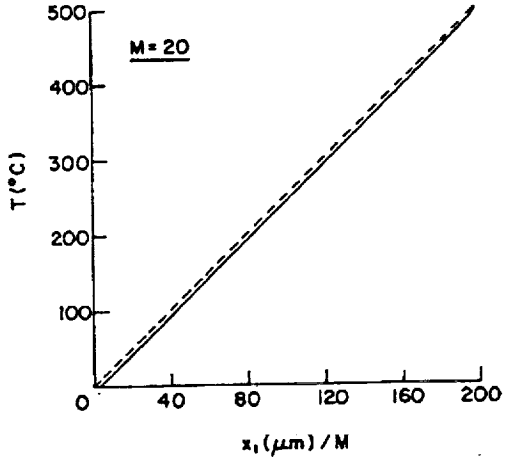

f) M = 20

Figure 6 - Through-the thickness temperature distribution in a unidirectional composite with uniformly spaced fibers in the cross-section containing matrix phase only (——) FG theory, (- - -) continuum theory.

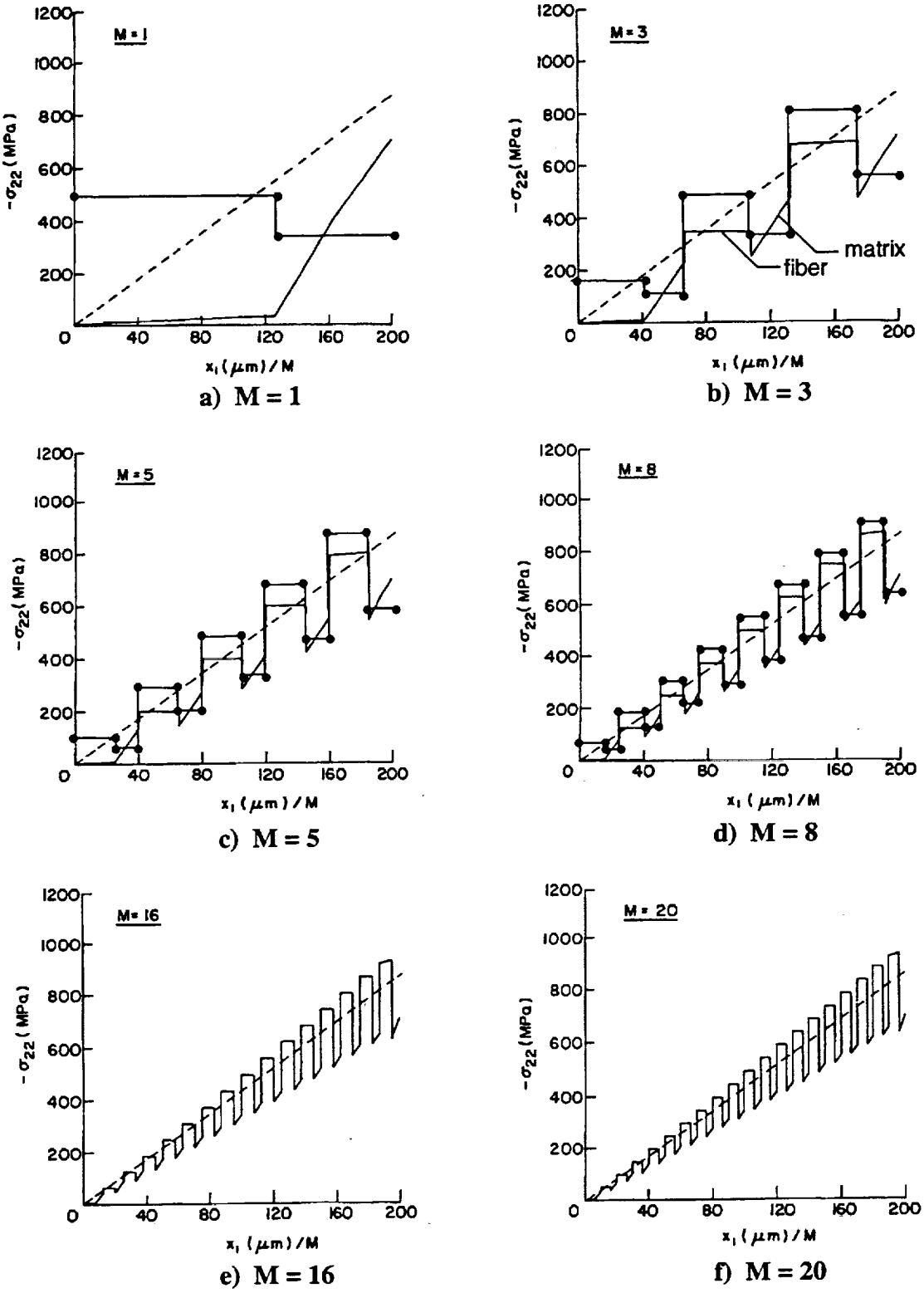

Figure 7 - Through-the-thickness normal stress σ_{22} in a unidirectional composite with uniformly spaced fibers in the cross-section containing both phases (——) FG theory, (- - -) continuum theory, (•——•) "primitive" micromechanics.

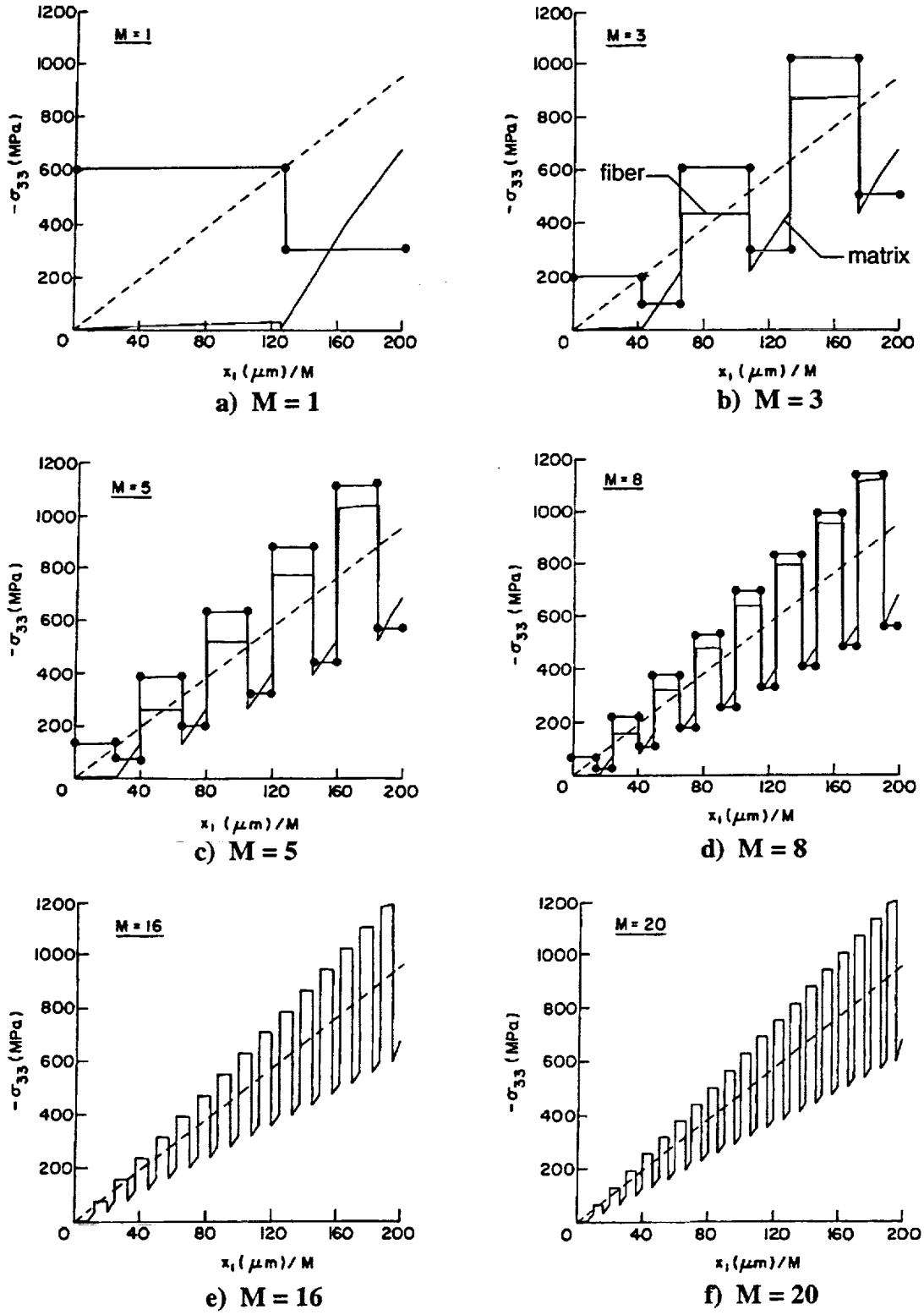

Figure 8 - Through-the-thickness normal stress σ_{33} in a unidirectional composite with uniformly spaced fibers in the cross-section containing both phases (——) FG theory, (- - -) continuum theory, (•——•) "primitive" micromechanics.

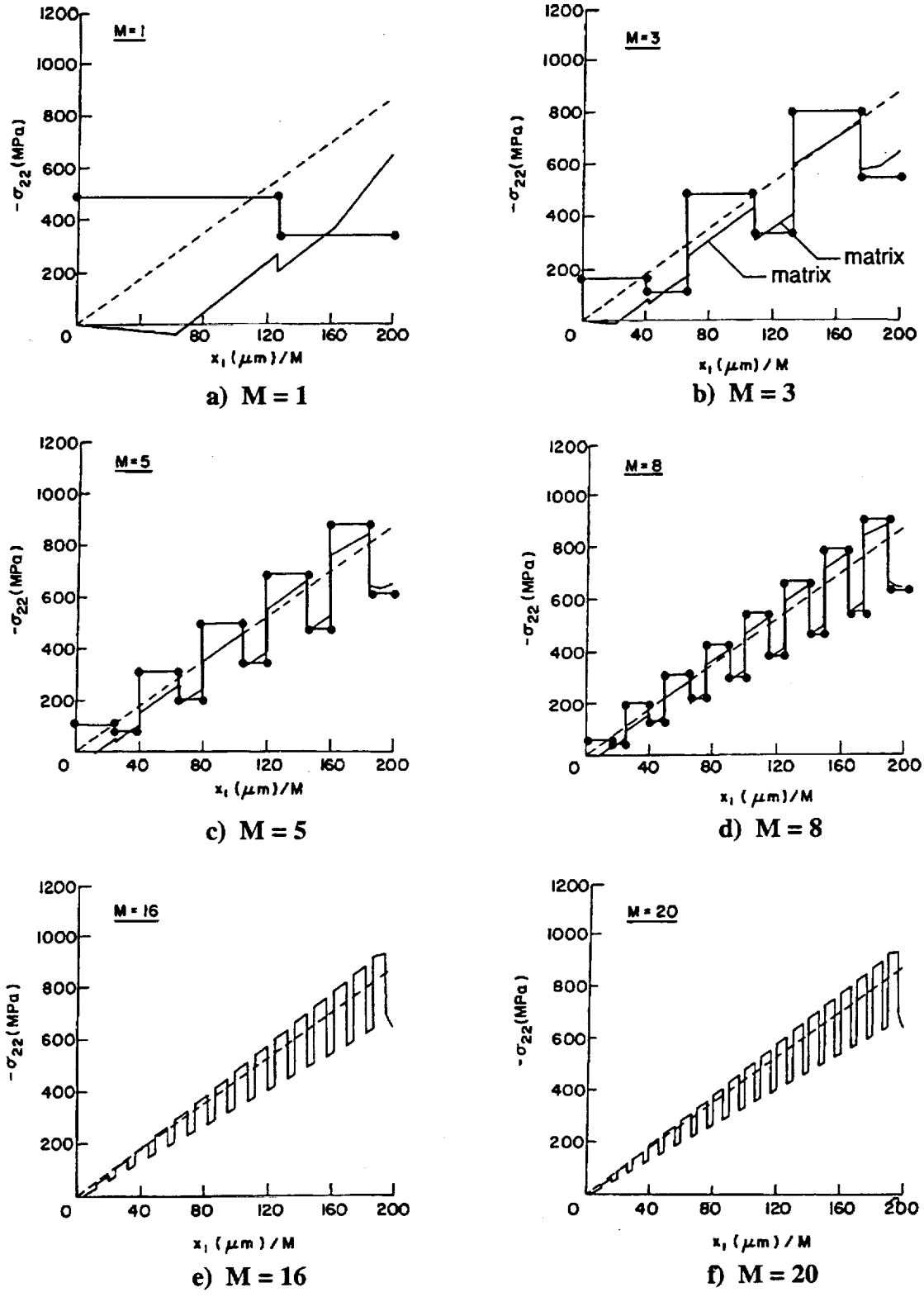

Figure 9 - Through-the-thickness normal stress σ_{22} in a unidirectional composite with uniformly spaced fibers in the cross-section matrix phase only (——) FG theory, (- - -) continuum theory, (•——•) "primitive" micromechanics.

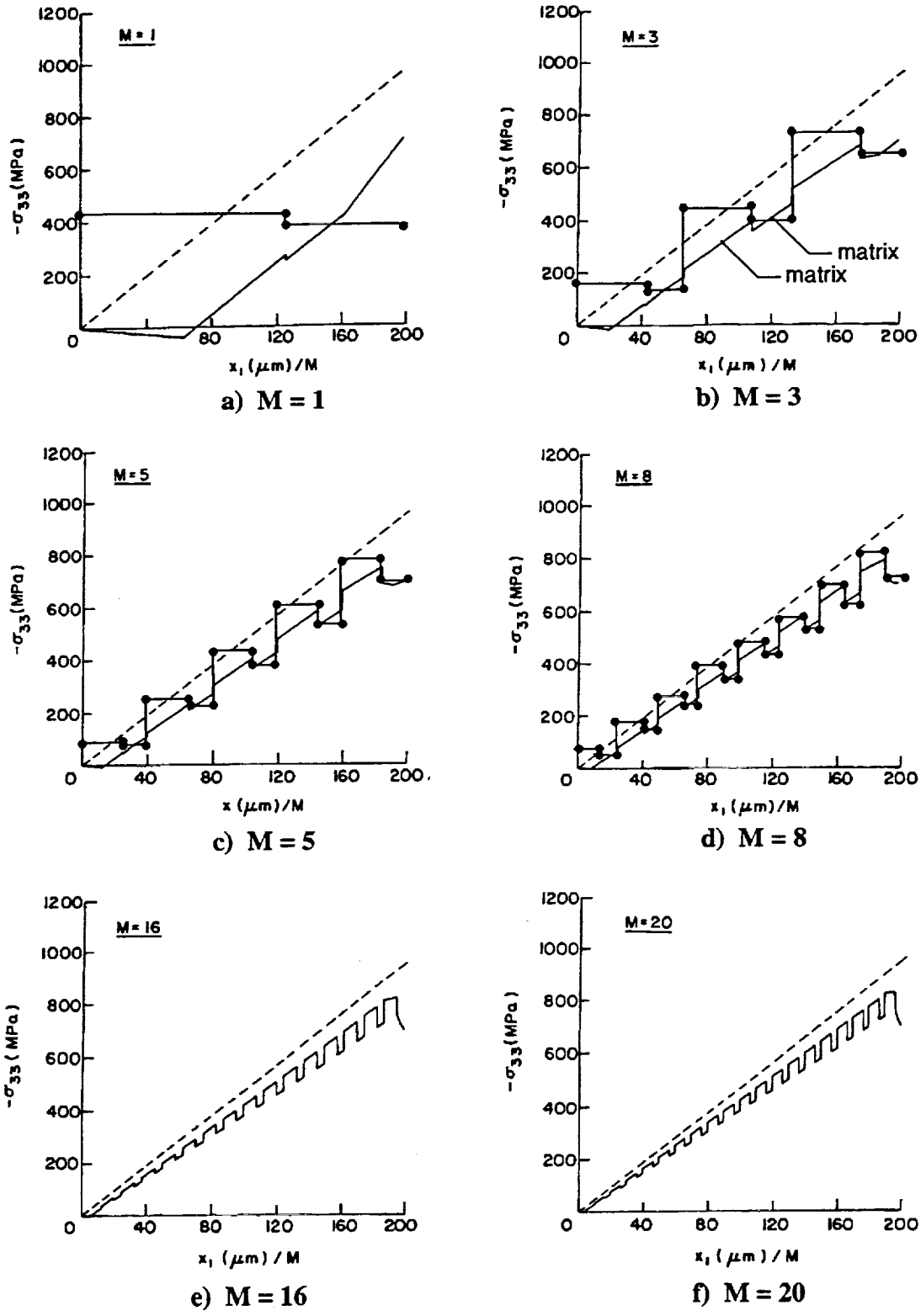

Figure 10 - Through-the-thickness normal stress σ_{33} in a unidirectional composite with uniformly spaced fibers in the cross-section matrix phase only (——) FG theory, (- - -) continuum theory, (•——•) "primitive" micromechanics.

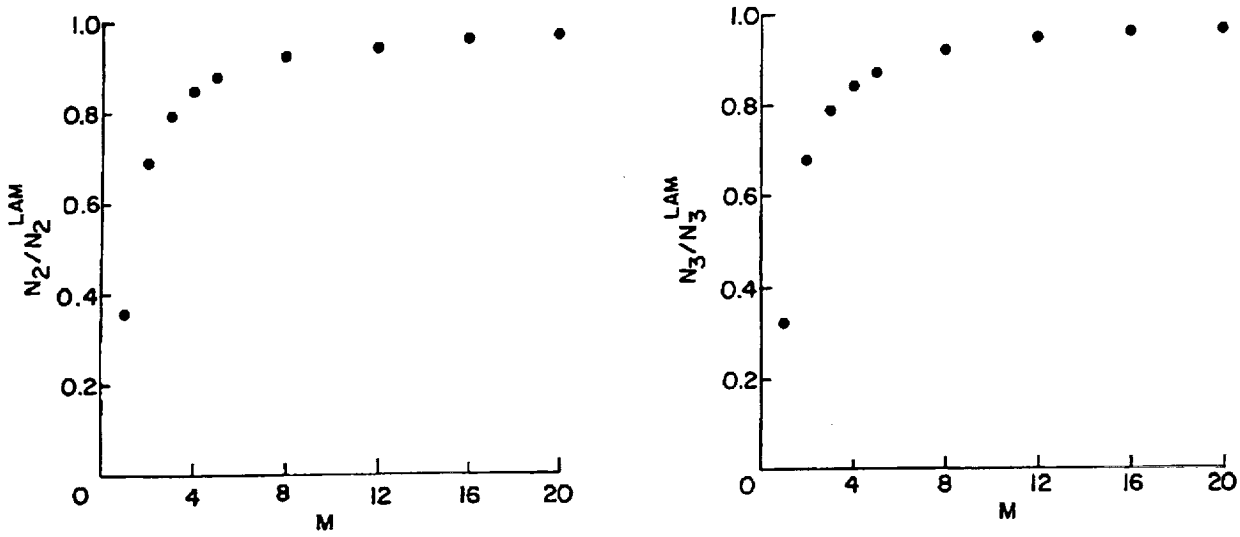

a) N_2 b) N_3

Figure 11 - Inplane force resultants in a unidirectional composite with uniformly spaced fibers in the thickness direction (normalized with respect to the continuum theory prediction).

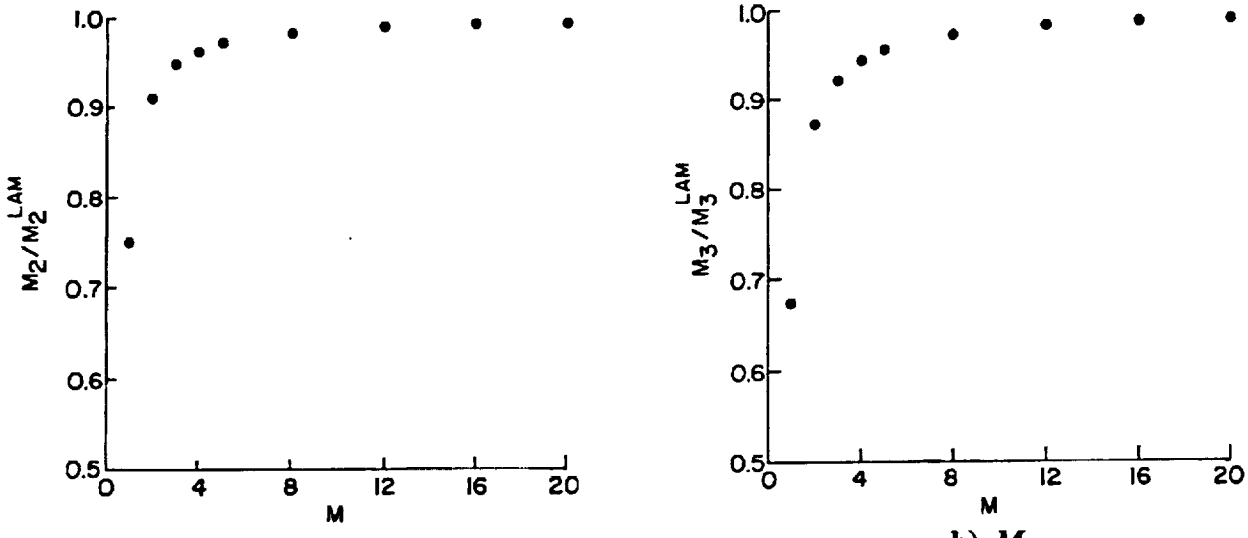

a) M_2 b) M_3

Figure 12 - Inplane moment resultants in a unidirectional composite with uniformly spaced fibers in the thickness direction (normalized with respect to the continuum theory prediction).

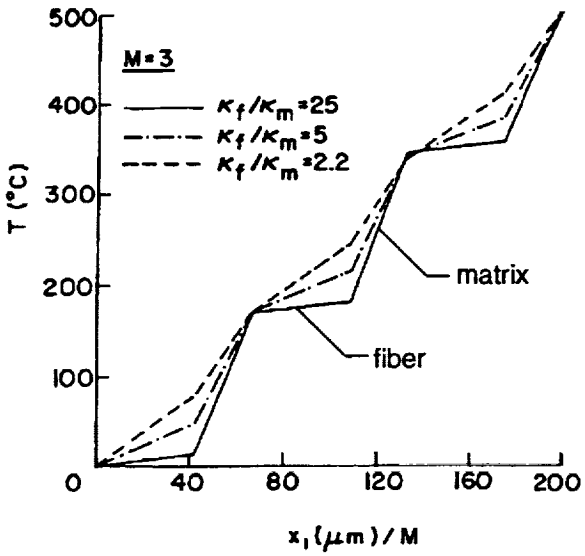

a) temperature distribution

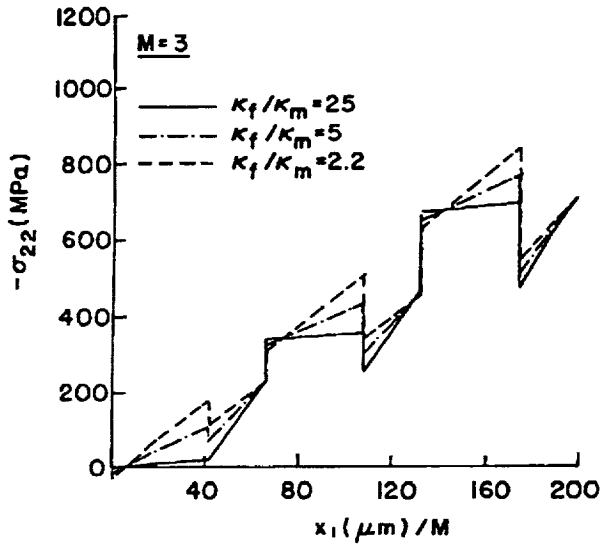

b) normal stress σ_{22}

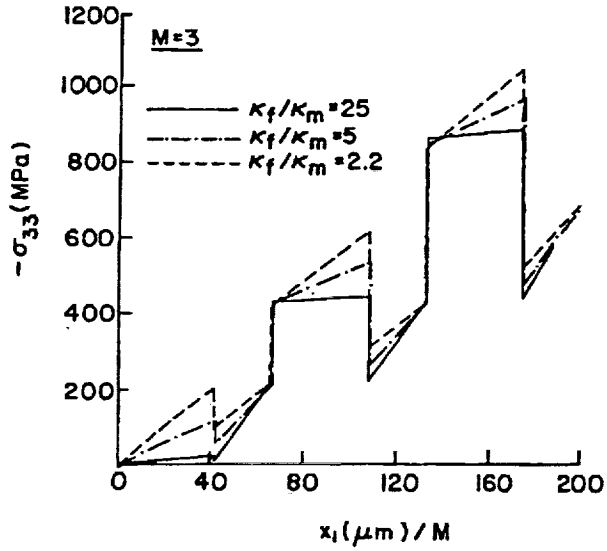

b) normal stress σ_{33}

Figure 13 - Effect of the thermal conductivity mismatch in a unidirectionally-reinforced material in the cross-section containing both phases.

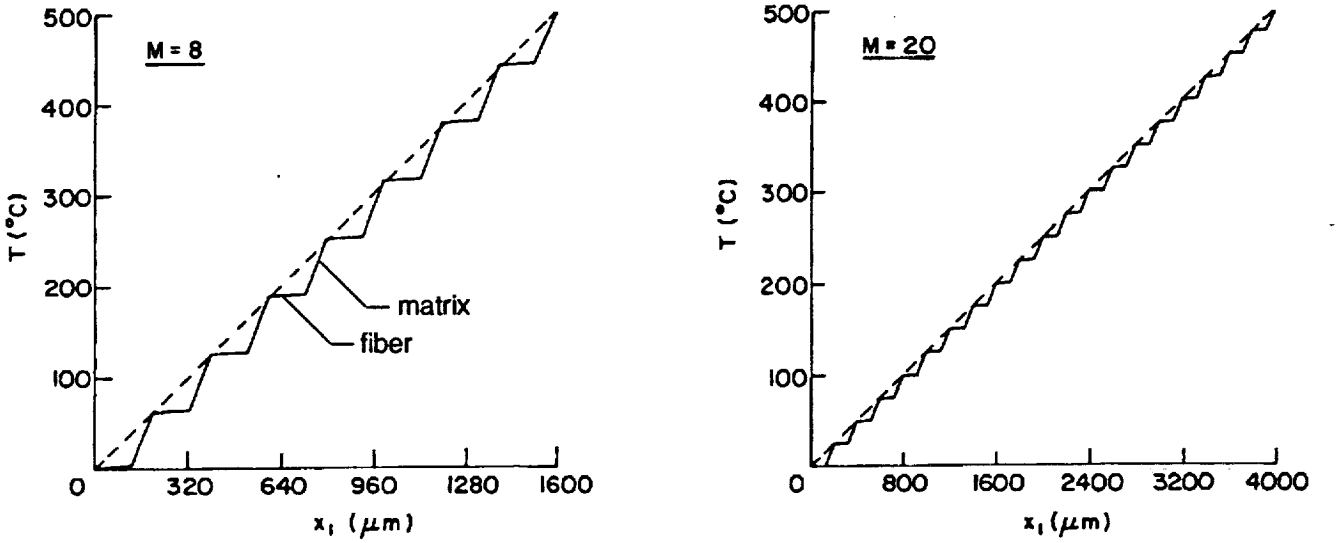

a) M = 8 b) M = 20

Figure 14 - Through-the-thickness temperature distribution in a bi-directional composite with uniformly spaced fibers in the cross-section containing both phases.

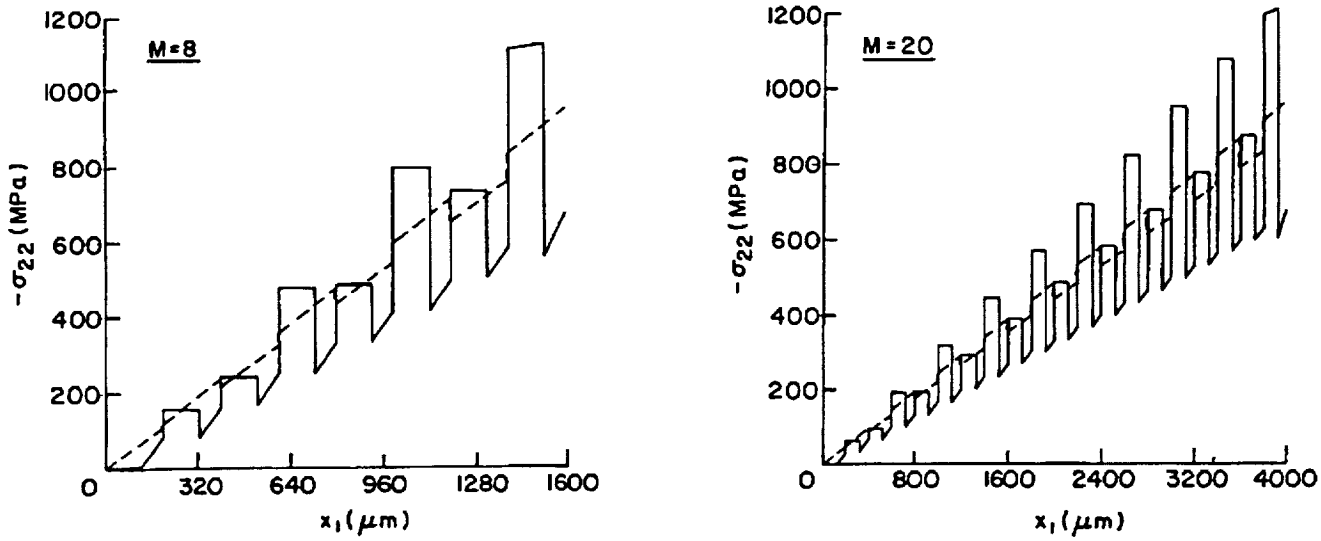

a) M = 8 b) M = 20

Figure 15 - Through-the-thickness normal stress σ_{22} in a bi-directional composite with uniformly spaced fibers in the cross-section containing both phases (——) FG theory, (- - -) continuum theory.

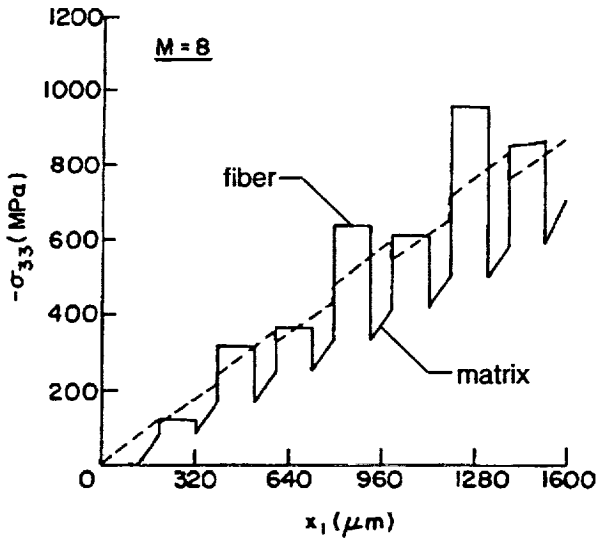

a) M = 8

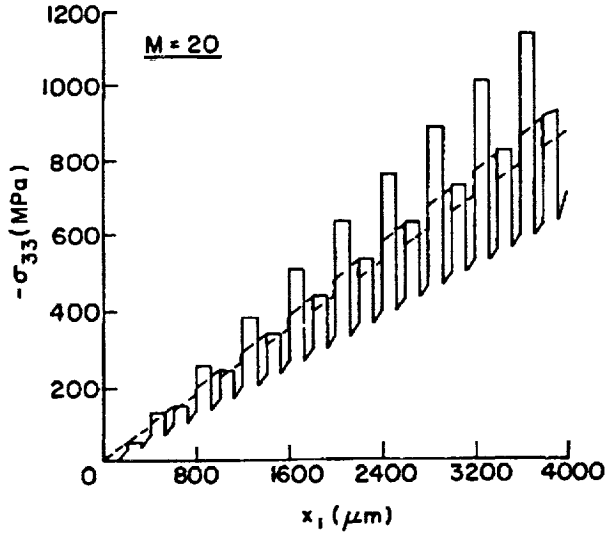

b) M = 20

Figure 16 - Through-the-thickness normal stress σ_{33} in a bi-directional composite with uniformly spaced fibers in the cross-section containing both phases (——) FG theory, (- - -) continuum theory.

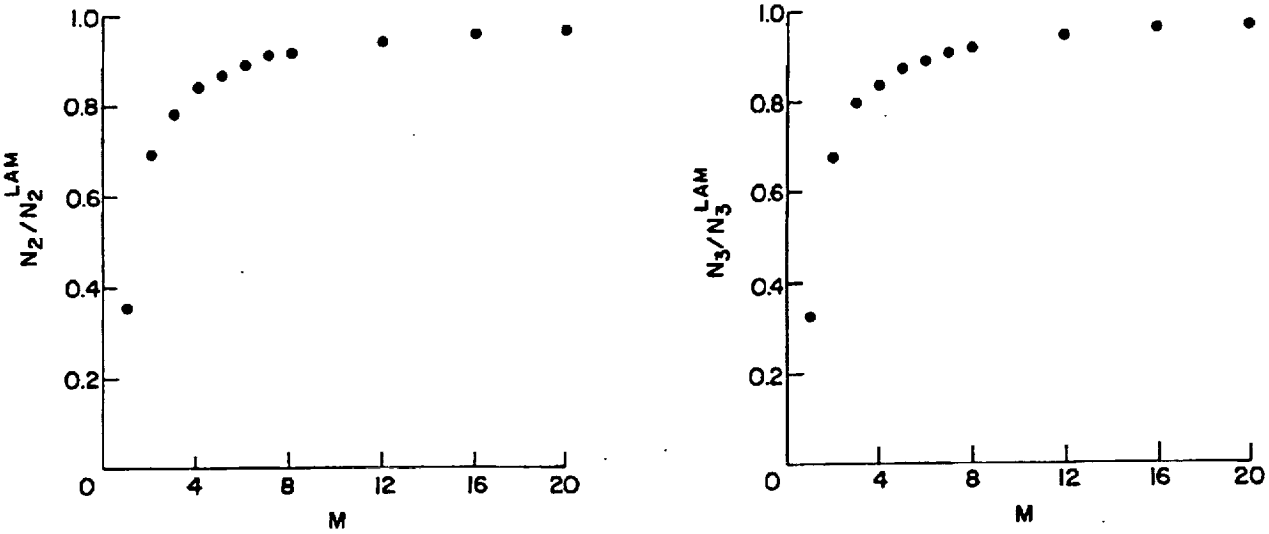

a) N_2 b) N_3

Figure 17 - Inplane force resultants in a bi-directional composite with uniformly spaced fibers in the thickness direction (normalized with respect to the continuum theory prediction).

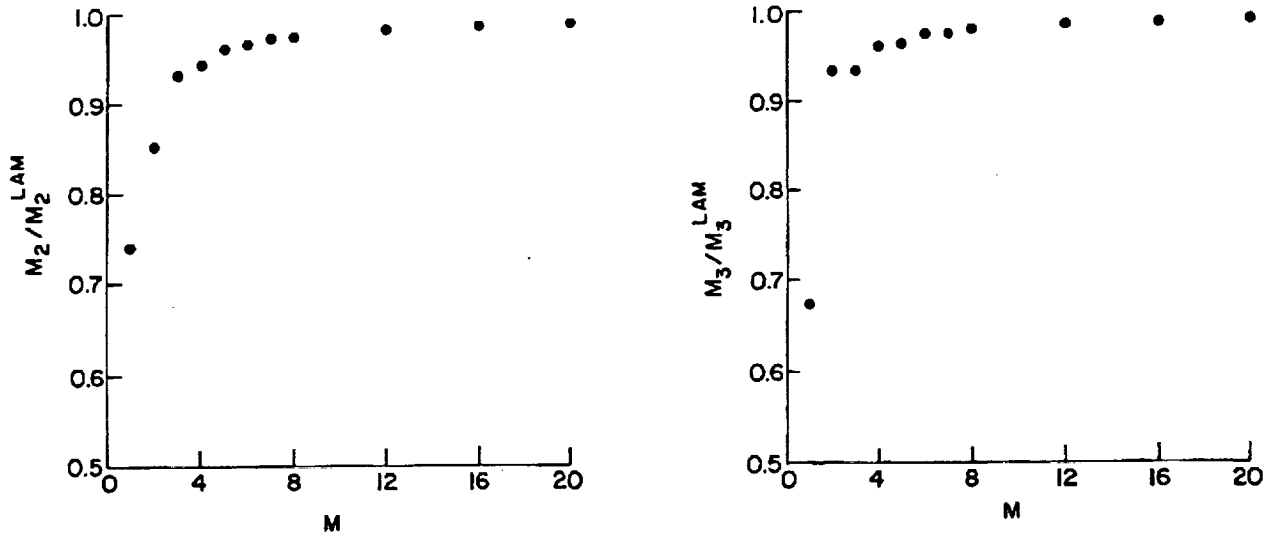

a) M_2 b) M_3

Figure 18 - Inplane moment resultants in a bi-directional composite with uniformly spaced fibers in the thickness direction (normalized with respect to the continuum theory prediction).

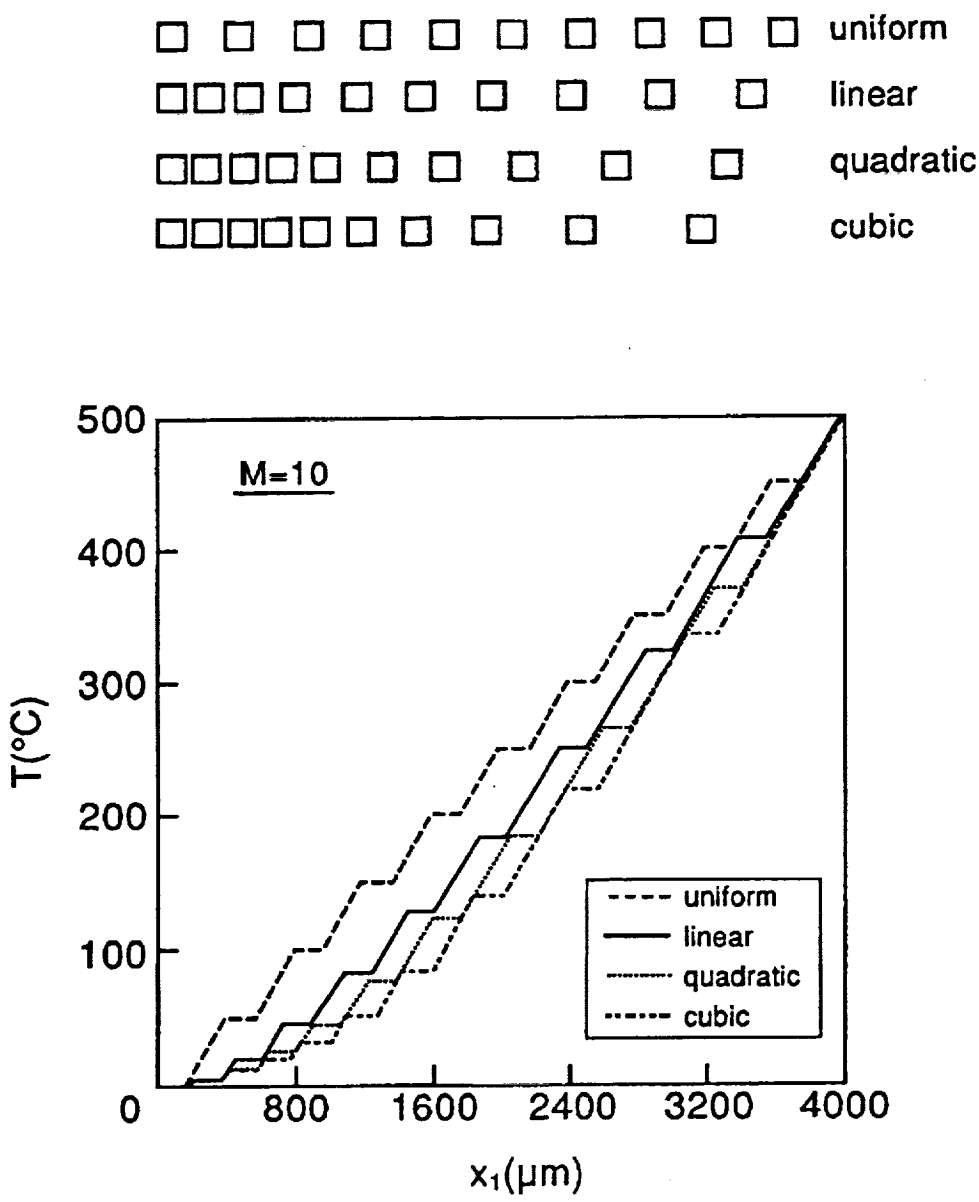

Figure 19 - Through-the-thickness temperature distribution in a unidirectional composite with linearly, quadratically and cubically spaced fibers. Comparison with uniformly spaced fiber composite.

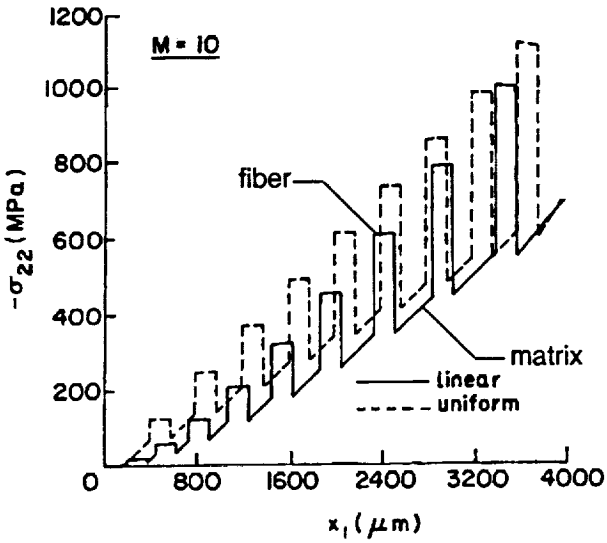

a) linearly spaced fibers

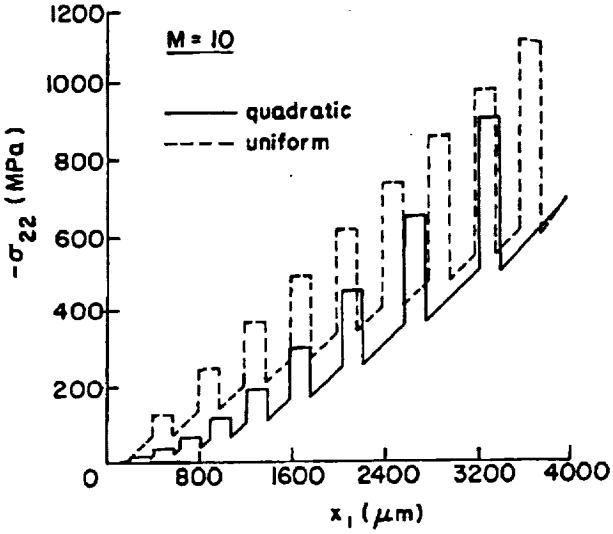

b) quadratically spaced fibers

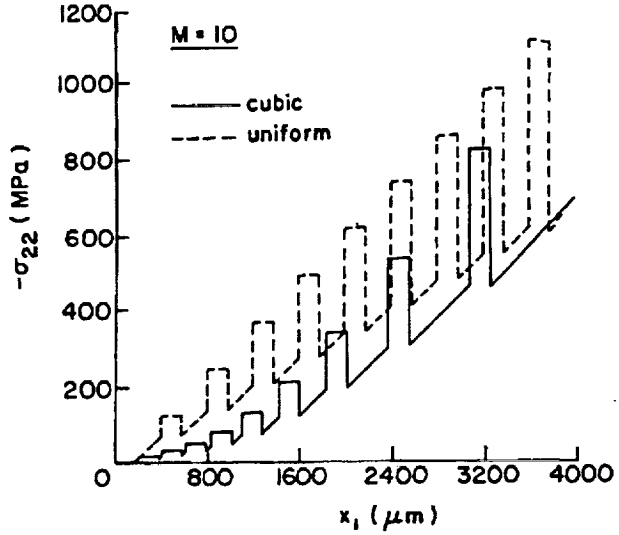

c) cubically spaced fibers

Figure 20 - Through-the-thickness normal stress σ_{22} in a unidirectional composite with nonuniformly spaced fibers. Comparison with uniformly spaced fiber composite.

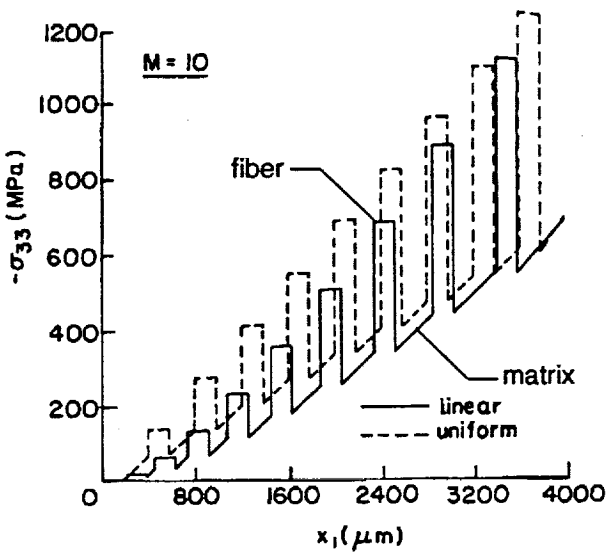

a) linearly spaced fibers

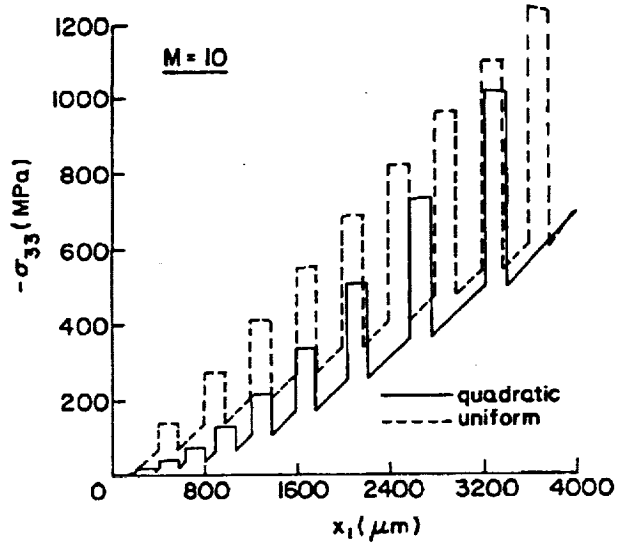

b) quadratically spaced fibers

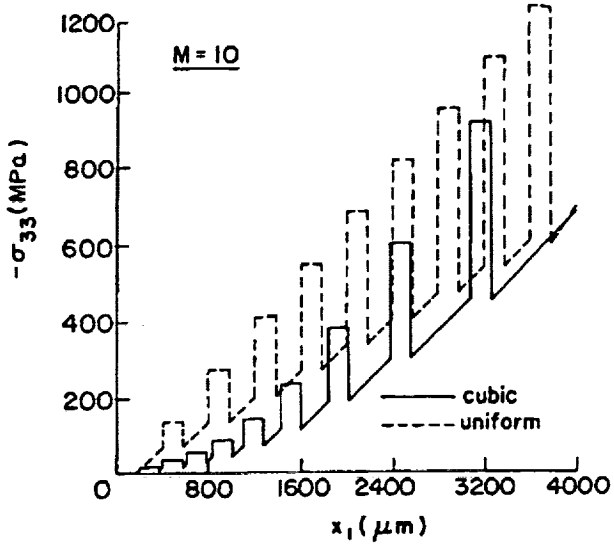

c) cubically spaced fibers

Figure 21 - Through-the-thickness normal stress σ_{33} in a unidirectional composite with nonuniformly spaced fibers. Comparison with uniformly spaced fiber composite.

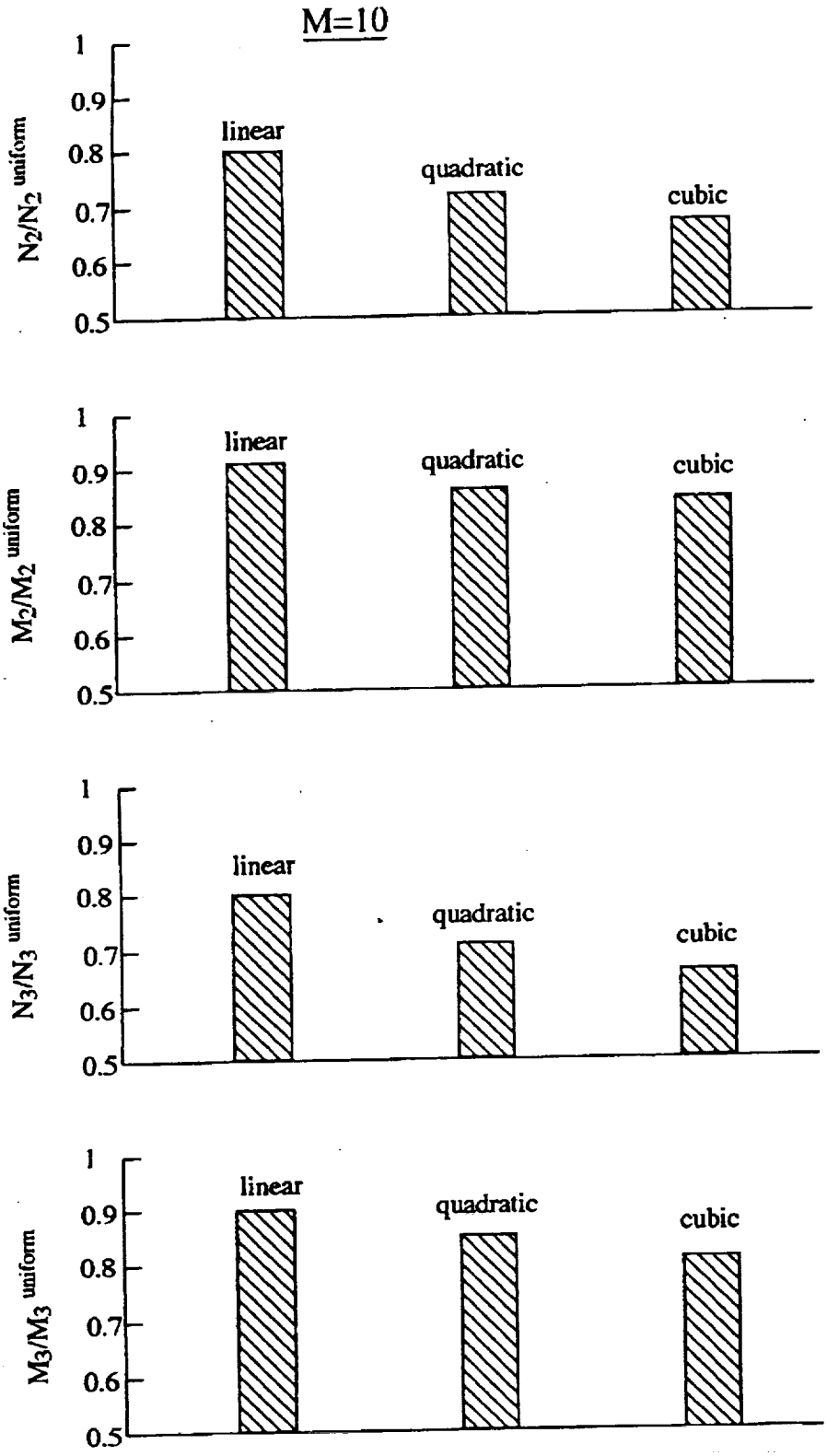

Figure 22 - Inplane force and moment resultants in unidirectional composites with linearly, quadratically and cubically spaced fibers, normalized with respect to the corresponding quantities in uniformly spaced fiber composites.

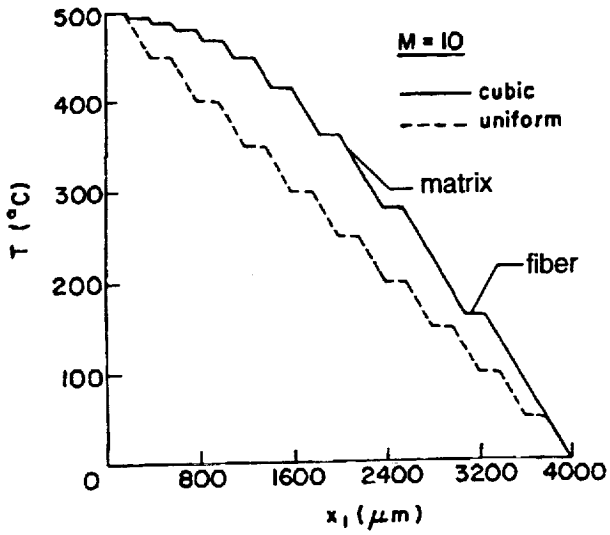

a) temperature distribution

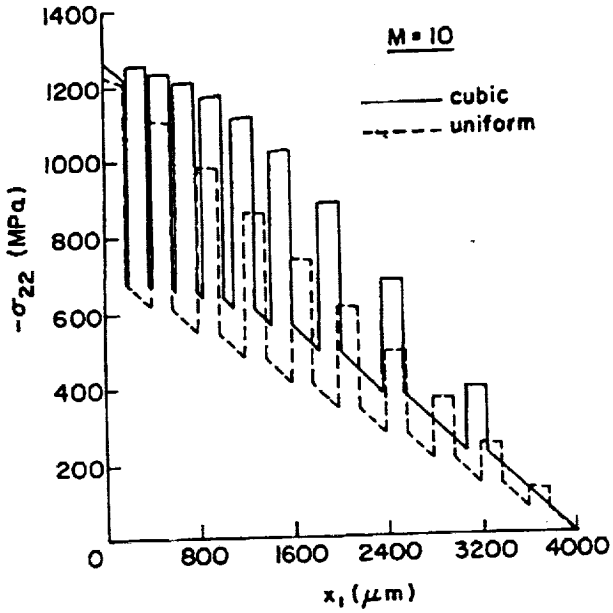

b) normal stress σ_{22} distribution

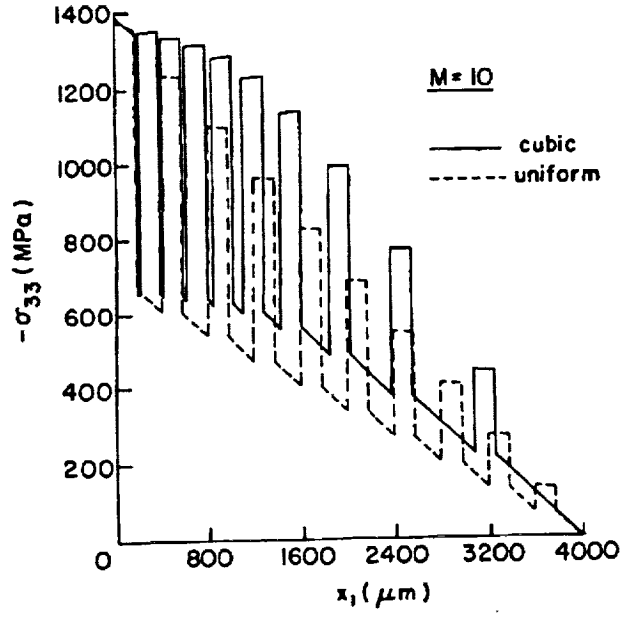

c) normal stress σ_{33} distribution

Figure 23 - Effect of reversing the direction of imposed thermal gradient in a unidirectional composite with cubically spaced fibers. Comparison with uniformly spaced fiber composite.

REPORT DOCUMENTATION PAGE

Form Approved
OMB No. 0704-0188

1. AGENCY USE ONLY (*Leave blank*)	2. REPORT DATE	3. REPORT TYPE AND DATES COVERED
	October 1993	Technical Memorandum

4. TITLE AND SUBTITLE

Thermoelastic Response of Metal Matrix Composites With Large-Diameter Fibers Subjected to Thermal Gradients

5. FUNDING NUMBERS

WU-510-01-50

6. AUTHOR(S)

Jacob Aboudi, Marek-Jerzy Pindera, and Steven M. Arnold

7. PERFORMING ORGANIZATION NAME(S) AND ADDRESS(ES)

National Aeronautics and Space Administration
Lewis Research Center
Cleveland, Ohio 44135-3191

8. PERFORMING ORGANIZATION REPORT NUMBER

E-8114

9. SPONSORING/MONITORING AGENCY NAME(S) AND ADDRESS(ES)

National Aeronautics and Space Administration
Washington, D.C. 20546-0001

10. SPONSORING/MONITORING AGENCY REPORT NUMBER

NASA TM-106344

11. SUPPLEMENTARY NOTES

Jacob Aboudi and Marek-Jerzy Pindera, University of Virgina, Charlottesville, Virgina, 22903 and Steven M. Arnold, NASA Lewis Research Center. Responsible person, Steven M. Arnold, (216) 433-3334.

12a. DISTRIBUTION/AVAILABILITY STATEMENT

Unclassified - Unlimited
Subject Category 24

12b. DISTRIBUTION CODE

13. ABSTRACT (*Maximum 200 words*)

A new micromechanical theory is presented for the response of heterogeneous metal matrix composites subjected to thermal gradients. In contrast to existing micromechanical theories that utilize classical homogenization schemes in the course of calculating microscopic and macroscopic field quantities, in the present approach the actual microstructural details are explicitly coupled with the macrostructure of the composite. Examples are offered that illustrate limitations of the classical homogenization approach in predicting the response of thin-walled metal matrix composites with large-diameter fibers when subjected to thermal gradients. These examples include composites with a finite number of fibers in the thickness direction that may be uniformly or nonuniformly spaced, thus admitting so-called functionally gradient composites. The results illustrate that the classical approach of decoupling micromechanical and macromechanical analyses in the presence of a finite number of large-diameter fibers, finite dimensions of the composite, and temperature gradient may produce excessively conservative estimates for macroscopic field quantities, while both underestimating and overestimating the local fluctuations of the microscopic quantities in different regions of the composite. Also demonstrated is the usefulness of the present approach in generating favorable stress distributions in the presence of thermal gradients by appropriately tailoring the internal microstructural details of the composite.

14. SUBJECT TERMS

Metal matrix composites; Large-diameter fibers; Thermal gradients; Functionally graded composites

15. NUMBER OF PAGES

76

16. PRICE CODE

A05

17. SECURITY CLASSIFICATION OF REPORT	18. SECURITY CLASSIFICATION OF THIS PAGE	19. SECURITY CLASSIFICATION OF ABSTRACT	20. LIMITATION OF ABSTRACT
Unclassified	Unclassified	Unclassified	